

Master Thesis, Department of Geosciences

Deformation bands in collapsed sandstone reservoirs

An example from Upper Jurassic Entrada Formation, Utah, USA

Ida Hope



UNIVERSITY OF OSLO

FACULTY OF MATHEMATICS AND NATURAL SCIENCES

Deformation bands in collapsed sandstone reservoirs

An example from Upper Jurassic Entrada Formation, Utah, USA

Ida Hope



Master Thesis in Geosciences

Discipline: Structure geology

Department of Geosciences

Faculty of Mathematics and Natural Sciences

University of Oslo

01.06.2015

© **Ida Hope, 2015**

This work is published digitally through DUO – Digitale Utgivelser ved UiO

<http://www.duo.uio.no>

It is also catalogued in BIBSYS (<http://www.bibsys.no/english>)

All rights reserved. No part of this publication may be reproduced or transmitted, in any form or by any means, without permission.

Acknowledgments

First of all, I would like to express my gratitude to my supervisors: Professor Alvar Braathen for guiding and help during field work as well as scientific discussions and feedback, and Elin Skurtveit for helpful advise and comments. I would also thank Helge Hellevang for helping me with questions regarding diagenesis.

In addition, I would like to thank the senior engineers: Berit Løken Berg for tutoring me in scanning electron microscope, and Salahalladin Akhavan for preparing my semi-consolidated sandstones into thin sections. Moreover, I would like to thank my fellow field trip student Eivind B. Larsen for keeping up the good mood even when the car was stuck in a muddy ditch for a whole day.

Last but not least, I will thank my family, friends and especially Magnus for always being there whenever I need them.

June 2015

Ida Hope

Abstract

Reservoir quality is of importance, related to extraction/production by: the petroleum industry, use of water aquifers and the assessment of CO₂ storage sites. A reservoir collapse would be critical for the reservoir performance. By studying an already collapsed reservoir, critical factors for collapsing can be revealed and avoided. An exhumed reservoir situated in Utah, USA was chosen. The studied sandstone reservoir in Humbug Flat reveals a quality reduction, addressed by occurrence of deformation bands decreasing the permeability. Four hypotheses were proposed explaining the collapse in the Humbug reservoir: 1) diagenesis, 2) fold strain, 3) fault leakage and 4) cap-rock burst. The orientation and density of the deformation bands were measured and counted in nine scan lines along Humbug Flat. Moreover, samples were collected from several deformation band types and areas, for identifying the chemical contents and the variations in grain size.

The field observations and laboratory work indicate an influence of CO₂-enriched fluids, which are suggested as the main cause of the reservoir collapse. The first assumed appearance of the reduced fluids is related to soft-sediment dike-intrusions. The fluid contributes to dissolution, alteration and increased pore-fluid pressure, reducing the yield-strength of the rock. Three deformation band populations found within the collapsed reservoir are associated with lower sandstone-strength. Two populations are related to the tectonic events: the uplift of the San Rafael Swell and the Moab Fault Array. The last deformation band population is mainly disaggregation bands associated with low burial depth. An important correlation between host rock grain size and porosity in deformation bands are observed. Areas with coarse host rock grain size tend to form low porosity deformation bands. This means that well-sorted, coarse grain sized reservoir rocks may form deformation bands reducing the permeability in greater magnitude than reservoirs with less host rock porosity.

Table of Contents

1 Introduction.....	1
1.1 Background	1
1.2 Field area.....	3
1.2.1 Fremont Bedding	3
2 Regional geology.....	5
2.1 Geological history of Utah.....	5
2.2 Stratigraphic description of succession exhumed in the NNE San Rafael swell... 	10
2.2.1 Navajo (120-200 m) and Page sandstones formations (0-12 m)	10
2.2.2 Carmel Formation (60-215 m).....	10
2.2.3 Entrada Formation (90-245 m).....	11
2.2.4 Dewey Bridge Member	11
2.2.5 Slick Rock Member	11
2.2.6 Moab Tongue Member.....	12
2.2.7 Curtis Formation (10-75 m).....	12
2.2.8 Summerville Formation (30-120 m).....	12
2.2.9 Morrison Formation (115-230 m)	14
2.2.10 Bukhorn Conglomerate (0-10 m).....	14
2.2.11 Cedar Mountain Formation (30-60 m)	14
2.2.12 Dakota Sandstone Formation (0-30 m).....	14
2.2.13 Mancos Shale Formation (600-760m+)	15
2.2.14 Mesaverde Group (300-600m+).....	15
2.3 Structural geology of the San Rafael swell and Utah	15
2.3.1 Moab fault array	16
2.3.2 San Rafael Swell.....	16
3 Conceptual framework for the thesis.....	17
3.1 Deformation bands	17
3.1.1 Kinematic classification	18
Volumetric deformation	18
Shear deformation	19
3.1.2 Classification based on deformation mechanisms	20
Disaggregation bands.....	20
Phyllosilicate bands.....	20
Cataclastic bands	21
Dissolution and cemented deformation bands	22

3.2	The load-carrying and fluid pressure influence on deformation bands.....	23
3.2.1	Fluid pressure	23
3.2.2	Bleaching and load-carrying cement	23
4 	Methods	25
4.1	Fieldwork	25
4.1.1	Lithostratigraphic log.....	25
4.1.2	Deformation band collection.....	25
4.1.3	Measuring the reservoir permeability	27
4.2	Laboratory work	28
4.2.1	Sample preparation and microtextural analysis	28
4.2.2	SEM: Scanning electron microscopy	29
4.2.3	ImageJ.....	30
5 	Datasets and analysis.....	31
5.1	Outcrops of study area	31
5.1.1	Lithostratigraphic log.....	33
5.1.2	Structural placement	36
5.1.3	Local non-strata form structures	37
Location V. and VI. (Figure 5.1).....	37	
Sandstone knob.....	38	
5.1.4	Deformation band characteristics.....	40
Deformation band truncations.....	41	
Ladder structures of deformation bands.....	43	
Deformation band clusters	45	
5.2	Field measurements	45
5.2.1	Deformation bands – distribution and orientation	45
5.2.2	The measured permeability differences	49
5.3	Microtextural analysis	50
5.3.1	General microtextural observations	50
5.3.2	Sample locations and thin sections	50
5.3.3	Host rock characteristics	53
Mineralogy	53	
Structures	53	
Porosity and grain size	53	
5.3.4	Deformation bands characteristics	55
Mineralogy	55	
Structures	57	

Porosity and grain size.....	57
6 Discussion.....	63
6.1 Regional setting.....	63
Deformation band chronology	63
WWS trending fold	64
6.2 Depositional characteristics of the Fremont Bedding and surrounding units.....	65
6.2.1 Pipe-structures, collapse or something else?	66
6.2.2 Is the Fremont Bedding bleached?.....	68
6.2.3 Deformation band occurrence in the Fremont Bedding.....	72
6.2.4 How did the deformation band form?	73
6.2.5 Burial evolution and deformation band formation.....	76
6.2.6 Are there a relationship between the dome-structure and the pale-colour?	77
6.3 The key to the collapse of Fremont Bedding	78
7 Conclusion	80
8 Recommendation	82
9 References	83

1 | Introduction

1.1 Background

Reservoir performance is economically of importance, as highlighted by resource extraction/production by the petroleum industry extracting oil and/or gas, use of water aquifers and the assessment of CO₂ storage sites. There are different aspects impacting the reservoir quality, and many are well studied. Nevertheless, there are still some less explored aspects, which the “Intergrated reservoir-seal bypass system analysis” project will address (UIO project funded by the research council of Norway). Deformation bands may or may not impact the reservoir permeability, which highly depends on the deformation band mechanism and distribution. Deformation bands mainly form in damage zones around faults, however they also exist in broadly disturbed populations (Brandenburg et al., 2012). The project is a collaboration between UIO teams working in SUCCESS, with contributions from partners such as NGI, UNI reasearch and university of Parma, exploring reservoir response to sedimentary architecture, deformation and pressure-driven and chemical changes.

For utilization, reservoirs need to be covered by a sealing cap-rock. Reservoir research of the connected reservoir cap-rock system can only be performed by either seismic imaging, well core analysis, or observation of old inactive reservoirs preferably exhumed to the surface. To perform highly detailed analysis of impacts by pressure-driven and chemical change, an inactive unroofed and exhumed reservoir was chosen. The target chosen was a reservoir situated in Utah’s Jurassic Entrada Formation. The reservoir site is in a sandstone shale succession, whereas assumed removal of hematite coating has created a bleached layer and bleached fracture systems, mimicking fluid mobility. The area consists mainly of red eolian sandstone deposits, except the assumed bleached layer. In addition to the chemical change caused by the bleaching of this layer, the bedding has experienced deformation in the form of mainly cataclastic shear and compaction bands.

The thesis addresses the deformation bands formed within the pale-coloured layer, and why and how they form. Four hypotheses are proposed by the “Intergrated reservoir-seal bypass system analysis” project:

Hypothesis 1 - Diagenesis: The analysed bedding is white and surrounded by red successions, indicating a chemical diagenesis with removal of red hematite. Reduced fluids may have travelled through the red rock, causing dissolution of the hematite coating that changed the sandstone colour from red to white. This chemical removal of load carrying hematite cement would perhaps create a higher porosity and permeability and reduce the shear strength of the rock. If the rock already experienced a significant stress, the removal of the hematite coating may have been the trigger for the sandstone to collapse by the formation of deformation bands.

Hypothesis 2 - Fold strain: The studied layer sits in an anticline. Deformation within a rock depends on yield strength. The pale-coloured layer represent a sandstone with the lowest shear strength, and because of this, the layer might collapse with local stress increase from folding. Hypothesis 2 suggests that if folding created the collapse, there should be more deformation bands around the fold hinge with the presumed highest strain.

Hypothesis 3 - Fault leakage: The upright anticlinal fold with a buoyant fluid creates pressure around the fold hinge. The pressure could reduce grain-contact friction so that the rock reached the critical strength limit, at that stage creating deformation bands. With several deformation bands and/or faults generations, a cyclic development might be a good explanation.

Hypothesis 4 - Cap-rock burst: With increasing pressure created by inflow of buoyant fluid the upright anticlinal might start to fracture, or/and reactivate pre-existing fractures. If this was the case, there should be more bleached fractures up along the fold hinge zone, from the pale-coloured layer into the cap-rock.

1.2 Field area

The field area is situated in central Utah, USA (Figure 1.1) along the NE margin of the San Rafael Swell. Geologically, Utah can be divided in two areas bounded by the “Wasatch line” or “Utah’s hingeline” (Berg and Skar, 2005; Hintze and Kowallis, 2009). The study area is localized to the central-east part of the state, east for the “Wasatch line”, where San Rafael Swell can be observed. The field area is located south of Book Cliffs, east of the Wasatch Plateau and west of Green River, in a Mid-Jurassic succession. The field data is collected in the area named Humbug Flat, which lies within the NNE-extent and east limb of the San Rafael Swell.

1.2.1 Fremont Bedding

The fieldwork is focused on an assumed bleached succession of the Jurassic Entrada Sandstone Formation, surrounded by red sandstones and some shale-mudstones above and below. The bedding can be followed along cliffs in what makes up a very gentle anticline with 3D closure. The studied bleached layer is crosscut by at least two faults, which have bleached patches along the slip surface (The following, bleached bedding will be termed Fremont Bedding to simplify the nomenclature). The sandstone succession makes up the Earthy Member of the Entrada Sandstone Formation, dominated by eolian, playa and fluvial overbank deposits. However, the studied bleached layer is of fluvial origin. In Figure 5.2, the readers will see examples of cross-stratification and colour change.

At the top of the Fremont Bedding, there is a thin layer consisting of similar bleached sandstone containing small traces of paleo-roots. The surface of this layer is exposed in several locations along the cliffs, showing a pillow-like top surface morphology interpreted to represent growth of grass and other vegetation.

In two sites along the cliffs there are observed pipe-like collapses or feeders of pale-coloured sandstone right underneath the Fremont Bedding. In addition, there is an alone standing bleached sandstone knob a few meter from the cliffs. The structures signal hydro-plastic sand mobility during deposition, and seem to impact observed deformation pattern.

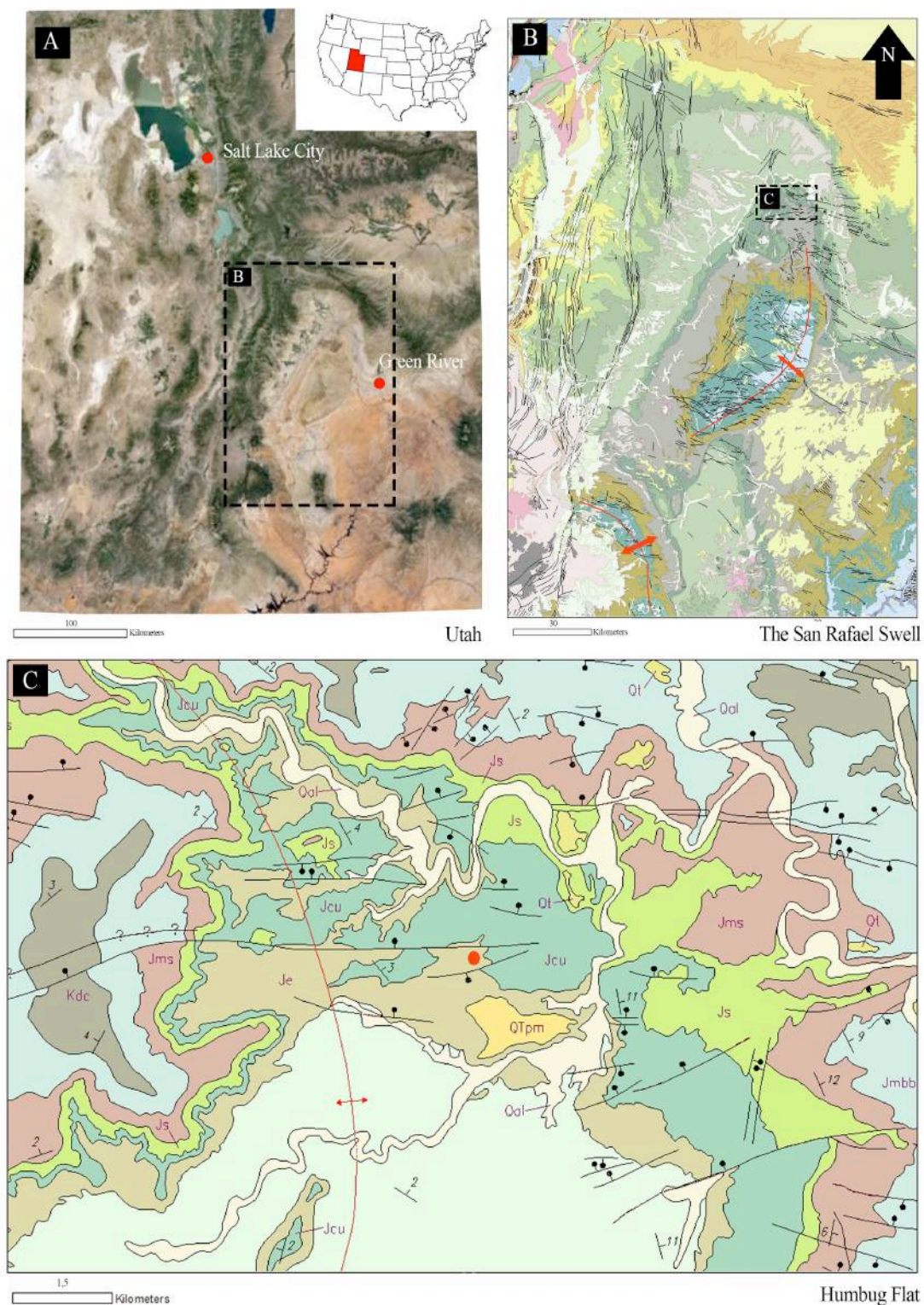


Figure 1.1: Location map displaying the field area. Humbug Flat is the geographical name of the study area. A) Image illustrating locations of Salt Lake City and Utah State, in addition to location within the USA. B) Geographical map showing the San Rafael Swell area and related anticlines. C) Detailed geological map describing the bedrock and structures in the area, including several faults. The red dot is the study area location. The map is based on Google Earth satellite image (2015) and a geological digitized map (Hintze et al., 2000).

2 | **Regonal geology**

2.1 Geological history of Utah

The North American basement rock was formed in several collisions, whereas gneisses, gneissic granites, schists and pegmatites are the dominantly formed rocks (Farmer and DePaolo, 1983; Whitmeyer and Karlstrom, 2007). Few early sedimentary deposits are conserved. The successions preserved before Neoproterozoic consisted of sedimentary basins related to rifting of Rodina and glacial deposits from the Cryogenian ice age (Crittenden Jr et al., 1983; Goodge et al., 2008; Whitmeyer and Karlstrom, 2007).

During the Neoproterozoic to Permian the western North American rift evolved, creating an oceanic basin within the craton. The eastern margin subsided slowly as it cooled, forming a shallow marine environment that was transgressed from what is today's western to eastern Utah (Burchfiel and Hickcox, 1972). This westward thickening wedge consists of km-thick carbonates and sandstone deposits (Burchfiel and Hickcox, 1972).

The marine environment was maintained through the Mississippian to Pennsylvanian period (Fillmore, 2011d). Especially the Pennsylvanian period experienced cyclic sea level fall and rise, reflecting glaciations in the Southern Hemisphere (Fillmore, 2011d). The assemblage of the supercontinent Pangaea in the late Paleozoic forced parts of Gondwanaland over Laurantia in an orogeny today found in Texas-Oklahoma (Dickinson and Lawton, 2003). The force of the collision caused warping and faulting further inland, producing the Ancestral Rockies and associated basins (Dickinson and Lawton, 2003). Within Utah's state borders, the Paradox and Oquirrh basins formed in this period (Fillmore, 2011d)(Figure 2.1). The Paradox Basin has especially seen detailed studies, since this region hosts petroleum. The Paradox Basin is ascribed to a sabkha environment with a 600 to 3000 m thick succession of partly organic evaporates and some salt, the latter being mobile, during subsequent tectonic events (Cater and Craig, 1970, 9; Hite and Buckner, 1981)

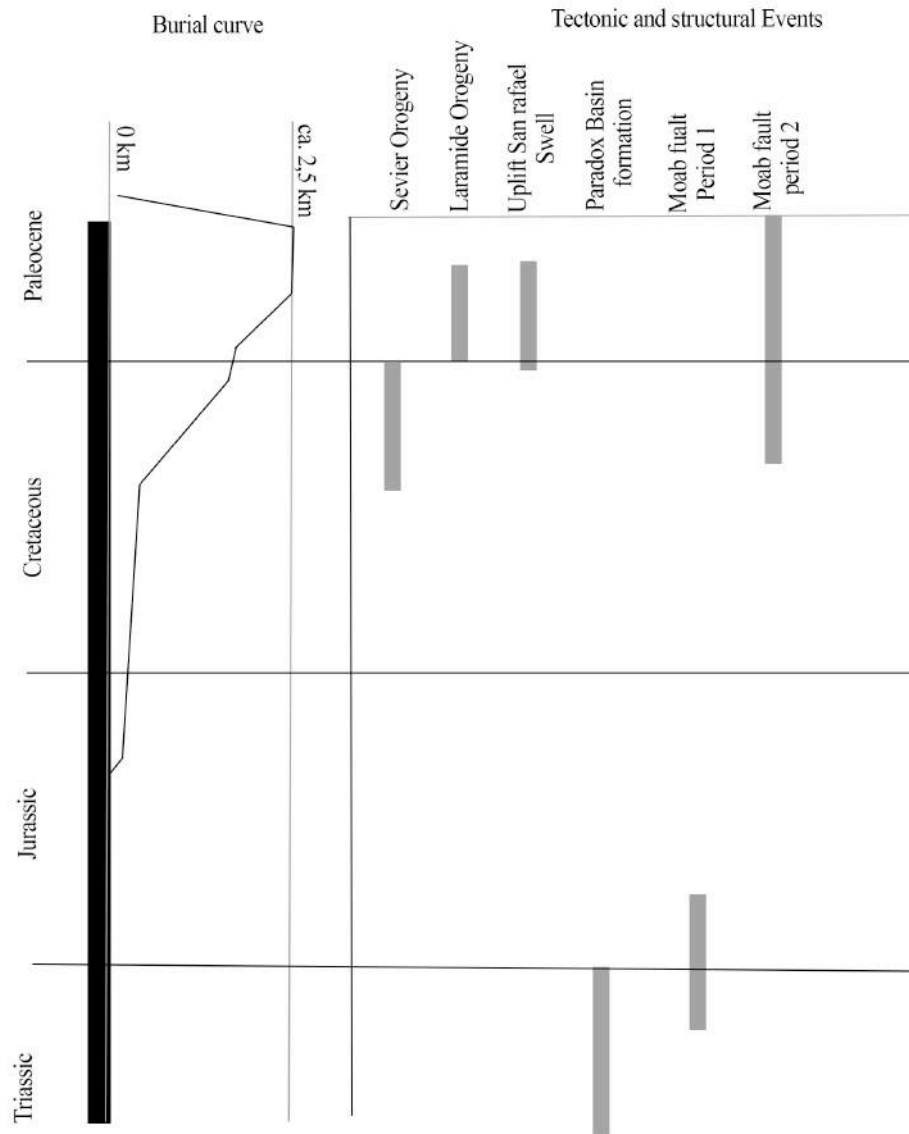


Figure 2.1: Timing of events in Utah. The burial curve for Entrada is shown in left of the figure, with ages at further left. The burial curve is based on Davatzes and Aydin (Davatzes and Aydin) study on Navajo Fm.

In the Early Mesozoic the Pangaea started to rift, forming narrow seaways which gradually grew into large oceanic basins (Fillmore, 2011c). The Mesozoic rifting eventually forced the North American continent to override the Farallon plate in the late Triassic (Burchfiel and Hickcox, 1972). This movement resulted in subduction, with related Andesitic magmatism, as seen in the Sierra Nevada Mountains and some granitic plutons in the Utah region (Fillmore, 2011c). In addition to magmatic activity, the thrusting caused a back-bulge stretching from Utah to Canada (Figure 2.2) (Willis, 1999). The Earthy Entrada Member formed within this middle Jurassic back-bulge setting, with mudflats, fluvial and eolian environments (Hintze and Kowallis, 2009). Subduction of the Farallon plate beneath North American continued from Jurassic to Cretaceous times, when the Sevier orogeny formed

(Fillmore, 2011c). Overall, Sevier thrusting caused mountain-building in west and a broad subsiding foreland basin system further east (Currie, 1997). As the thrust front reached Utah, the Idaho-Utah-Wyoming fold-thrust belt formed a frontal imbricate stack shedding sediments into a foreland basin system in eastern Utah and Colorado (Currie, 1997; Currie, 2002), seen in the famous Book Cliffs.

In the Late Cretaceous, the global sea level raised simultaneously as Utah experienced local high subsidence rate in the foreland basin system (Fillmore, 2011a) (Figure 2.1). The combination of sea level raise and high subsidence resulted in a deep seaway (Figure 1.1), causing deposition of a thick, deep marine layers of mud, represented by the Mancos Fm Shales. The more proximal facies, hosting sandstones is found in the Mesaverde Group (Fillmore, 2011a).

About 60 million years ago, in the Early Paleogen (Early Tertiary), most of the Farallon Plate was overridden by the North American continent and the progressive younger oceanic crust caused shallower subduction (Fillmore, 2011e; Dickinson et al., 1988). This resulted in stronger coupling between the plates, triggering the Laramide Orogeny. This tectonic province is characterized by deep-seated, basement-rooted thrusts that cut into overlying cover sediments, setting up major thrust-tip monoclines across the Colorado Plateau (Erslev and Rogers, 1993). In Utah, the largest of these up-thrusts is the Unita Mountains with the Unita Basin as flexural syncline to the south (Fillmore, 2011e). Other Laramide upthrusts are the San Rafael Swell, and the Circle Cliffs and Mountain Upwrap. Since the Sevier and Laramide orogenies overlap in space and time, it is debated if they actually represent one or two orogenies (Fillmore, 2011e) (Armstrong, 1968).

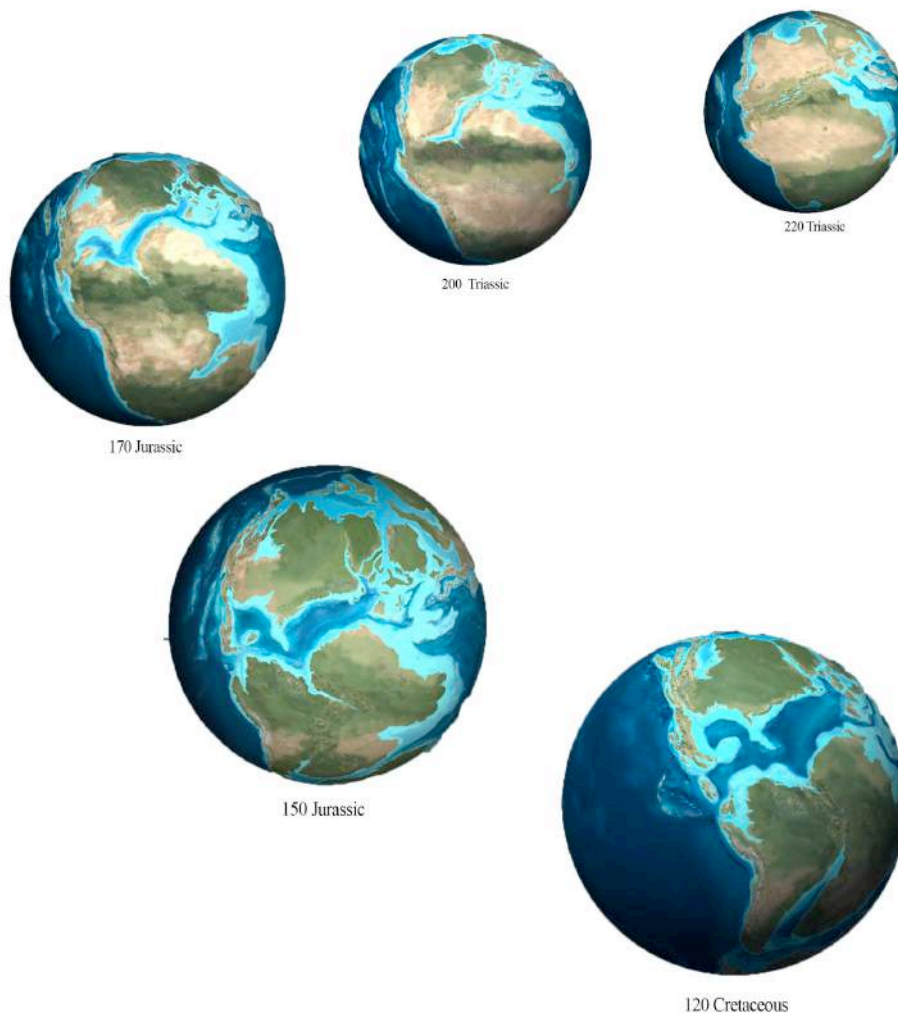
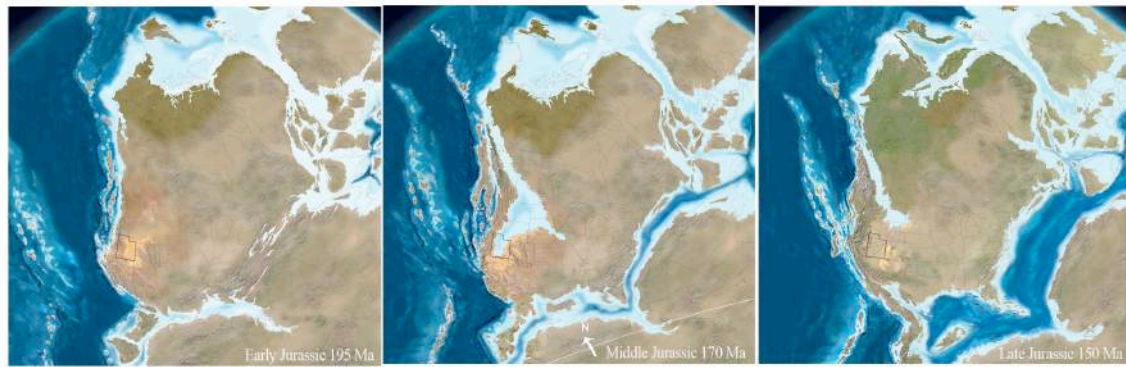
By the Oligocene epoch, volcanic activity was common in western parts of Utah (Fillmore, 2011e), during the so-called magmatic flare-up (ca. 20 Ma)(Coney, 1978). The volcanic activity was caused by a collapse of the Farallon slab, allowing magma to heat and elevate western North America (Nelson and Davidson, 1997). Both volcanoes and intrusions made up of felsic material (andesite, dacite and rhyolite) contributed to the formation of western Utah's topography (Fillmore, 2011e). Striking plutons in today's morphology are the Henry and La Sal mountains.

Late in the Cenozoic Eon, the San Andreas Fault system established, with a pull on the Californian region northward (Atwater, 1970). This tectonic event replaced subduction with

transform movement and extension, causing substantial normal faulting further east, which eventually created the current setting of the Basin and Range province (Stewart, 1998).

At approximately 20 000 years ago the climate cooled, as the Pleistocene ice age began. Utah's mountains were covered by glaciers, and the valleys were filled with lakes and rivers (Madsen and Currey, 1979). During this Epoch, the Lake Bonneville covered large parts of western Utah, of today, only parts of this super-lake remain: Utah Lake, Sevier Lake, Bear Lake and the Great Salt Lake (Madsen and Currey, 1979).

Jurassic Paleogeography



Triassic to Cretaceous Paleogeography

Figure 2.2: Overview of the Paleogeography from Triassic to Cretaceous. In this period the North America and South America divides, causing a large seaway in-between. The Earthy Entrada Member is the main succession analysed in this study, which makes Jurassic paleogeography important related to this thesis' context. The uppermost illustration shows early Jurassic to late Jurassic paleogeography, with in a continent-seaway-continent environment. Illustrations are based on Blakey (No date) Global Paleogeography.

2.2 Stratigraphic description of succession exhumed in the NNE San Rafeal swell

The compilation of Hintz and Kowallis (2009) forms a fundament for understanding the stratigraphy of Utah and the attached logs or type-sections inform this chapter.

The field area is located to an outcrop area within the San Rafael swell. The San Rafael Swell hosts the: Mesaverde Group, Mancos Shale, Dakota Sandstone Formation (Fm), Cedar Mountain Formation (Fm), Buckhorn Conglomerate, Morrison Formation (Fm), and the San Rafael Group. This last group (San Rafael Group) are made up of the Summerville, Curtis, Entrada (Earthy facies), Carmel, and Page formations (Hintze and Kowallis, 2009). The ages of the San Rafael Swell-successions are from Middle Jurassic up to late Cretaceous. The formations were deposit in the Jurassic period occurred simultaneously with the beginning of the Sevier Orogeny. The Jurassic succession is usually divided into three parts: Early Jurassic deposits are non-marine sandstones with marine intrusions. The overlying Middle Jurassic sandstones are a result of changing environments, mostly due to development of the epicontinental seaway from Canada to Utah. The Late Jurassic rocks formed within the non-marine Morrison basin. The Cretaceous successions are widely influenced by Sevier thrusting with related development of mountains in the west and the evolving Cretaceous foredeep oceanic basin (Hintze and Kowallis, 2009).

2.2.1 Navajo (120-200 m) and Page sandstones formations (0-12 m)

Page Sandstone Formation (Fm) forms the base of San Rafael Group. This sandstone is identical with the sandstone underneath, which is the Navajo sandstone Formation (Fm). The Page and the Navajo sandstones (fms) are considered as individual units, as they are separated by the J-2 unconformity (Fillmore, 2011b). Both units are eolian, deposit in a north-south belt, along the coastal plain separating the epicontinental sea from the western continental margin (Fillmore, 2011b).

2.2.2 Carmel Formation (60-215 m)

The middle Jurassic Carmel Formation (Fm) is made up of marine fossil-bearing limestone and marine shales (Hintze and Kowallis, 2009). In addition local evaporate deposits are present, seen as by gypsum layers and gypsum noduls in shale. Common lithologies in the Carmel Fm are gray-green shale and mudstone, red earthy sandstone and a yellow sandstone. The Formation appears strikingly layered, due to shifts between the gray-green shale, white

gypsum and yellow and red sandstones. In certain areas there is soft sediment deformation (Mathis, 2000).

2.2.3 Entrada Formation (90-245 m)

The succession encountered in the study area of the Humbug Flats, Utah, is essentially consisting of the Entrada sandstone Formation (Fm). This unit contains three members, from older to younger: The Dewey Bridge Member, the Slick Rock Member and Moab Tongue Member (Chan et al., 2000). Regional correlations remain somewhat uncertain, as in the study area, the Slick Rock and Moab Tongue Members are replaced by the Earthy Member. There is a gradual shift in facies from the SE towards the field area in the NW reflected by the mention replacement of members by fms. The Earthy Member consists of more mudstone interlayered with sandstone deposit in a coastal plain mud-flat environment. The Slick Rock and Moab Tongue eolian deposits are replaced with changing fluvial overbank, playa lakes, soil profiles and eolian deposits of the Earthy Member and marginal marine deposits of the Curtis Fm.

2.2.4 Dewey Bridge Member

The Dewey Bridge Member is found towards the SE near Moab and consists of sandstone and siltstone, formed as sabkha and/or eolian deposits (Chan et al., 2000). The red- to brown-coloured unit is more sandy in the lower part, giving way to interbedded, poorly sorted, fine-grained sand- or siltstone (Blakey et al., 1988). Parts of the Dewey Bridge Member are proposed to interfinger with to the marine Carmel Formation located further west (Blakey et al., 1988). Near Moab the contact between Slick Rock and the Dewey Bridge members is visible as a brown, undisturbed, planar, mudstone bed (Fossen, 2010). In the field area, the top of the Dewey Bridge Member or Carmel Fm, consist of meter-thick fine-grained fluvial sandstone. In a regional sense, it is debated if the Dewey Bridge Member belongs to the Entrada or the Carmel formations. Either way, the encountered sedimentary facies depends on location (Figure 2.3).

2.2.5 Slick Rock Member

The Slick Rock Member is a white-, pink-, and salmon-coloured resistant sandstone, with meter-scale dune sets (Chan et al., 2000). The Slick Rock Member marks a transition from the muddy Dewey Bridge Member to sand-dominated facies. The unit are consisting of thin, laterally continuous dune sandstones of eolian affinity, with interbedded eolian wet dune

deposits and muddy to sandy sabkhas (Chan et al., 2000; Foxford, 1996). The sandy parts of the Slick Rock Member are predominantly quartz arenites, with well-sorted fine to medium grain size. Permeability is mainly high, except in areas where thin interbedding with muddy sabkha exists (Foxford, 1996).

2.2.6 Moab Tongue Member

The third and last member of the Entrada Fm Sandstone is known as the Moab Tongue Member or Moab Member. This unit is primarily white-coloured and thin, representing eolian dune deposits partly reworked as beach deposits (Chan et al., 2000). The Moab Tongue Member is a result of more arid conditions than the Slick Rock Member. Dune sandstones and interbedded eolian interdune are represented at the Moab Tongue Member base, with large-scale eolian dune sets closer to the top of the member. The sandstone consists of about 98% quartz and only small amounts of alkali feldspar. Generally, Moab Tongue Member is better sorted and less fine-grained than the Slick Rock Member (Foxford, 1996). The J-3 unconformity is recognized right above the Entrada Sandstone in the San Rafael Swell and in the Uinta Mountains and in northwestern Colorado. Chert pebbles are observed on or at least not far above the J-3 surface (Piperinos and O'Sullivan, 1978). As shown in Figure 2.3 Carmel Fm. replaces the Dewey Bridge Member.

2.2.7 Curtis Formation (10-75 m)

The Curtis Formation (Fm) is a marginal marine near-shore sediment, dominated by sandstone situated on top of the Jurassic J3 unconformity (Mathis, 2000). The lower part of the Curtis Fm is fine-grained sandstone, continuing as an upward coarsening succession. The uppermost sequence of Curtis Fm are deposited during a maximum flooding event, representing the boarder between the Summerville and Curtis formations (Mathis, 2000).

2.2.8 Summerville Formation (30-120 m)

The summerville Formation (Fm) consists of thin bedded strikingly red and brown alterations of mudstone and sandstone. There are also usual to find inter-beds with secondary white gypsum veins and concretions (Fillmore, 2011c; Mathis, 2000). There are locally oscillation ripples in the sandy units, mudcracks in the clay rich parts and gypsum indicating a flat, low-laying, tidally-influenced depositional environment (Fillmore, 2011b)

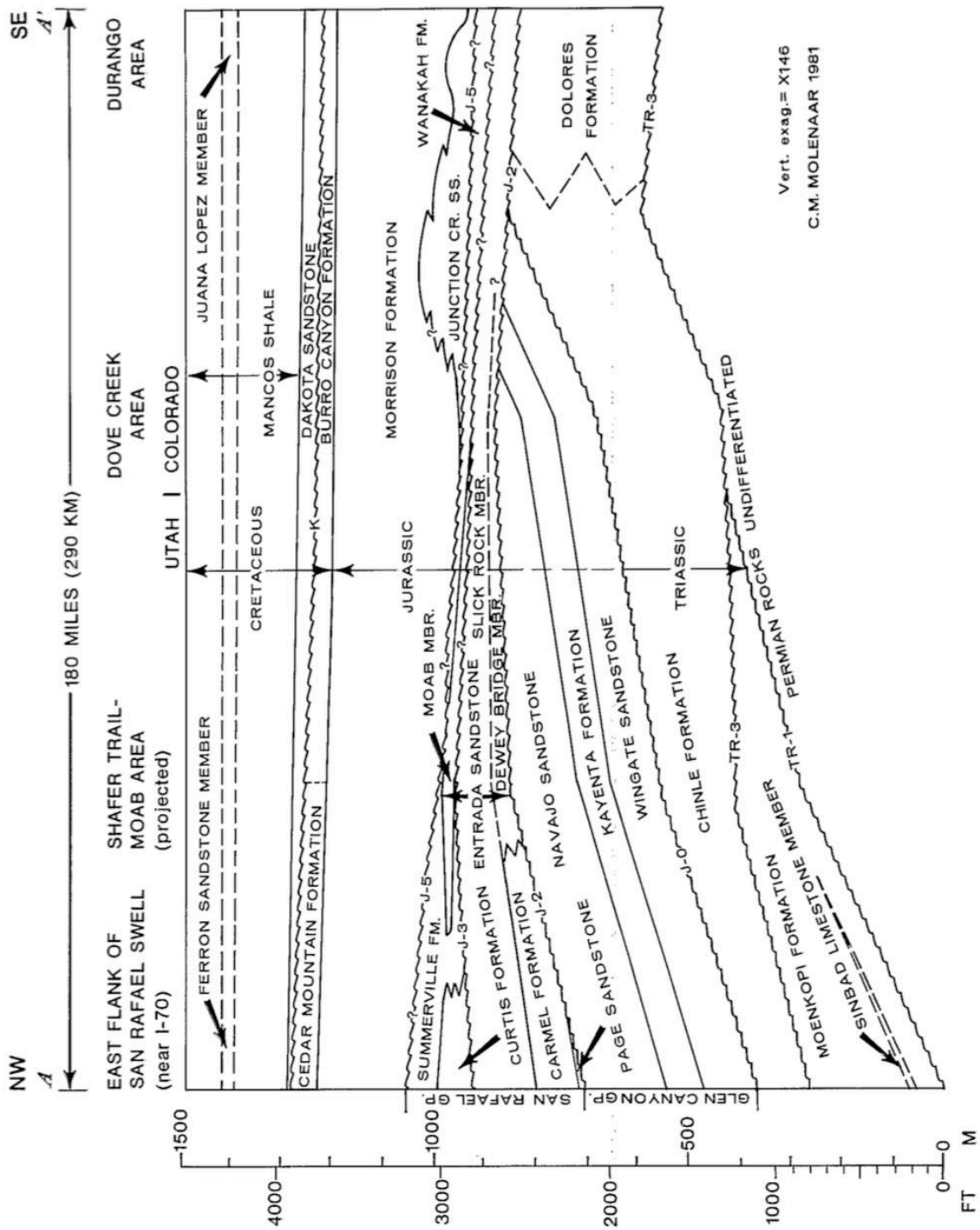


Figure 2.3: Overview of the stratigraphy of east flank of San Rafael Swell. Mark that Dewey Bridge Member are replaced by Carmel Fm. and that Moab Member does not cover the San Rafael swell Moleenaar (1981). This illustration describe the are east for the field area.

2.2.9 Morrison Formation (115-230 m)

This is the first upper Jurassic deposit, situated above the J-5 unconformity (Fillmore, 2011b). It is strikingly colourful. The unit is continental, with stacked fluvial sandstone channels, and fine overbank deposits (Fillmore, 2011c; Humez et al., 2014). The Morrison Formation is divided in three members, based in the abundance of channel deposits (Mathis, 2000). The oldest member is the Tidwell, consisting of alluvial plain sediments. The middle Salt Wash Member is mainly constructed of fluvial channel and floodplain deposits. The youngest Brushy Basin Member is a combination of wetland and lacustrine deposits, with local fluvial channels (Mathis, 2000).

2.2.10 Bukhorn Conglomerate (0-10 m)

The Bukhorn Conglomerate was defined by Stokes (1944) and was considered as a member of Cedar Mountain Formation until the discovery of the significant unconformity between the Bukhorn and Upper shale Member (Currie, 1997; Aubrey, 1996). According to Currie (1997) and Aubrey (1996), the Bukhorn Conglomerate is closer related to the Upper Jurassic Morrison Formation than the Early Cretaceous deposits. The Bukhorn Conglomerate is up to 35 m thick, consisting mostly of black shale pebbles with a mean diameter of 3 centimetres (Currie, 2002; Kirkland et al., 1999).

2.2.11 Cedar Mountain Formation (30-60 m)

Since the Bukhorn Conglomerate is no longer considered as Member of Cedar Mountain Formation (CMF), the Upper Shale Member is the only component part of CMF (Aubrey, 1996). This Member is a non-marine sequence consisting of sandstone, conglomerate and a sand rich mudstone with small micritic limestone beds (Yingling and Heller, 1992). Several lithofacies in addition to the micritic limestone indicates fluvial and lacustrine origin (Yingling and Heller, 1992; Currie, 2002). There is generally agreement among geologists that the variation in depositional environment is connected to the Sevier Orogeny (Kirkland et al., 1999)

2.2.12 Dakota Sandstone Formation (0-30 m)

The earliest Cretaceous records of seaway deposits, separates the CMF from the Dakota Sandstone Formation (Fm.) (Young, 1970). The marine Dakota Sandstone Fm. consist of three members; the oldest member is a combination of sheet sandstone and conglomerate,

and the middle and upper member contain paralic marine deposits with shale and sandstone (Yingling and Heller, 1992).

2.2.13 Mancos Shale Formation (600-760m+)

Mancos Shale Formation (Fm.) is mainly dominated by mudrock, deposited in a deep marine basin (Hettinger and Kirschbaum, 2002; Weimer, 1960). The Mancos Shale Fm. is divided into three members. The oldest Tununk Shale Member is above a transgressive disconformity contact with Dakota Sandstone. In late Cretaceous time the marine accumulation were interrupted by eastward regression of the shoreline between the western continent and the eastern foredeep Mancos Sea. The first marine regression is seen as deltaic sandy deposits, which today is encountered by the Ferron Sandstone Member of the Mancos Shale Fm. The youngest member, the Blue Gate, is related to the Blue Gate transgression and is dated by the inoceramid bivalve *Mytilodites dresdensis labiatoidiformis* to be approximately 87 Ma old (Ryer and McPhillips, 1983).

2.2.14 Mesaverde Group (300-600m+)

According to Lawton (1986) the Mesaverde Group deposits were laid down due to a transition from the Sevier Thrust Belt to Laramide basement controlled uplift within the foreland basin. The mesa Verde Group reflects a regression from marine to delta-top deposits, and is sandstone dominated as seen in the Book Cliffs. The Mesaverde Group contains mostly marine sandstones, with layers of shale, coal and brackish and fresh-water sediments (Spiker and Reeside, 1925). The group is divided into four members. The oldest is the Star Point Sandstone, which represents the retreating Mancos Sea. With the first appearance of coal the Blackhawk Formation starts, shifting into Castlegate Sandstone with a base of pebbly coarse-grained sandstones. The youngest Mesaverde Group Member is the Price River Formation, which contains of gray sandstone, grits and conglomerate (Spiker and Reeside, 1925; Lawton, 1986).

2.3 Structural geology of the San Rafael swell and Utah

The field area is situated along the NNE part of the N-S trending San Rafael Swell, believed to be an East-verging Laramide-style monocline. The area also in a broad sense offers a segment of Moab fault array.

2.3.1 Moab fault array

The Moab fault itself is 45 km long, strikes SSE-NNW, and has a maximum-throw about 960 m at the surface (Fossen, 2010; Jones et al., 1998; Foxford et al., 1998), its evolution is related to deep salt movements (Hintze et al., 2000). The type area of this normal fault is located near Moab town in the northwestern part of Paradox basin. There, the Moab fault truncates at least a 5000 m thick succession consisting of sediments of Carboniferous to Cretaceous age (Berg and Skar, 2005; Foxford, 1996). According to Foxford et al. (1996), the activity on the Moab fault happened in two different periods: the first from Triassic until Mid-Jurassic and the second from Mid-Cretaceous to Paleogen. The Moab fault itself contains a meter wide shear zone fault core encased by deformation band swarms in damage zones, up to 70 m wide (Foxford et al., 1998; Aydin and Johnson, 1978). The Moab fault is followed to the WNW by a series of WNW-ESE striking fault segments. Near Moab, these segments are the hard-linked Courthouse, Tusher and Bartlet Segments. They give way to the soft-linked Salt Wash Graben and Little Grand Wash fault farther WNW (Dockrill and Shipton, 2010). From the Green River towards the San Rafael Swell there is a series of smaller isolated near E-W striking normal faults, they are found all the way to the eastern and NNE limb of the San Rafael Swell.

2.3.2 San Rafael Swell

The Laramide style San Rafael Swell is a doubly-plunging, asymmetric East-verging monocline, covering an area that is 120 km long and 60 km wide (Zuluaga et al., 2014). Along the center of the swell, the monocline has a steep east limb, however, the east limb dips more gently to the north and south (Fillmore, 2011b). The long west-limb dips less than 5° to the west. The Laramide orogeny is assumed to have reactivated faults deep in the crust, causing movement both along the old faults and in the overlying lithologies. Accordingly the swell is assumed to have formed due to reactivation of older faults and/or fractures, and formed into a monoclinial fault propagation fold with the largest throw, or upfolding, near the center, declining in intensity to the north and south towards the terminations of the swell. (Zuluaga et al.)

3 | Conceptual framework for the thesis

3.1 Deformation bands

Deformation bands are tabular zones, often but not necessarily with small-scale displacement, which occur only in highly porous lithified and non-lithified deposits (Fossen, 2010; Fossen et al., 2007). Deformation bands are observed at shallow depth (< 3 km) in low confining pressures (<40 MPa). However, the occurrence is highly variable due to the physical properties of the host rock (Nicol et al., 2013). There are several factors controlling the occurrence of deformation bands, including mineralogy, grain size, grain shape, sorting, burial depth, deviatoric stress and pore fluid pressure (Fossen et al., 2007). The host rock conditions in addition to the physical environment control the deformation style and therefore determine which type of deformation band that occur. There are two types of nomenclature for the deformation bands based on either kinematics (Aydin and Ahmadov, 2009; Schultz and Fossen, 2008; Johansen and Fossen, 2008) or deformation mechanism (Fossen et al., 2007). In this thesis the classification of deformation mechanism are used. However, the classifications can be compared as the Figure 3.1 shows.

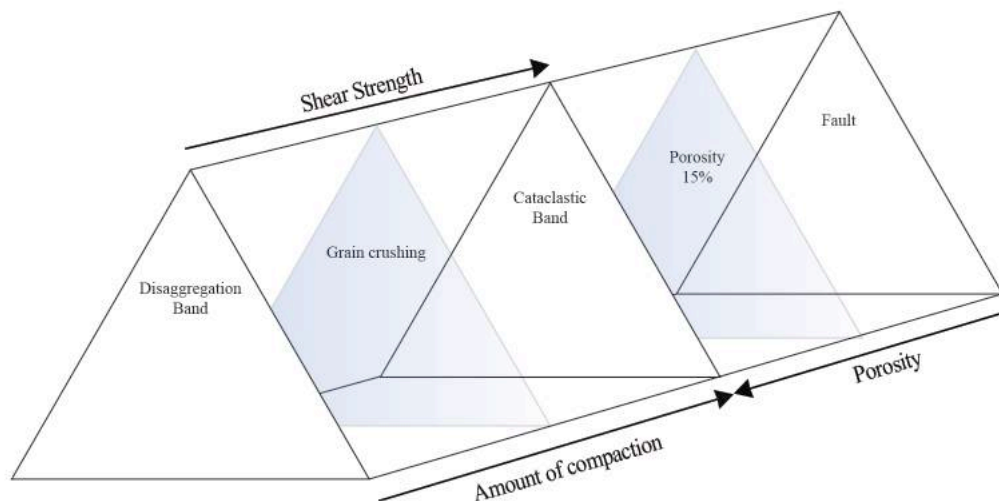


Figure 3.1: Comparing kinematic and mechanical Classification. Inspired by Schultz and Fossen (2008) figure comparing faults and kinematic classification of deformation bands. Amount of shear strength and compaction are the kinematic properties causing either disaggregation or cataclastic bands. With high compaction and/or shear strength, cataclastic band will form rather than disaggregation bands. If the porosity is approximately lower than 15 %, faults occur instead of cataclastic bands.

3.1.1 Kinematic classification

The kinematic classification divides bands into five different types; dilation bands, dilational shear bands, shear bands, compactional shear bands and compaction bands. In nature the compactional shear bands are the most frequently observed structures, where as dilation bands occur locally especially in the fault tip regions (Johansen and Fossen, 2008).

Volumetric deformation

Compaction bands

The obvious characteristic of compaction band is the lack of any shear offset (Aydin et al., 2006). Mollema and Antonellini (1996) divided the compaction band in “thick” and “crooked” compaction band based on their morphologic attribute. The “thick” compaction bands are described as straight 0,5-1,5 cm thick deformation zones with orientation parallel to crossbed laminae (Mollema and Antonellini, 1996). “Crooked” compaction bands are wavy with a length up to 2 m and a thickness between 0,1-0,5 cm (Mollema and Antonellini, 1996). Generally, compaction bands are thicker than an average shear band at the same locality (Aydin et al., 2006).

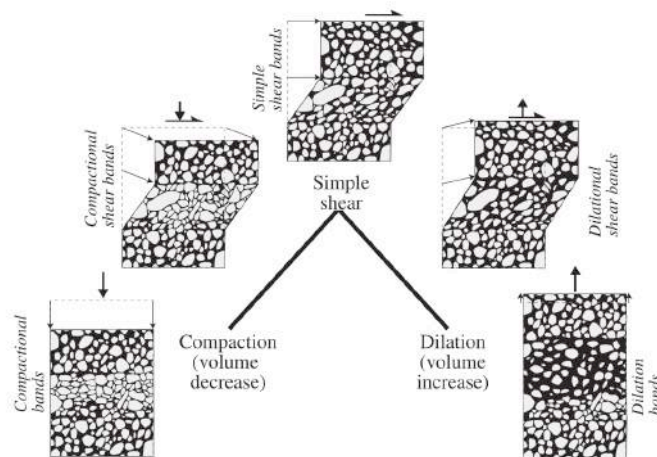


Figure 3.2: Overview of the kinematic classification of deformation bands. The figure is taken from Fossen et al. (2007), describing the kinematic classification of deformation bands. The figure shows the three main classification groups; dilation, compaction and simple shear. Moreover, the intermediate classification groups represent the dominant occurrence of the deformation bands in outcrop; compactional shear bands/shear enhanced compactional bands, dilation shear bands and shear enhanced dilation bands.

Pure compaction bands are rare geological structures, probably since compaction bands form during large loading stresses and require a high porosity (Eichhubl et al., 2010). Moreover, the differential stress in active tectonic settings promotes shear stress related failure rather than pure compaction (Eichhubl et al., 2010). Overall, the microstructures in compaction bands are associated with grain crushing and compaction, resulting in decreased porosity (Mollema and Antonellini, 1996). Eichhubl et al. (2010) claims that previous work on compaction bands actually addresses shear-enhanced compaction bands, which are common.

Dilation bands

Opposite to compaction bands, dilation bands show increase in porosity compared to the host rock, and true dilation without shear (Du Bernard et al., 2002). Dilation bands are also rare; however, a few observed dilation bands are described near the tip region of shear bands (Du Bernard et al., 2002; Johansen and Fossen, 2008). Poorly consolidated sand under near-surface conditions is the circumstances requested to form dilation bands (Du Bernard et al., 2002). According to Du Bernard et al. (2002), dilation bands can be recognized by the characteristic large pores, which have seemingly grown due to grain displacement over a zone of finite width. In thin section, pore space within a dilation band is filled by dark clay or/and organic matter (Aydin et al., 2006).

Shear deformation

Shear bands

Unlike volumetric deformation bands (compaction and dilation bands), most shear bands undergo a significant grain-size reduction (Eichhubl et al., 2010). Pure shear bands can be separated in an inner and outer core. The inner core has no “survivor grains” and a high degree of grain-size reduction and the outer has some “survival grains” additional to the high grain size reduction (Eichhubl et al., 2010). Compaction occurs due to significant pore collapse. On the contrary, near-surface shear bands formed by granular flow, so-called disaggregation deformation bands, show isochoric or mild compaction. Grain breakage does not exist, but transitions to grain abrasion and mild crushing can be seen (Fossen, 2010). Aydin et al. (2006) divided shear bands into; Isochoric shear bands, Compactive shear bands and Dilatant shear bands. Isochoric shear bands represent the “simple shear” deformation,

which have no volumetric change (Aydin et al., 2006). Eichhubl et al. (Eichhubl et al.) described a new transitional type of band: Shear-enhanced compaction bands. This is a transitional deformation band type a combination of shear-dominated and pure compaction bands (Ballas et al., 2012).

3.1.2 Classification based on deformation mechanisms

The deformational mechanism classification primarily divides bands into three different types (Fossen et al., 2007): disaggregation, phyllosilicate, and cataclastic bands (Figure 3.3 E). Herein the dissolution and cementation bands are regarded as cataclastic bands, since their mechanisms occur after or at the same time as the cataclastic deformation bands form (Fossen et al., 2007). In addition, the deformation mechanism classification divides into phyllosilicate disaggregation bands and regular disaggregation bands.

Disaggregation bands

This type of bands is difficult to recognize in outcrop, despite that disaggregation bands can form at a variety of depths in porous sands or sandstones (Fossen, 2010). Disaggregation or reorganization bands are dominated by granular flow (Fossen, 2010). The non-destructive granular flow mechanism reorganizes the sediments during grain rolling and grain sliding along grain boundaries. In homogeneous sediments, bands will hardly show up in outcrops and could be challenging to recognize in microtextural analysis. However, heterogeneous layering or lamination can demonstrate the appearance of disaggregation bands when the bands offset the layers. Disaggregation bands have typically an offset of a few centimeters, the lengths are up to tens of meters and their thickness depends on host rock grain size or mineral composition (Fossen, 2010; Torabi and Fossen, 2009). The thickness of disaggregation bands will increase with increased grain size and phyllosilicate content of the host rock (Fossen, 2010). The occurrence of disaggregation bands is commonly related to shallow burial, such as in a syndepositional setting (Fossen, 2010). The disaggregation bands are rare at depth exceeding 2-3 km (Fossen, 2010).

Phyllosilicate bands

The Phyllosilicate bands occur where the sand or sandstone contains more than 10-15% phyllosilicates (Fossen et al., 2007). With a sufficient amount of platy minerals, frictional sliding along grain contacts will occur rather than grain crushing (Fossen et al., 2007). This granular flow deformation mechanism relates phyllosilicate bands to disaggregation bands.

However, the physical properties between the disaggregation and phyllosilicate bands are different: Phyllosilicate minerals tend to create a local fabric along the band, formed due to shear-induced rotation (Fossen et al., 2007). These fabrics decrease the porosity and permeability in greater magnitude than regular disaggregation bands (Torabi and Fossen, 2009). The color and fabric are often visible in outcrop. In addition, platy minerals can slide more easily causing a larger offset (Fossen et al., 2007). Hence, these bands commonly show shear offsets of 1-5 cm (Fossen et al., 2007).

Cataclastic bands

Cataclastic bands differ from disaggregation bands by their grain crushing and predominant compaction mechanisms (Fossen et al., 2007). The cataclastic band can be divided in two zones, a core and the marginal rims. The core is identified by a wide range of grain size distribution, angular grains, low porosity and high matrix content (Fossen et al., 2007). The matrix consists of crushed sand grains, originally from grains inside and along the margin of the core. The matrix fills the pore space creating a low porosity and permeability.

Commonly, the porosity and permeability are recorded to be one and three orders of magnitude smaller, respectively, compared to the host sandstone (Fossen et al., 2007).

Several cataclastic bands forming a cluster represent a cumulative low-perm ability zone that may prevent fluid to flow through the sandstone, and will therefore affect the quality of reservoirs (Antonellini and Aydin, 1994). The marginal rims of bands represent mm-wide zones that are mainly characterized by compaction (Fossen et al., 2007).

The grain crushing leads to reduced grain size, compaction and higher amount of angular grains, which interfere with shearing displacement and contribute to strain hardening (Fossen et al., 2007). This is perhaps the cause of the less displacement described for cataclastic bands compared with disaggregation bands (Fossen et al., 2007). Along with the physical property differences of these two band types, they are formed under different conditions. Cataclastic bands form at greater depths, whereas disaggregation bands develop under a range of depths up to 2-3 km (Fossen, 2010).

Dissolution and cemented deformation bands

These types of deformation bands develop after or during deformation (Fossen et al., 2007). To form both cementation and dissolution within a deformation bands, the depth usually has to be greater for accelerate the chemical reactions (Fossen et al., 2007). The dissolution and cementation happens faster with fresh exposed quartz boundaries and available clay minerals, which is why chemical change preferentially occurs along new deformation bands after the deformation (Fossen et al., 2007). When highly reactive surfaces are exposed (Fossen et al., 2007), dissolution reaction is enhanced by clay minerals along grain boundaries (Fossen et al., 2007).

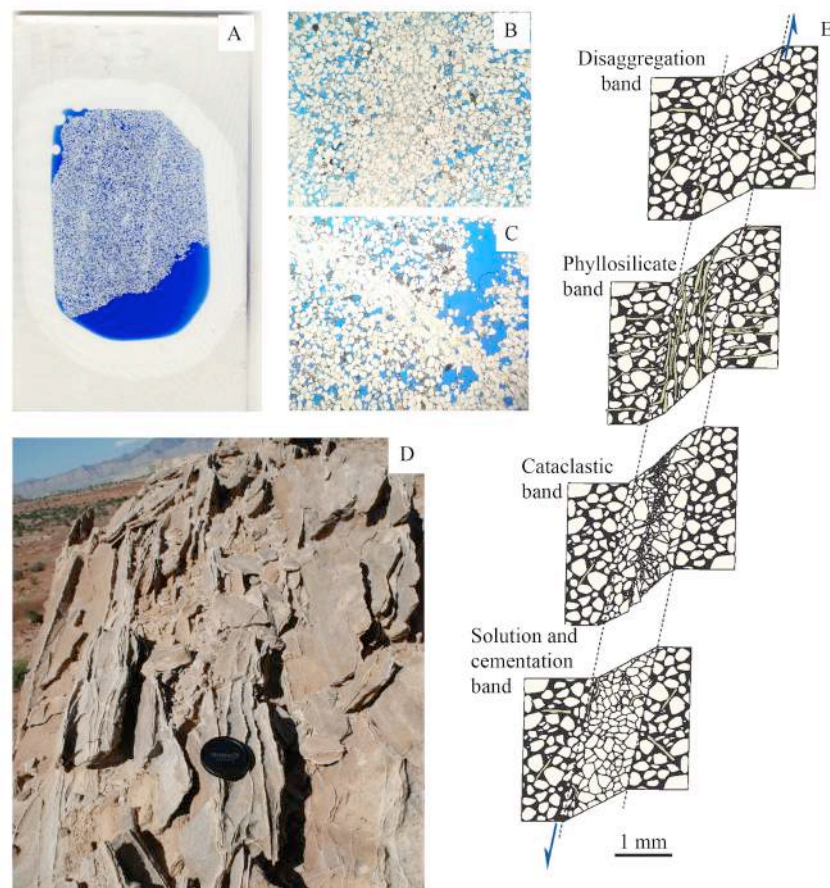


Figure 3.3: Illustration and description of deformation bands. A) Thin section with two parallel deformation bands. B) Compaction band in thin section. There is higher porosity seen as blue epoxy representing the porosity both to the left and right of the deformation band in the middle of the picture. C) Cataclastic deformation band. The porosity difference is easy to recognize, displaying a diagonal deformation band from lower left corner to upper right corner. D) Cataclastic deformation bands in clusters situated in outcrop. The deformation bands are highly weathering-resistant, and stand out of the host rock. E) Illustration E is taken from (Fossen et al., 2007), displaying different mechanisms and types of deformation bands.

3.2 The load-carrying and fluid pressure influence on deformation bands.

The main aim of this thesis is to point out mechanisms, which can affect the reservoir quality for Carbon capture and storage (CCS), water, oil and gas by forming deformation bands. Fluid pressure, folding and bleaching are put forward as possible hypothesis for forming deformation bands in the field area.

3.2.1 Fluid pressure

Increasing fluid pressure or pore fluid pressure decreases the effective stress within the sandstone, which eventually can evolve into rock failure (Handin et al., 1963). The Mohr circle represents the effective stress, which is the total stress minus the pore pressure. For increasing pore pressure, the Mohr circle is shifted to the left along the normal stress axis toward lower effective stress (Twiss and Moores, 2007a)(Figure 3.4). Due to fluid pore pressure the differential stress may decrease in necessary amount to permit failure, deformation band or fracture, which otherwise would be stable or in ductile behaviour (Twiss and Moores, 2007a). In other words, the deformation bands may form formed due to the presence of an inducing pore fluid pressure (Figure 3.4).

The overall stress and the fluid pressure will increase with depth, whereas fluid pressure can be as high as the normal stress when a barrier restrict free communication of the fluid and the surface (Twiss and Moores, 2007a). The fluid pressure increases since the sand and sandstones get denser grain packing, causing pressure to increase in values approximately of the weight of the overlying column (Harms, 1965). Although, the change in packing have to occur more rapidly than the fluid can escape, to increase the fluid pressures (Harms, 1965).

3.2.2 Bleaching and load-carrying cement

The bleaching of the sandstone will affect the rock in several ways, whereas the dissolution of grain coating can change a cement-carrying rock into a grain-carrying rock. The Load-bearing stress on grain contacts will become much higher than the overall mean effective stress, because of the small contact area between the grains (Bjorlykke, 2010a). If cement or coating of the grain is present, a larger contact surface is established. Due to these stress surface differences, the cementation or coating can prevent deformation and fracturing from occurring (Figure 3.4).

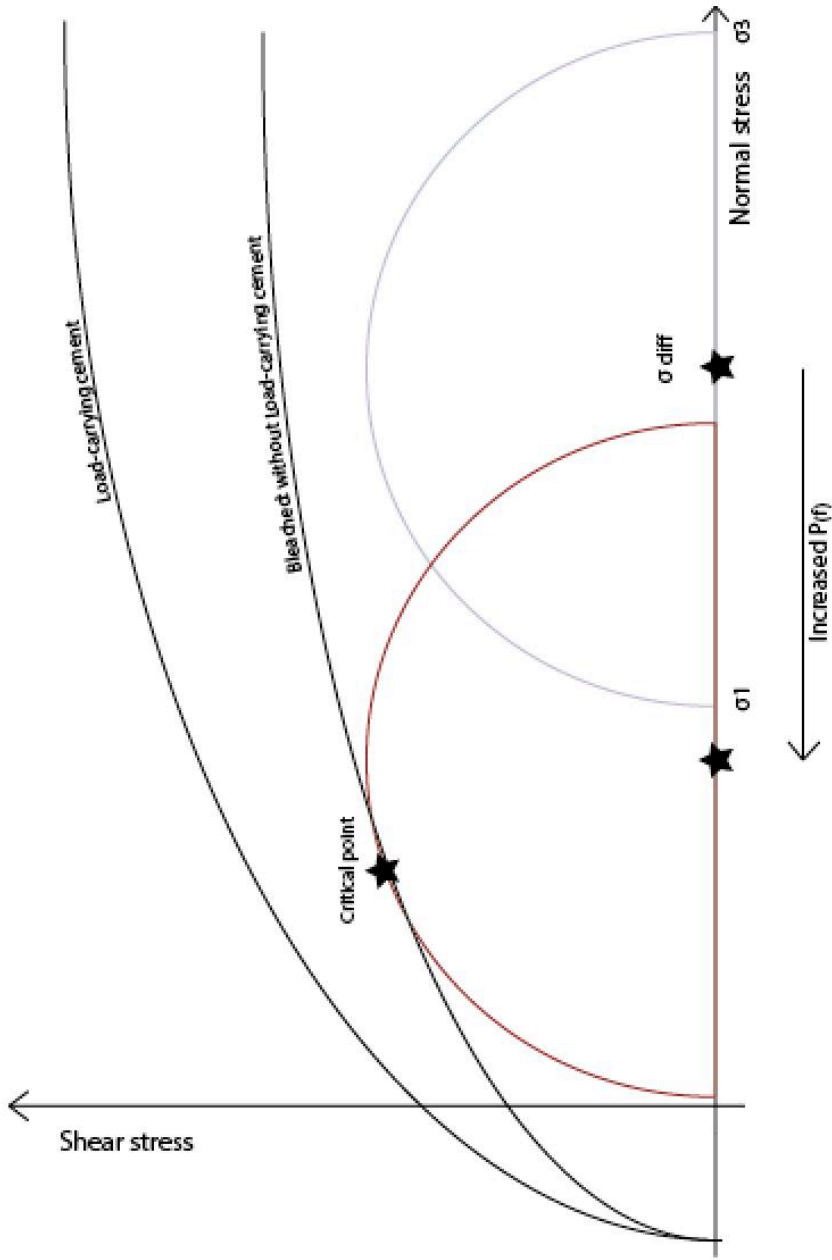


Figure 3.4: Mohr's circle showing influence of bleaching and pore fluid pressure. With increased pore fluid pressure, the effective stress decrease and may cause failure within the rock. Removal of coating around quartz grains entails higher stress at each grain, which reduces the strength of the rock and may cause fracturing and deformation band occurrence. The blue circle describe a normal stress state, the left red circle is showing an increased pore fluid pressure. The uppermost failure line represents a load-carrying cement rock, which prevent high grain boundary stress. The lower failure line represents a grain-carrying rock. The shear strength of the rock reduces when coating is absent or removed.

4 | Methods

4.1 Fieldwork

As mentioned, the study area is situated along the NNE San Rafael Swell in central Utah. The fieldwork was concentrated around the Fremont Bedding, gently folded into an anticlinal fold or dome. The bedding is of great interest due to the high content of deformation bands localized in this particular layer. There is an absence of deformation bands in over and underlying layers, which brings about the question of bleaching, folding and faulting as possible causes to the deformation bands formation. To obtain evidence of relevance to this question several methods have been used to collect datasets. The fieldwork performed has mainly focused on samples of the Fremont Bedding with deformation bands and observations around occurrences of deformation bands. The field equipment applied consisted of a Silva Expedition S compass, hammer and chisel, meter stick, log paper, field book, camera, Iphone with a GPS app and a TinyPerm 2 instrument.

4.1.1 Lithostratigraphic log

To achieve information about the field lithology and the relatively age of the bleached bedding, there were conducted a log through the area. A Lithostratigraphic log is an idealized summary of the preserved rocks and have especially advantage because of; the succinct method of summarizing, gives an immediately impression of the vertical succession, useful for identification of repetitions and major changes in the sedimentary facies (Coe et al., 2010). The log is mapped with a vertical 1:100 scale and the common used horizontal scale ranging from siliciclastic clay to granules. Moreover, a Lithostratigraphic log template was used for drawing. 3D examination of the sedimentary structures was impossible and therefore a 2D identification method is used to obtain an interpretation. The lower part of the log is accurate performed apposed to the uppermost parts, which were not available for close observation. In addition to detailed descriptions of colour, internal layer structures, grain size thickness and photographs from each layer were taken. The log was composed in collaboration with Eivind B. Larsen.

4.1.2 Deformation band collection

The main field method for reworking of deformation band distribution was linear traverses (scan lines) through parts of the Fremont Bedding (Figure 4.1). Each scan line was bedding-parallel and 10 m long. The individual scan lines were distributed through the field area to

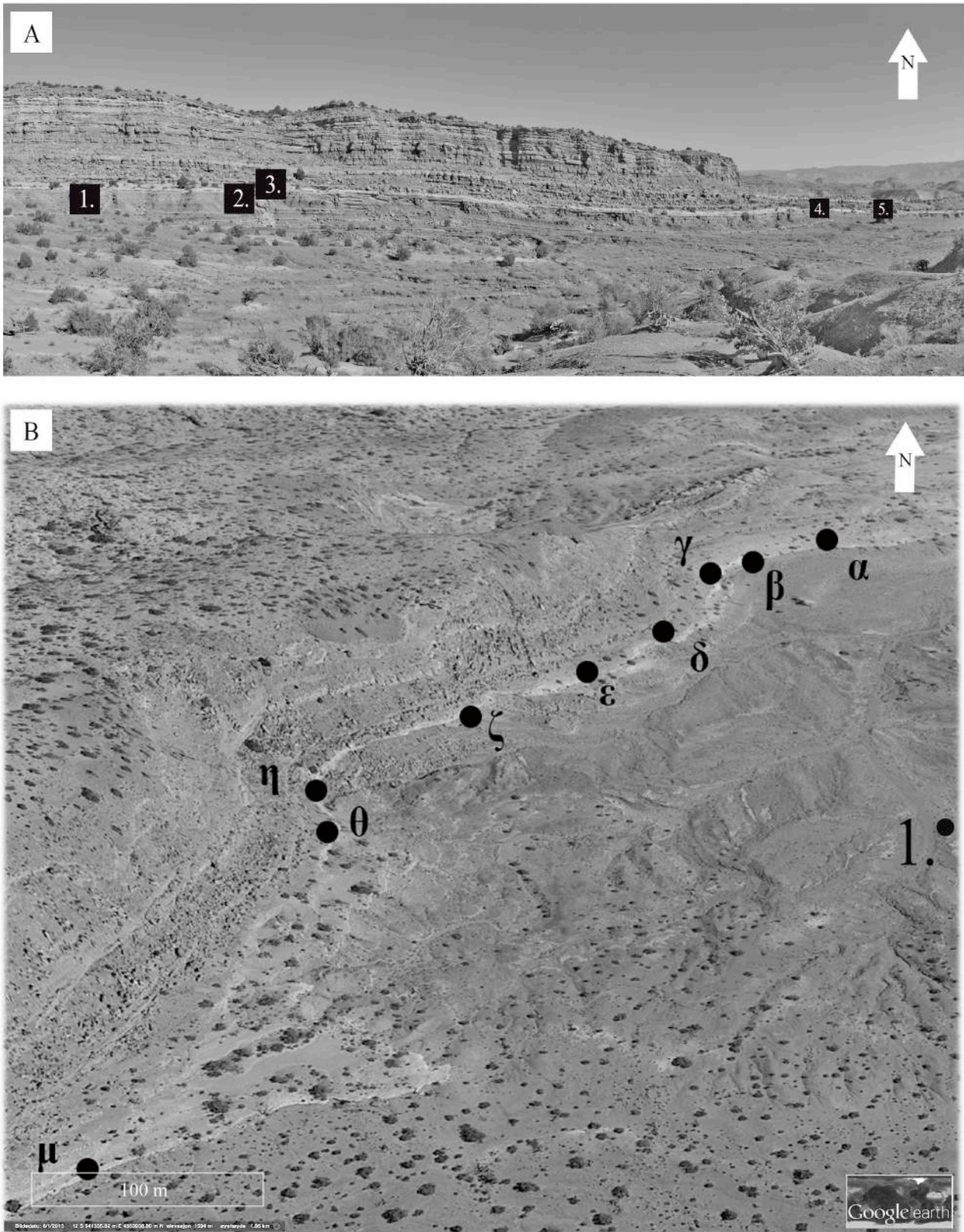


Figure 4.1: Samples and scan line locations in the field area. A) Photograph showing areas where 11 samples have been taken. B) Google Earth overview of the study area with a bird perspective 1,86 km above the ground surface. Greek letters α - μ in photo B represent the startpoint of each scan line, each of which continues 10 m in the direction of the next letter.

Deformation band orientation, morphology and crosscutting relationships were recorded for each deformation band of the Fremont Bedding. Along the Fremont Bedding, nine individual scan lines were collected. In each of these scan lines, every individual deformation band were measured with right hand strike and dip measurement technique. The data collected is divided in m-wide groups illustrating the distribution within the scan line and the total distribution along the Fremont Bedding cliff. For further reading on other usages of scan line, see Bonnet et al. (2001).

4.1.3 Measuring the reservoir permeability

The permeability was measured in-situ with a portable air permeameter, the TinyPerm 2 minipermeameter of New England Research. These probe permeameters benefits from providing a non-destructive permeability, which according to Filomena et al. (2014) give the best 3-D permeability, estimates of anisotropy effects, and heterogeneity.

The probe permeameter's nuzzle has to be pressed against the rock, and when fully sealing it will be able to measure permeability, related to the time the instrument used to recover the vacuum created by pressing the piston. A microcontroller measure the air volume withdrawn from the rock in addition to the transient vacuum (Filomena et al., 2014). The TinyPerm 2 value (T), is a result of calculations connected to the air permeability (K) through Equation 1 (Filomena et al., 2014):

[Equation 1]

$$T = -0,8206 \log_{10}(K) + 12,8737$$

K is given in millidarcy (mD).

The range of the value T correlates with measuring time and the time varies with rock permeability. The time of measuring is therefor calculated by the permeameter to achieve high accuracy.

The TinyPerm 2 is designed for fieldwork, where the user has to handhold the probe. The lower measuring threshold is approximately 10 mD according the manufactures. This limit gives permeability equivalent to a 5 min measuring time (Filomena et al., 2014). However, in the study of Magnabosco et al. (2014) a threshold of > 1 mD can give meaningful values if corrected for a systematic bias.

To obtain permeability measurements of high quality, three measurements were conducted on each bedding-spot. The mean value from these three T- measurements was used to calculate permeability for the given bed. When or if a clear bias where observed in two new measurements were added.

4.2 Laboratory work

4.2.1 Sample preparation and microtextural analysis

From the 12 samples selected in the field area, seven were prepared into thin sections. The preparation was carried out by Salahalladin Akhavan of the Department of Geosciences at the University of Oslo. Pore space of the samples were saturated with blue epoxy, then dried and glued onto a 4,5 cm X 2,5 cm glass slide, before being polished down to a thickness of 30 μm . A Nikon Optiphot-pol petrographic microscope was used to preform an optical study of sandstone texture, structure and mineralogy.

Table 4.1: Relation between samples, field area and thin sections. The number given in "situated in field area" is connected to Figure 4.1, showing the area in photo A. Samples/ thin sections labelled AB was collected by A. Braathen in 2013. Positions are given in WGS84 coordinates. Due to low accuracy on the coordinates, they are not placed in Figure 4.1.

Thin section and samples			
Thin section nr.	Sample	Situated in field area	Analyzed in SEM
1)	IH-03	2.	X
2)	IH-04	3.	X
3)	IH-05	3.	X
4)	IH-06	2.	X
5)	IH-07	4.	
6)	IH-11	5.	X
7)	IH-12	5.	
8)	AB13_2	N39°19,44 E110°31,27	X
9)	AB13_1	N39°19,44 E110°31,27	X
10)	AB13_4B	N39°20,10 E110°31,07	X
11)	AB13_5	N39°20,10 E110°31,07	X

The main aim of the microtextural analysis was to describe the differences between the deformation bands and the host rock. Both plane polarized light (ppl) and cross-polarized light (xpl) added value to the study. The ppl was used to determine relief, color, pleochroism, size, roundness, cleavage, crystal shape and fractures. Xpl were mainly used for identification of twinning and for revealing difficult minerals, using determination methods such as birefringence, extinction and optical sign. The mineral observations were later verified by a SEM study.

4.2.2 SEM: Scanning electron microscopy

The scanning electron microscope was SEM used to confirm chemical composition, crystallization features and derived mineralogy linked to observations in the microscope. The SEM instruments used in the analysis are a JEOL JSM 6460LV scanning electron microscope with a LINK INCA Energy 300 (EDS) from Oxford Instruments. Of the total 11 thin sections (Table 5.1), five were analysed in SEM.

To perform analyses on the SEM, the thin section have to be coated with a conductive material, if the minerals are not already conductive. At the Department of Geosciences, either Carbon Coater Cressington 208C or Gold Coater Quorum Q150R S is used. SEM analysis was preformed with guidance from Berit Løken Berg. The performed analysis was mainly conducted with backscatter electron (BSE) images to obtain mineralogy. Images from four different thin sections were subsequently used in further investigations with the photograph editing software ImageJ.

SEM is mainly used to achieve information on morphology and on micrometre scale textures, crystal intergrowth, chemical analysis and reaction relationships (Klein and Dutrow, 2007). Surface morphological features are obtained using secondary electron imaging, whereas Backscattered-electron images are manly used to observe compositional variations (Reed, 2005). The JEOL JSM-6460 LV has several detectors; one for secondary-electron images, backscattered electron image, cathodoluminescence (Schultz and Balasko, 2003) and another that offers a X-ray spectrometer for element mapping (Reed, 2005). In depth information of the methods are given in *Electron Microprobe Analysis and Scanning Electron Microscopy in geology* written by Reed (2005).

Several limitations such as resolution, depth of focus, etc. are disadvantages related to analysis in a SEM. Apart from the disadvantages, which may occur, the image can be

defective in many other ways. Some examples can be statistical noise, when the image is recorded with too fast scan rate (Reed, 2005), coating artefacts because of coating that is not entirely structure free (Reed, 2005), and specimen charging when something non-conductive such as fingerprints and dirt pollute the conductive coating (Reed, 2005).

4.2.3 ImageJ

ImageJ is a scientific image processing program, which is able to measure distances, angles and perform calculations of area and pixel value statistics in addition to create density histograms and line profile plots (Ferreira and Rasband, 2011). The ImageJ was in this thesis used to calculate grain size of host rocks and deformation bands.

The ImageJ analysis requires a good image of the thin section, such as a backscatter image from the SEM study. The format used is TIFF with a high resolution of 640X480 ppi up to 2560X1920 ppi. The unfortunate problem is that ImageJ struggle to identify individual grains when the sandstone is closely packed. To rectify this, one can draw individual borders of each grain, which is a very time consuming process. The advantage is that ImageJ can calculate the grain size with good precision when the digitizing of the grain borders is completed. The grain size distribution or variation is calculated manually. The calculations were preformed in area-measurement reduced to the radius value and grouped into bins of 0-10, 11-20 etc. continuing up to 100 micrometre.

5 | Datasets and analysis

This section gives a presentation of the geology and observed structures of the studied layer/reservoir of the Humbug Flat area, including a detailed description of the deformation bands and their microstructural characteristics. In the field area is displayed, showing locations of several important features regarding the observation and analysis.

5.1 Outcrops of study area

The succession encountered in the study area is part of the Earthy Member of Entrada Sandstone Fm, deposited in a coastal plain mud-flat environment. The lithostratigraphic log composed from the field study shows predominately fine-grained sandstones with thin inter-layers varying from siltstone to coarse sandstone. The fine-grained sandstone beds contain different sedimentary structures, whereas cross-stratification, ripple laminations, biological trace as burrows and roots, massive and layered structures are recorded. At the top of the cliff the Entrada Fm sandstone is separated from the Curtis Formation by the J-3 unconformity, which is marked by a widespread chert pebble conglomerate layer (Piperinos and O'Sullivan, 1978). This J-3 unconformity is the last noted layer observed in the lithostratigraphic log. However, bleaching in the Curtis Fm is seen to be conformable to the contact.

In addition, pipe-structures and an overall dome geometry are recorded. In this section, stratigraphy, structures and deformation bands will be described in detail.

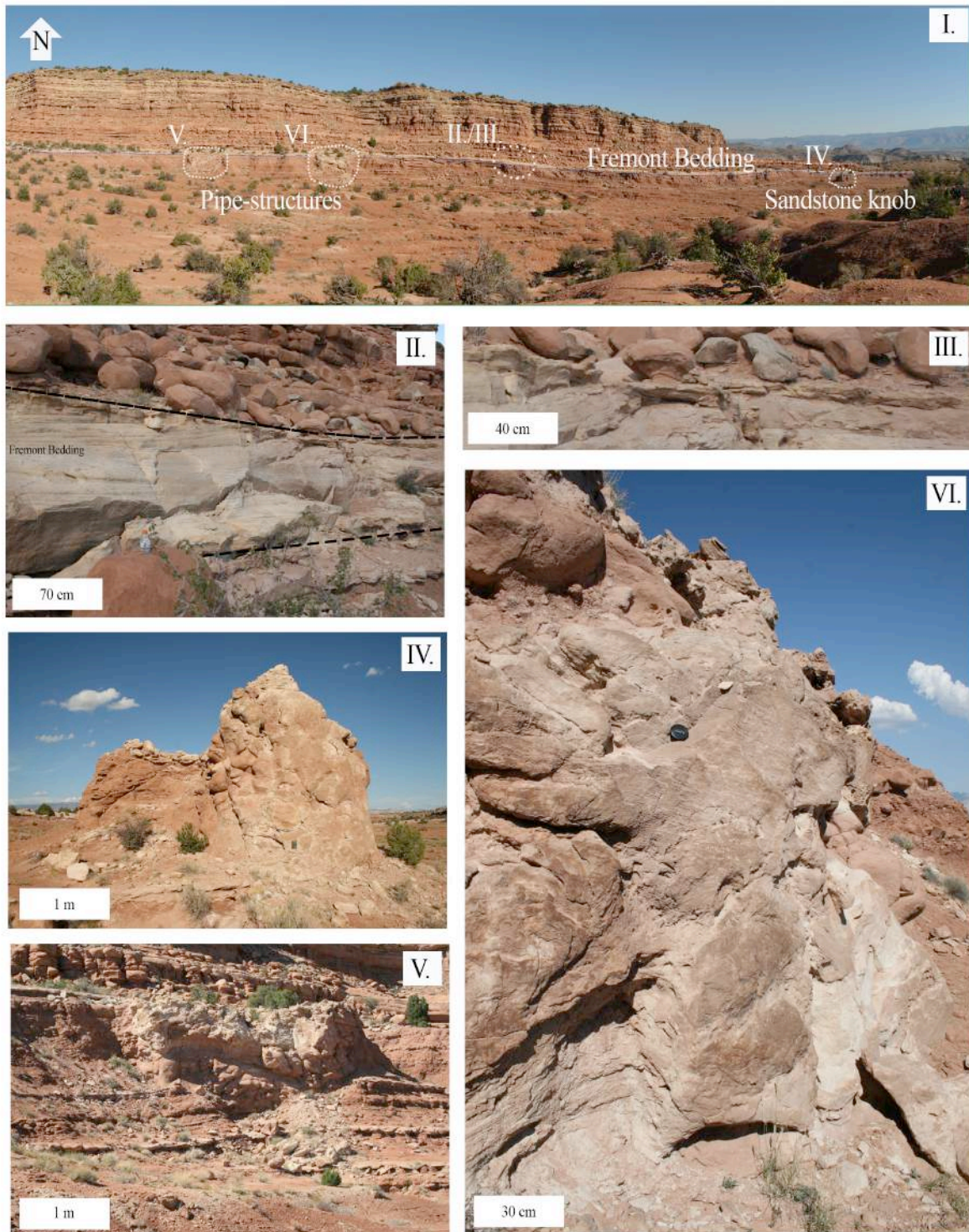


Figure 5.1: **I.)** photograph displaying different locations related to features described in this chapter. The blue dotted lines display displays the Fremont Bedding path. **II.)** Image displaying the bleached Fremont Bedding. In this picture, cross-stratification is barely visible and deformation bands are absent. In general, the deformation bands are present in the Fremont Bedding, with only local exceptions. **III.)** Thin bed on top of Fremont bedding. This layer is yellow and contains slightly lighter areas, which show evidence of roots. **IV.)** Sandstone knob, with visible breccia on the east/right side. **V.)** Photograph illustrating a collapse with bleached sandstone, distorted and rotated large clasts. **VI.)** Image showing a close-up of the collapse structure A (see figure 5.1 I.). Clasts and a bleached matrix are present, indicating a collapse.

5.1.1 Lithostratigraphic log

The log displays the studied succession from a few layers below the Fremont Bedding (pale-coloured bedding) and up to the J-3 unconformity Figure 5.2. The facies-description shown in Table 5.1 is divided in four dominating facies.

The predominantly succession is the massive red sandstone A representing a facies outlined in Table 5.1, which occur as thicker beds in the lower part of the Humbug area cliff. Beneath the Fremont Bedding is a thin layer with coarse calcite-cemented sandstone. The Fremont Bedding (B) contains low-angled tabular cross-stratification, deformation bands in addition to distinctive lighter colour than other beddings in the field area. On top of the Fremont Bedding is a yellow layer with signs of rootlets and an uneven pillow-like exposure surface, accordingly formed as a vegetation-rich surface.

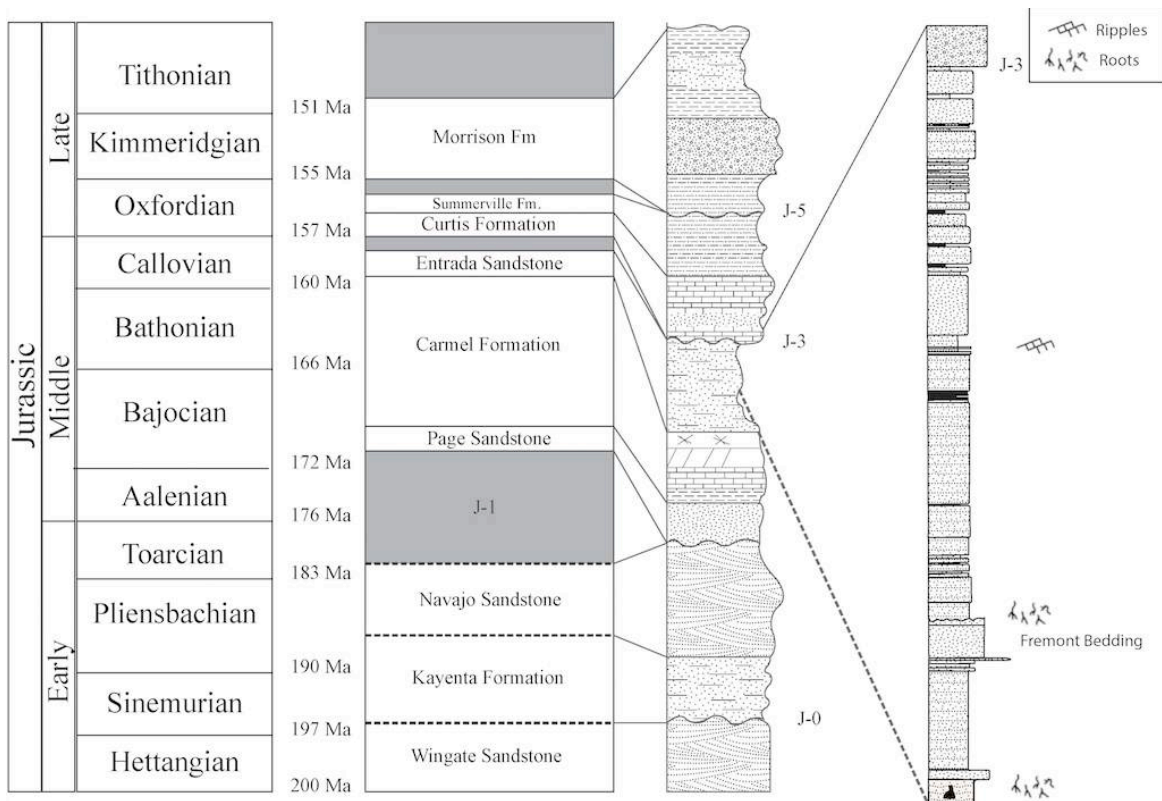






Figure 5.2: Overview of San Rafael Swell's Jurassic successions. The right log shows the field area cliff, with Fremont Bedding situated in the lower part. The second log from the right illustrates the Jurassic succession in relative thickness. The field log covers the upper part of Entrada and the lower Curtis conglomerate. Third column from the right illustrates succession related to age, listed in the left column. The two middle logs are taken from "Geologic History of Utah", written by Lehi F. Hintze and Bart J. Kowallis, page 59 and 209. Right log made by Eivind B. Larsen and Ida Hope

Table 5.1: Facies description for Humbug Flat. The predominantly beddings are divided in four main facies, A-D. The fourth column from left describes assumed depositional conditions. The third column from left is photographs taken from the lithostratigraphic log. The sedimentary and depositional environment is the main description of the dominantly facies. The first column is the name of the facies, given for simplifies of the description of the log. The facies description are based on “principles of Sedimentology and Stratigraphy”; Boggs (2011b).

<p>A</p>	<p>Massive red sandstone (f-m sand): Massive red sandstone with fine to medium grain size. The bed-type thickness is between one to six meters thick, and are the most abundant bedding in this area. No internal structures are observed. Nevertheless, wind erosion seems to have affected the surface.</p>		<p>Proposed to form by rapid deposition, to obtain a homogeneous mass. Use of x-ray techniques, could reveal internal structure. Proposed to form in an eolian environment.</p>
<p>B</p>	<p>Pale-coloured sandstone with cross stratification (m-c sand): Fremont bedding; the main studied layer. Tabular cross-stratification is the predominant structure in addition to the pale colour. However, at the base small trough cross-stratifications are observed. Indications of low angle cross-stratification at the top, possible with bi-directional vergence. Nevertheless, the main flow direction is measured and have a 193° strike. In upper part of the bedding signs of root growth is found.</p>		<p>Formed mainly by large-scale, straight-crested ripples or dunes, this is associated with the lower flow regime. Suggested depositional environment: fluvial origin.</p>
<p>C</p>	<p>Thin layers of consolidated pale sandstone (s -sand): Occur as thin layers with a thickness between 5-10 cm. Mainly horizontal layered with a few exceptions, small ripples further up in the succession. Moreover, the thin consolidated pale sandstone occurs with interlayers of red sandstone/mudstone (layer D).</p>		<p>The alternating silt and vf-f sandstone/mudstone indicate flood plains.</p>
<p>D</p>	<p>Semi-consolidated heterolithic red sandstone (f -m sand/mudstone) The semi-consolidated red sandstone/mudstone seems to be present in-between Layer C (thin layers of consolidated pale sandstone). The thickness varies in-between 10-60 cm. The grain sizes within the layers seem to be coarser in the uppermost section of the succession.</p>		<p>The alternating silt and vf-f sandstone/mudstone indicate a flood plain in some sort.</p>

Bedding situated over the yellow layer change from massive red sandstone (A, Table 5.1) to layered red sandstone, split by few thin layers of red and white very fine sandstone (Changing in-between C and D, Table 5.1). Over the Fremont Bedding, the massive red sandstone (A, Table 5.1) is changing from approximately 4-6 m to thinner beds around 1 m in thickness. Moreover, the beds are less massive further up the succession, whereas facies C and D gets more frequent (Table 5.1). In addition, two thin coal laminas are observed in the uppermost part of the succession, right underneath massive red sandstones (A, Table 5.1). Facies C seems to have the same pale colour as the bleached bedding (Fremont Bedding). However, in relative thin layers compared to the Fremont Bedding.

The lithology changes from medium to coarse sandstone in the thicker layers into silt and very fine sand-grain size in the thinner parts. Especially at the top of the succession the massive layers seem to get larger grain sizes. A conglomerate bed is known as the marker for the J-3 unconformity and the change from the Entrada Sandstone Fm to the Curtis Fm (Piperinos and O'Sullivan, 1978), which can be observed at the top of the Humbug cliff. Due to the steep cliff limiting access in the area, the draping conglomerate was observed from distance.

5.1.2 Structural placement

Along the Fremont Bedding, strike and dip was measured on numerous sites to find the structural architecture of the study area and particularly this bed. The documented structure is an anticlinal dome, however the dome hosts complications. In Figure 5.3 a stereonet and a map with strike and dip are displayed, showing an anticlinal fold along the cliff. In addition to the anticlinal fold with a fold-hinge trending approximately northwest, several minor anticlinal folds and a synclinal are present. The bedding dip range from 2° to 26° out from the dome with a mean dip value of 14° . The white or lighter layer in Figure 5.3 represent the Fremont Bedding and can be followed around the entire study area (see Figure 5.3 for more information).

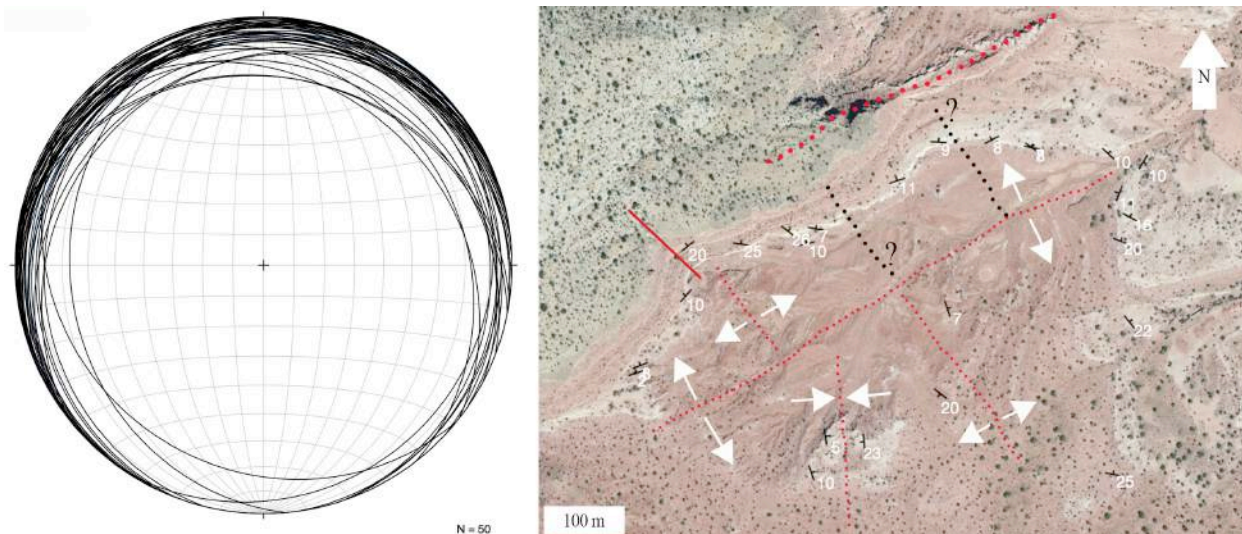


Figure 5.3: Stereonet and mapped strike and dip are displayed. The stereonet shows a small dip for all measured places. The predominantly orientation are southwest, due to more measurements along the Humbug Cliff. The map to the right shows the variation in strike, demonstrating a complex folding event or events. The red dotted lines are representing an approximately measured fold-hinge, whereas the white arrows describe either a synclinal or an anticlinal. Anticlinal: arrows away from the red dotted line. Synclinal: arrows towards the red dotted line. The larger red-dotted line represent the large fault array related to Moab Fault. Mark that both the fold-hinge and the fault array have same orientation, northwest. The red stretched line displays the other fault found in this study area, situated close to the fold-hinge oriented northwest. The black dotted line point out the structures visible from above, which have not been observed during the field study. The black lines show a curve in the pale-coloured bed, indicating a fold in the area. Steronet3D software for mac was used for both the stereonet and the map.

5.1.3 Local non-strata form structures

Several non-strata form structures were observed in the section below the Fremont Bedding (Figure 5.1). In Figure 5.1 three pipe-like features are marked (Figure 5.1 V., VI. and IV.). They reveal a pale-coloured sandstone with blocks of sandstone, making up a breccia. The crosscutting nature with respect to bedding and their circular geometry in horizontal, suggest they are sand dykes. Two of the pipe-like features (V. and VI.) are close both in geographical location and lithologically. The isolated sandstone knob (IV.) has similar texture as the pipe-like features. However, geographically the sandstone knob is alone-standing pipe-form.

Location V. and VI. (Figure 5.1)

These two features represent pale-coloured pipes. The material has a landslide looking texture, with a matrix of nearly unconsolidated, distorted sandstone without layering. Two minor faults are observed, presumably associated with the pipe-form and the pale-colour in location V. (Figure 5.1 and Figure 5.4). The dominating rock is the pale-coloured sandstone matrix surrounding a few larger pale-red sandstone clasts, with a deflected texture illustrating flow pattern around. Associated with the pipe, clustered deformation bands occur in areas above both locations V. and VI. The source is considered as unknown, regardless of the present deformation bands in some of the clasts. Location V. and VI., are similar structures. However, location V. has more clasts than location VI. The clasts/blocks located within the pipe-structures have clusters of cataclastic deformation bands. They have no obvious origin.

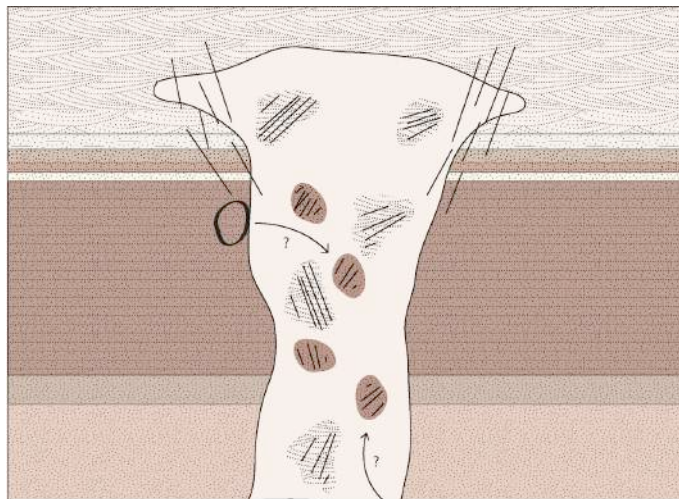


Figure 5.4: Illustration of pipe-structure V. (Figure 5.1). The pipe contains blocks with deformation bands. The block source is unknown. The uppermost layer in this illustration is Fremont Bedding. The black lines within the deformation bands represent deformation bands. The larger black lines crosscutting the succession represent small normal faults.

Sandstone knob

The third location is a pale-coloured sandstone knob situated about 20 m south of the exposure of the Fremont Bedding. The right part on Figure 5.5 is bleached inequality to the surrounding red sandstone. The pale-cloured area contains different sizes of clasts; rotated, angular and with deformation bands. The matrix is a pale-coloured sandstone with a flow pattern changing from homogeneous bleached to heterogeneous red and bleached sandstone. Based on occurrence of the clastic angular large clasts and matrix, this area is classified as a breccia, although there are no faults along the sandstone knob. There are clusters of parallel deformation bands in almost all of the clasts, each in different directions. The breccia clasts have an unknown source, probably originating from the bedding below or above. In Figure 5.5, the black lines show bended layers, probably formed when the sandstone knob formed.



Figure 5.5: Overview of the sandstone knob. 1) This picture shows a close-up of the leftmost knoll displayed in picture 4. Showing a lower part of the knot, with fluid flow pattern. The sandstone matrix has a red colour, with deformed clasts. The matrix has signs of visible fluid flow pattern in outcrop, and seems to have been flowing around the present clasts. 2) Image displaying a large clast with several deformation bands. The clast is light red consolidated sandstone. Close-up of the largest clasts shown in picture 3. 3) An overview of clasts with surrounding bleached sandstone. The clasts are angular and fit the classification of breccia. The only explanation of the breccia formation has to be a collapse, either related to gravity or pressure. 4) Image displaying the local knot, with the Fremont Bedding and Humbug flat cliff at the left side. The bleached matrix is situated at the right side with huge clasts. Half way out on the left side the matrix is red sandstone with bleached, small clasts. Leftmost, the sandstone is homogenous red sandstone. At the top, the whole knot is bleached, with occasional deformation bands. The black lines represent continuous layers with consolidated light red sandstone

Geometrically, the sandstone knob emerges as semi-circular. The uppermost black line is bended upwards, dividing the sandstone knob from the red succession. Moreover, the pale-coloured part seems to have a pipe-like circular structure, if the red sandstone is excluded from the interpretation.

5.1.4 Deformation band characteristics

Within the field area, the deformation bands are uniquely located in the Fremont Bedding. The deformation bands occur individually, in clusters or as stepped ladder structures, in which the thickness and length appear to be consistent. The thickness of individual deformation bands is about 1-2 mm, and the length are restricted by the thickness of the bedding itself. The deformation bands are easy to recognize because of the white colour and the fact that they are standing out of the rock, a result of weathering and/or erosion impacting the undeformed sandstone. In different locations along the Fremont Bedding individual deformation bands and band populations make occur in two sets with roughly 80-100° bisector angle. No consistent crosscutting relationship and common master structures suggest they formed in conjugated sets.

The deformation band populations are divided into four sets, each with there own orientation and formation mechanism (see Table 5.2 for an overview of the deformation bands sets). Originally, the deformation bands were divided into three groups. However, the decision to divide population 1 and 2 into different population, is made because of similarities with the fault orientation.

- Population 1: Deformation bands formed in conjugated sets (1 and 2), with orientation 280/(60-70)° and 100/(60-70)°, dominated of cataclastic deformation bands. The deformational kinematics is both shear and compaction.
- Population 2: Deformation bands formed in conjugated sets (3 and 4), with orientation 260/(50-70) ° and 080/(40-70)°, dominated of cataclastic deformation bands. The deformational kinematics is compaction and shear
- Population 3: Deformation bands formed as a conjugated sets (5 and 6) and as single sets with orientation 180/(40-60)° and 360/(40-60)°. They occur in clusters mostly as cemented cataclastic deformation bands with high shear strength. These clusters are rare in an overall perspective, and occur mostly next to other clusters of deformation

bands. Compared with population 1 and 2, deformation band population 3 are thinner and less weather resistant.

- Population 4: Deformation bands formed in ladder structures and other random orientations, which do not fit into other populations. The deformation bands formed in the ladder structures are predominantly disaggregation bands, with mainly shear with some compaction.

Deformation band truncations

Individual deformation bands in conjugated sets are typical for the Fremont Bedding. Anyhow, there are a few observations with clear truncations. Figure 5.6 shows the largest offset observed, where set 4 (185°) crosscuts set 4 (092°). The W-E (population 1 and 2) sets and especially population 1 is the most dominant of the conjugated sets. In optic analysis performed on this truncation, a slight difference between the two deformation bands is shown. The offsetting deformation bands observed in optic microscope have less cementation and high amount of crushed quartz than the crosscutting deformation band. Deflected deformation bands or tabular truncations (Figure 5.6B), shows similar directions at the offset A Figure 5.6, anyhow without differences in deformation band characteristics (cataclastic cemented). The difference between the tabular offset and the truncation is the amount of catalasis and shear in set 5.

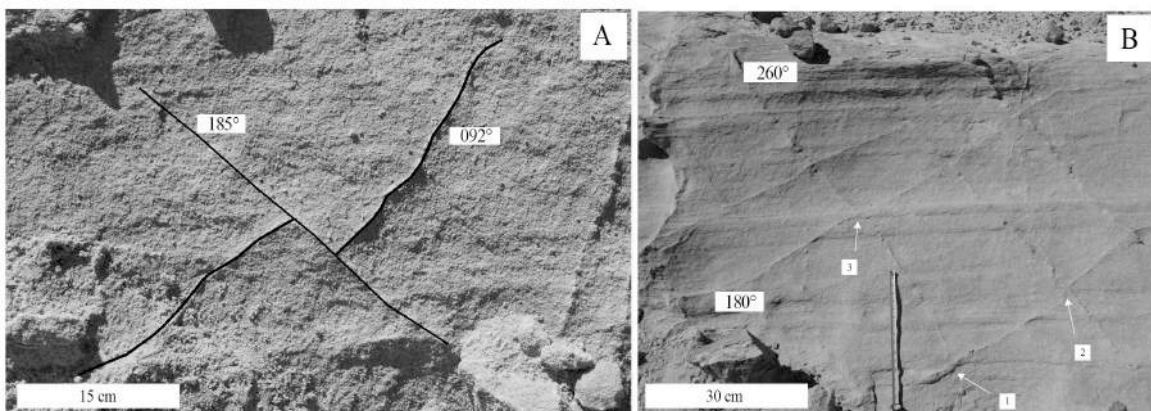






Figure 5.6: Deformation band truncation in Fremont Bedding. A) The image shows offset of a deformation band 092° (set 4), by younger deformation band 185° (set 5). There are two examples of this kind of offset, however there are several occurrences of deflections in same direction. B) The image display several deflections caused by another deformation band. Deflection 1 and 3 shows similar orientation as offset A, anyhow the deflection 2 are opposite and the 180° (set 5) are affected.

Table 5.2: Overview of deformation band populations with characteristics. The four population suggested are divided into sets and populations primary based on orientation and outcrop studies. Kinematics and deformation mechanism are similar in population 1, 2 and 3. The last population 4 have a small amount of porosity reduction between host rock and deformation bands, indicating shear-bands with some compaction.

Illustration	Population	Set	Kinematics	Mechanism	Orientation	Area (Figure)	Occurrence	Thin sections
	Through-going Population 1	Conjugated Set 1 and 2	Shear enhanced compaction bands	Cataclasis	1-280/(60-70)° 2-100/(60-70)° WVN/EES	All scan-lines	Individual	IH_06
	Folding Population 2	Conjugated Set 3 and 4	Shear enhanced compaction bands	Cataclasis	3-260/(50-70)° 4-080/(40-70)° WWS/EEEN	β, γ, δ and θ	Individual	IH_06
	Clustered Population 3 (and 3.1)	Partly conjugated Set 4 and 5 (Set 6 and 7)	Shear enhanced compaction bands	Cataclasis	5-180/(40-60)° 6-360/(40-60)° S/N 7-(200/(40-50)°) 8-(020/(40-50)°)	1: γ and θ 2: ε and θ 3: δ and ζ 4: ζ	Clusters	IH_04 IH_11
	Ladder structure and random Population 4		Shear bands	Disaggregation	Random	ζ	Ladder structures	IH_03

Ladder structures of deformation bands

Structures first named by Davis (1999) as either “ladder structures” or “radiator rock” is observed in a few locations in the field area. The ladder structure occurs with short parallel diagonal deformation bands (rungs) bounded by thicker and longer zones of bands (flanks), consisting in a network. The rungs form preferentially at the west/left side of the ladder structure, opposite to a few diagonal short steps starting at the east/right side (Figure 5.7). The tips of the bounding bands are propagating further over at the facing side, either overlapping by other bounding bands or cut by a larger vertical deformation band. The location of the few ladder structure observed in the area are next to either a fault or the pipe structure. However, the pipes and faults are closely spaced making it difficult to relate the ladder structure to an individual fault or pipe collapse event.

The z-shaped formation can be related to R- and R'-shear, due to ladders formed with given space and later interpreted as Riedel shear zones in regular mode two (Schultz and Balasko, 2003). The narrow angled darker deformation bands form as R-shear with about 20° to main displacement direction, without crossing the ladder structure entirely (Figure 5.7). The R'-shear is formed with an angle approximately $75-85^\circ$ to the prime deformation band direction and opposite shear sense to the main fault (Twiss and Moores, 2007b). The R and R'-shear set can be considered as a conjugated set with approximately 30° to the short axis of the strain ellipse associated with simple shear. Larger structures, as flower structures, may have a connection to the Riedel shears in a large-scale/small-scale relation. In theory, related T- and P-share may form in these kinds of situations. Nevertheless this ladder structure have a known overall displacement and bounding compaction bands (Schultz and Balasko, 2003). The ladder structures show a slightly normal-shear offset (Figure 5.7). The ladder flanks is thicker than the diagonal bounding steps in addition to being more weathering-resistant.



Figure 5.7: A ladder structure illustration. The illustration is drawn on the basis of a photo from Fremont bedding. The vertical, darker markings are representing thicker deformation bands. The lighter, diagonally running deformation bands are less weathering resistant. The red lines illustrate layers in the sandstone, showing direction of movement. In thin sections the diagonal deformation bands are absent of grain crushing and cementation, and therefore classified as disaggregation bands. The stress is displayed in a focal diagram in the upper right corner. The ladder structure has a normal displacement. The focal diagram shows stress areas, which may contribute to understanding the occurrence of diagonal deformation bands.

Deformation band clusters

Deformation band population 3 occur in clusters and in individual bands. In this thesis a cluster is defined as 18 individual deformation bands in one set over a small tabular zone around 5-10 cm wide (Figure 5.8). Compared with individual bands the clustered areas seem to be more weather resistant, since the deformation bands stands out of the host rock. Moreover, the clusters are restricted to areas around and over the pipe-structures.

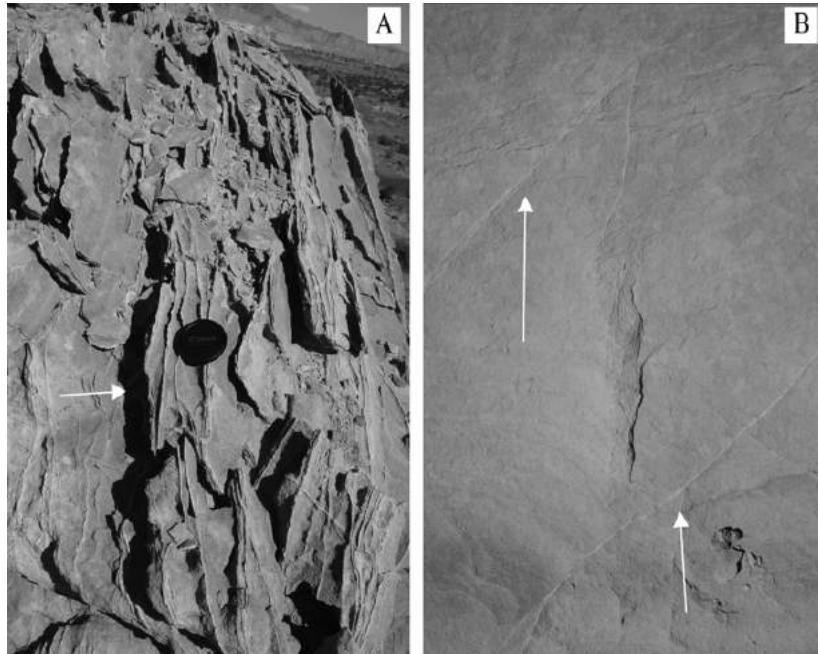


Figure 5.8: Overview of deformation band occurrences. A) Deformation bands in clusters with one orientation (population 3). B) Photograph of single isolated deformation bands with similar orientation (population 4).

5.2 Field measurements

5.2.1 Deformation bands – distribution and orientation

Distribution and orientation of the deformation bands within the Fremont Bedding was recorded to obtain the spatial arrangement. The results are entirely obtained from the Fremont Bedding, as this is the only unit in the study area with deformation bands, hence there are no other layers to compare with. The distribution of deformation bands was measured along the cliffs in nine different scan lines, 10 meters long. For each line, the orientation of the Fremont Bedding was determined and the orientation of the scan line

recorded. The fracture and fault sets are observed and recorded by Eivind B. Larsen. (2014), and compared to the deformation band data in Figure 5.9.

The orientation of each deformation band is given with strike and dip. The dip ranges between 40° - 70° , whereas the strike varies between deformation band population 1, 2, 3 and 4. Figure 5.9 displays the mean deformation band orientations as well as the direction of the fault at fracture system in the study area. Three conjugated sets are observed: N-S strike (population 3), WNW-EES strike (population 2) and WWS-EEN strike (population 1). As these sets show no clear crosscutting relationship, the sets-couple are interpreted as a conjugated population, formed in the same stress regime. Set 5 and 6 (population 3) occur in clusters, conjugated sets and as single non-conjugated deformation bands. In some few areas, set 5 occur without set 6 and set 6 occur without set 5. However, in an overall perspective set 5 and set 6 occur as a conjugated set in population 3.

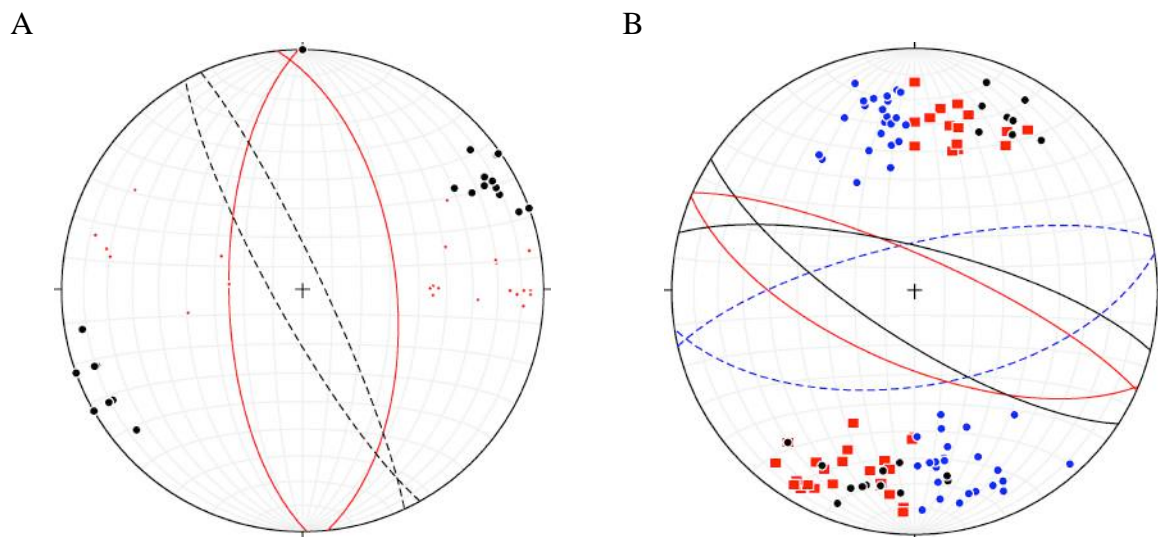


Figure 5.9: Stereonets showing deformation bands, faults and fractures in the study area. **A)** Showing orientation to fracture/fault set (dotted-plains) and the deformation band set 3 (red plains). **B)** Showing one fracture/fault set (black plains) and two deformation band set (blue dotted plain and the red plain). Measurements on fault/fractures

The scan lines vary greatly with respect to the three populations identified in the overall stereoplots. The strike and dip are displayed in stereonet within Figure 5.10, for each scan line (Figure 4.1).

For all of the scan lines, population 1 is present (red plain displayed in Figure 5.10). Population 2 occur in 4 scan lines (β , γ , δ and θ), and set 5 and 6 (population 3) occur in total 5 scan lines (γ , δ , ε , ζ and θ).

The outer scan lines (α and μ) contain few deformation bands, compared to high numbers in the next scan lines (β , γ , η and θ). The three scan lines in the middle (δ , ε and ζ) again contain few bands. The high densities in some of the scan lines are partly caused by clusters, but individual deformations bands are also more frequent. For instance in γ and θ there are a few peaks in the diagram, these representing clusters higher than the total mean count (population 3).

Band density and orientation can be compared between locations. In γ and θ the density is high and population 3 as present as clusters. However, in scan line θ population 1 and 2 are more frequent than the mean count in addition to clusters (population 3). Population 1 is distributed along the entire bedding, with a frequency peak in scan lines β , ζ and θ . Scan line β and θ are located close to the sandstone pipe-formations and ζ are next to the main fault in the study area. Population 2 occurs in four scan lines. Anyhow, there are only in scan line β and θ the population 2 is present in a substantial amount. The density increases with scan-lines closer to the faults. Nevertheless, the high-density of deformation bands also correlates with the pipe-structures. Scan line η and θ are both close to the eastern pipe structure (V.), while γ and β are closer to the pipe-like sandstone knob.

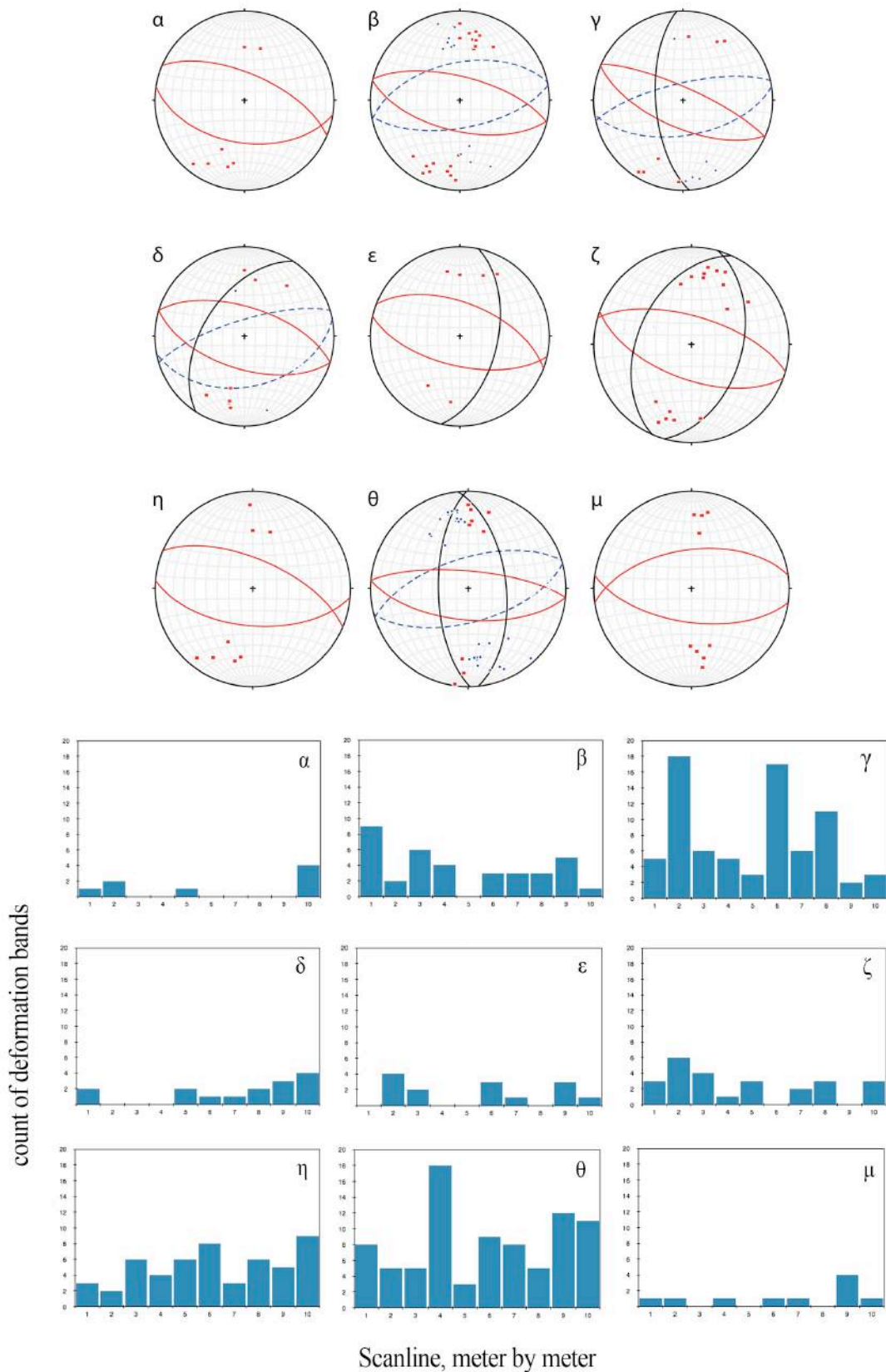


Figure 5.10: *Deformation band* orientation and frequency distribution. **A)** Scan lines α - μ and the mean direction in form of plain and poles. The stereonets and the deformation band orientation are similar for scan lines A, B, G and H, while C, D, E and F show more randomly distribution. **B)** Frequency of each scan line plotted in 1 m intervals. Scan lines B, C, G and H stand out by having higher deformation band density compared to the other sites.

5.2.2 The measured permeability differences

Permeability measurements using the TinyPerm2 probe were performed at four sites, on the Fremont bedding and on two beds below and one above the Fremont Bedding, measurements were taken on location around the line of the lithostratigraphic log.

As visualised in Figure 5.11, L3 is the Fremont bedding, L1 and L2 are beds below and L4 the bed above. The permeability is given with logarithmic scale because of the high differences in permeability. The L1, L2, L3 and L4 are based on the mean value of three measurements, where deviations from the mean value are illustrated with error bars. The mean permeability of for the Fremont bedding is $K=399\text{mD} \pm 33\text{mD}$. There is a positive correlation between permeability and porosity, which gives an indication of porosity values in the nearby beddings.

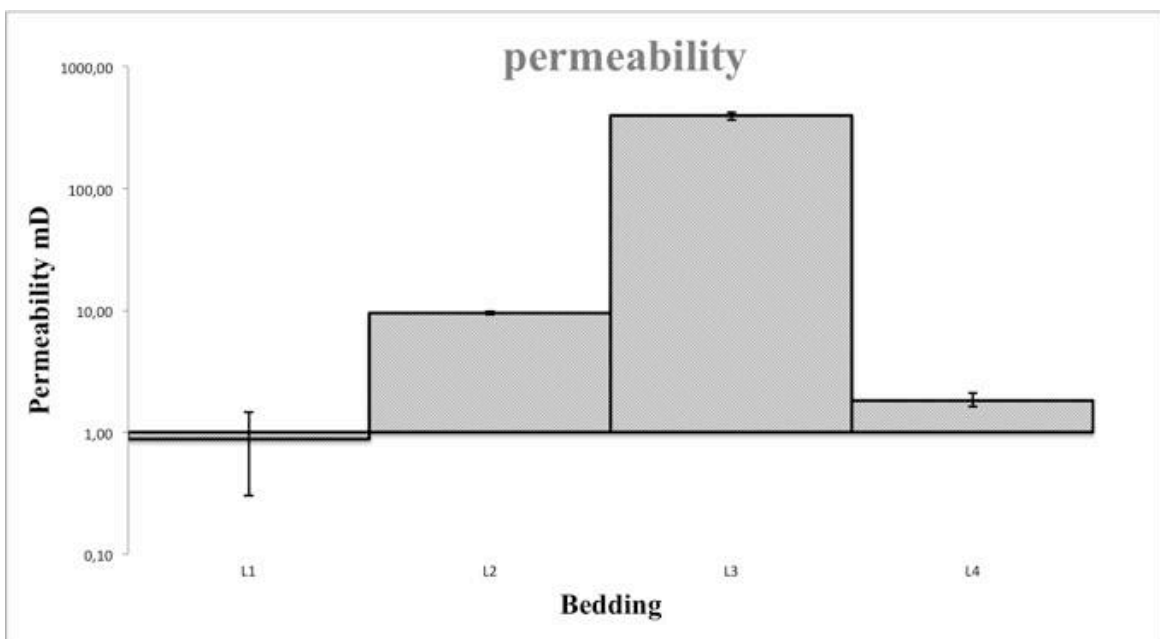


Figure 5.11: Permeability measured using a TinyPerm 2 probe. Note that the permeability scale is logarithmic due to high variety in the measured values. Four beds were measured: the highest peak are the Fremont bedding with a K value at 399 mD, the bed below the Fremont have permeability at 10 mD. The other two beds have permeability below the confidence level given by the instrument. The vertical lines are error bars showing the variation of three readings on one spot.

5.3 Microtextural analysis

5.3.1 General microtextural observations

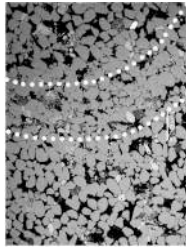
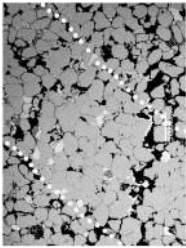
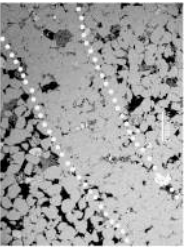
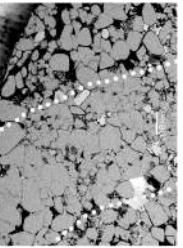
For further investigating of the four deformation band populations, samples were collected from each deformation band type and later cut and worked into thin sections. In this section population 1 and 2 are treated as one, since that was the originally interpretation of the band populations. A classification of the deformation bands is possible, due to the microscopic observations of the characteristics of the microtextural properties (Table 5.3). There are different deformation bands formed by different mechanisms. Crosscutting deformation bands are observed in thin sections as well as the outcrop.

Firstly, there is some quartz cement in thin sections with cataclastic deformation bands. Illite mainly coats quartz grains outside the deformation bands, though there are also observed some quartz grains with illite coating inside the deformation bands. Overall, the quartz grains are sub-rounded with mainly tangential contact within the host rock. In addition, some quartz grains are “floating”. The coating is thin or absent between grain contacts. Calcite is present in the analysed thin sections, situated predominately in pore space as a diagenetic mineral. However, there is also calcite inside deformation bands both as cement and as grains. Pore space and porosity is lower in the cataclastic deformation bands compared to the disaggregation bands observed in the ladder structures. The cataclastic bands are thicker; however, both disaggregated and cataclastic deformation bands show compaction and shear.

5.3.2 Sample locations and thin sections

In Figure 4.1 the field area with sampling locations is shown. Location 3 (Figure 4.1 and Figure 5.12) was collected to examine the deformation band population 2. Texturally, the consolidated sandstone hosting the population 2, has a grey colour in addition to a bleached appearance. Location 3 differs from other areas, because of the grey colour, the high degree of consolidation and the dominating population 2. The thin section made for this location, (IH_06) verifies that these bands are cataclastic bands.

Table 5.3: Overview of deformation band population with a micro-textural approach. The table shows the relations between the different populations and micro-textural properties. The picture is taken in SEM with backscatter detection. There is a high uncertainty to the numbers on porosity and grain size. They are based on a limited number of observation points.

Backscatter image	Thin section	Population	Deformation mechanism	Host rock grain size	Host rock porosity	Deformation grain size	Deformation band porosity
	IH_03	Population 4	Disaggregation, shear band (compaction)	71-80 μm	21 %	61-70 μm	16%
	IH_06	Population 2	Cataclasis, Shear enhanced compaction bands	>101 μm	24 %	81-90 μm	9 %
	IH_04	Population 3	Cataclasis, Shear enhanced compaction bands	91-100 μm	18 %	>101 μm	11%
	IH_11	Population 3	Cataclasis, Shear enhanced compaction bands	51-60 μm	25 %	11-20 μm	18%

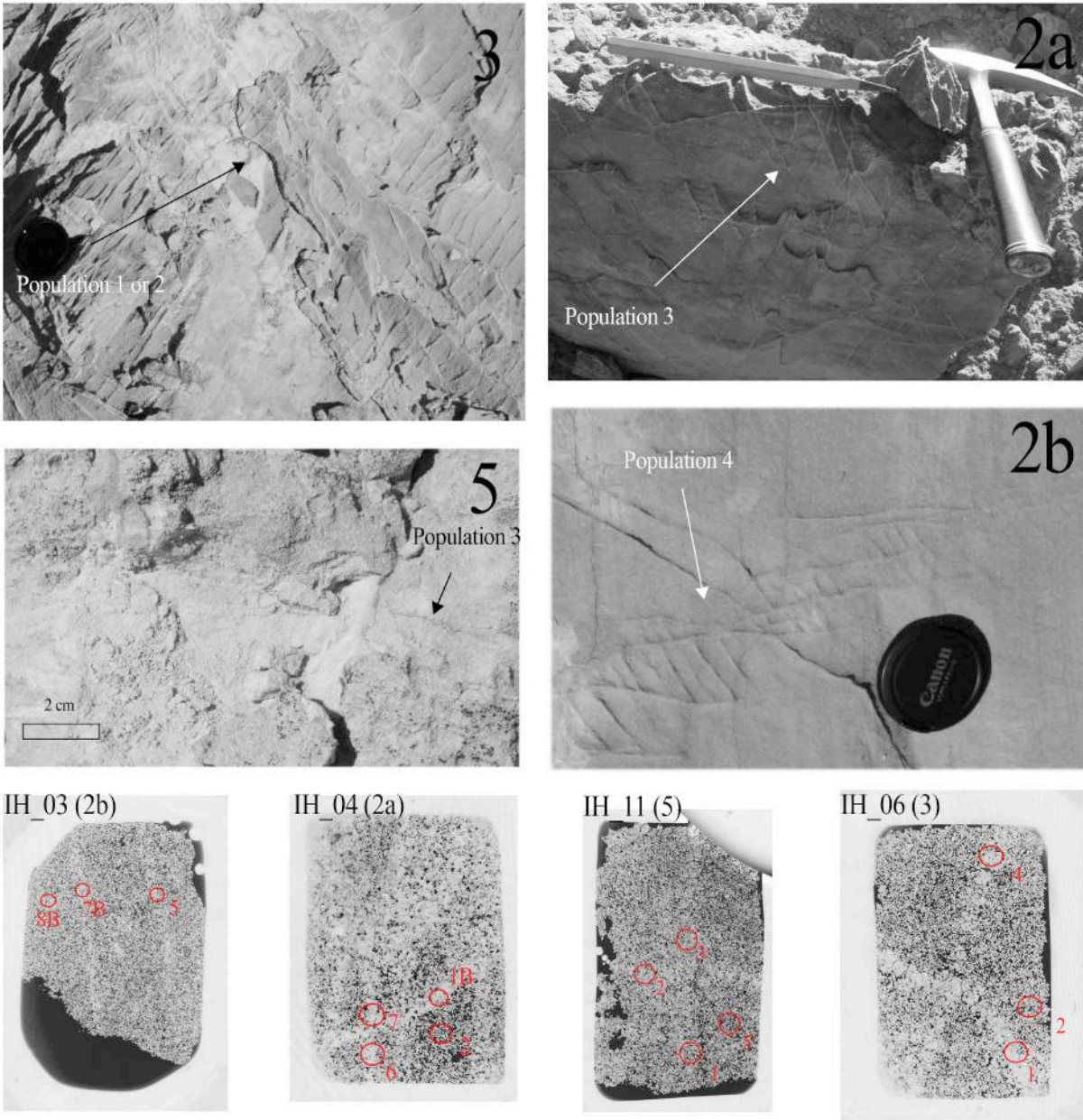


Figure 5.12: Outcrop locations 1– 5 is shown in Figure 4.1. The four images in the middle are location 2a, 2b, 3 and 5. Location 3 shows consolidated grey sandstone with clusters of parallel deformation bands. Location 2a contains red sandstone with crosscutting deformation bands. Outcrop 5 shows unconsolidated bleached sandstone with clustered parallel deformation bands. Location 2b shows a ladder structure. The lowermost row shows the thin sections used for grain size variation and distribution analysis. The spherical red markers illustrate locations of the analysis. The site numbers (beside the red circles) were given when the backscatter images were taken

Location 5 (Figure 4.1 and Figure 5.12) is situated on top of the sandstone knob, comprising a pale red coloured sandstone. Compared to location 3, this sandstone is clearly semi-consolidated and can be disintegrated by hand. The deformation bands are located in rotated blocks, making the deformation band strike meaningless to record. However, these deformation bands are similar to population 3 in location 2a (population 3), which is why this location is chosen in the first place. The deformation bands are mainly oriented in one direction (population 3), barely noticeable in some parts and distinctive in others. The deformation bands form dense clusters, with a few crosscutting bands. For location 5 thin section IH_11 was prepared, showing two deformation bands deflecting one another.

At location 2 (Figure 4.1), the characteristics of the deformation bands change from nearby the pipe and further away from the pipe. Samples from location 2a (Figure 5.12) are collected at the edge of the pipes showing several deformation bands, while samples from location 2b (Figure 5.12) targets a single stepped deformation band structure.

Location 2a (Figure 5.12) represent the population 3. This location shows deformation band sets that are more resistant to weathering than the light red host rock. The white coloured bands have two sets, the most frequent has a strike and dip direction around $180^{\circ}/60^{\circ}$ (population 3). In Figure 5.12, photograph 2a displays some examples of the conjugate deformation bands that exist in location 2a. There are no records of visible offsets in the outcrop descriptions. In thin section IH_04 (sampled from location 2a) there are several deformation bands crosscutting, with no visible offset (Figure 5.12).

The 2b location (Figure 5.12) represents a stepped deformation structure (population 4). The long and continuous deformation bands are thicker than the short, diagonal bands. The tabular offset is visible because of the layered pale-red surface, which have a normal shear displacement. The weathering-resistance is approximately the same for both host rock and deformation bands. There are several stepped deformation band structures in the field area and some of these have better weathering resistance than the structure in location 2b. In thin section IH_03 (sampled from location 2b) there are two parallel deformation bands, which represent the short, diagonal bands (Figure 5.12).

5.3.3 Host rock characteristics

Mineralogy

The mineralogy in the host rocks and in the deformation bands, is similar besides from a few exceptions, as described in Table 5.4 and Table 5.5. In the host rock, quartz, k-feldspar and albite are the main constituents with accessory minerals being dolomite and larger calcite grains. Present accessory to rare minerals are: pyrite; titanite; barite; halite, whereas there are of trace elements hematite/goethite and apatite. The halite, pyrite and titanite are situated inside quartz grains, while barite, hematite/goethite and apatite are formed as individual grains in available pore space. Quartz grains situated in the host rock are coated with illite.

An example from site 2 (Site within thin section IH_04 in Figure 5.12) in thin section IH_04 represents the normal host rock (Figure 5.15 B). This site has a high porosity around 24 %. The large grains neighbouring the pore space are coated with illite. In addition the illite mineral are surrounding small, euhedral calcite grains formed in clusters. Kaolinite, albite, dolomite and k-feldspar are also present as euhedral to sub-hedral grains.

Structures

K-feldspar shows signs of chemical weathering and fracturing Figure 5.14 B, C, D and F grains show two sets of transangular fractures. Similarities between grains illustrated in these backscatter images are two micro-fracture directions, crosscutting each other. Especially image F shows an offset indicating relative ages of transangular shear fractures. The fractured grains displayed in figure Figure 5.14 are all k-feldspar, representing the least weathering-resistant mineral in this rock.

Porosity and grain size

The porosity varies from 19 % to about 24 % in the host rock area. Population 3 in IH_06 and population 2 in IH_04 have the most frequent grain size above 100 μm . Population 4 in IH_03 and population 3 in IH_11 have significant smaller grain size than population 2 (IH_06) and population 3 (IH_04). Population 3 in IH_11 has small peak in frequency around 51-60 μm in the host rock area and population 4 in IH_03 has the most frequent grain size around 71-80 μm . Generally, Fremont Bedding is poorly sorted sandstone with sub-rounded grains.

Table 5.4: Result from analysis performed in SEM and electron microscope. The mineralogy is accomplished by SEM; grains size and percentage are based on electron microscope. Note that size and percentage of the minerals are estimates.

Mineralogy occurrence in host rock			
Mineral	Description	Grain size	Percentage
Quartz	Rounded to subrounded	20 -100 μm	60-80 %
K-feldspar	Altered grains	60 μm	5-12 %
Illite	Quartz coating	5 μm	5-10 %
Kaolinite	Cloudy appearance	5 μm	2-5 %
Calcite	Anhedral crystals	5-150 μm	5-10 %
Dolomite	Euhedral crystals	50-100 μm	2-8
Pyrite	Spherical crystals	10 μm	0-0,1 %
Apatite	Euhedral and anhedral crystals	15-30 μm	0-0,1 %
Titanite	Anhedral crystals	1-5 μm	0-0,1%
Hematite	One observed grain	1-5 μm	0-0,1 %
Barite	Matrix, cementation	1-5 μm	0-0,1 %
Halite	Crystal growth	1-2 μm	0-0,1 %
Albite	Replacing k-feldspar	10-100 μm	0-1 %

5.3.4 Deformation bands characteristics

Mineralogy

In the deformation bands, the main difference from the host rock is lower porosity and grain fractured into a fine-grained matrix. The band has some quartz cement, and some calcite and other minerals related to diagenesis. These deformation bands are classified as cataclastic, contrary to the disaggregation bands that formed without crushing. Inside the cataclastic deformation bands illite are absent, and the pore space is often filled with kaolinite or small grains of calcite. Accessory minerals present in deformation bands are situated inside the quartz grains and are halite, pyrite and titanite. There are differences between the appearance of deformation bands, which can be analysed in the thin sections IH_03, IH_04, IH_06 and IH_11.

The IH_06 thin section from location 3 (Figure 4.1) represents a grey host rock with clusters of population 3 deformation bands. In site 1 (site 1 within thin section IH_06, see Figure 5.12) inside the deformation band, the porosity is 10 % and pore space are filled with crushed parts of quartz grains interspersed with calcite matrix. Areas where pore space occurs, and illite are present as a thin layer coating around the quartz grains. Site 4 (site 4 within thin section IH_06, see Figure 5.12) is similar to site 1 (site 1 within thin section IH_06, see Figure 5.12), aside from having less crushed quartz material, higher porosity and more calcite present. The difference in porosity is noticeable in Figure 5.15.

Thin section IH_11 sampled from the semi-consolidated location 5 (Figure 4.1), show deformation bands deflecting each other. In Figure 5.12, within site 2 (site 2 within thin section IH_11, see Figure 5.12), thin section IH_11 host deformation bands with an unknown strike. Similar to the other deformations bands in the field area, this shows a high amount of quartz grains, however this section also contains more phyllosilicates in form of kaolinite, illite and more grains of dolomite and calcite. The porosity is higher in these deformation bands compares to other bands analysed.

Location 2a consist of population 2 in red coloured host rock. Site 1B (site 1B within thin section IH_04, see Figure 5.12) are situated within one of the deformation bands in thin section IH_04, consisting of quartz grains, quartz matrix and pore space filled with kaolinite, k-feldspar, dolomite and small rounded calcite grains. Site 6 (site 6 within thin section IH_04, see Figure 5.12) is located in an area with a deformation band containing large quartz grains together with matrix of small grains and cemented quartz. Calcite minerals are present within the core as a minority, nevertheless the calcite can be considered as a part of the deformation band matrix. Outside the deformation band's inner core; illite, kaolinite, k-feldspar, albite and dolomite are present. Site 7 (site 7 within thin section IH_04, see Figure 5.12) is located in an edge where two deformation bands crosscut. Population 2 are thicker and has more cemented matrix than the population 3. The matrix of the population 3 consists of smaller grains of quartz and other minerals. There are a minority of calcite, kaolinite, illite in both deformation bands.

The location 2b (Figure 5.12) with thin section IH_03 represent the diagonal deformation bands in the analysed ladder structure. Site 7B (site 7B within thin section IH_03, see Figure 5.12) is located in one of the present deformation bands, showing just a few signs of grain crushing and low porosity loss. The deformation bands from location 2b are less wide and

rich in quartz than the other deformation bands described in this section. Site 5 (site 5 within thin section IH_03, see Figure 5.12) is located in the other present deformation band. It is harder to recognise the deformation band in site 5 (site 5 within thin section IH_03, see Figure 5.12), anyhow an indefinite boundary can be observed. Similar to site 7B (site 7B within thin section IH_03, see Figure 5.12) only few signs of grain crushing and low porosity loss are present. Differences between host rock and deformation bands regarding mineralogy, grain size and roundness are difficult to recognize. The description of thin section IH_03 indicates a disaggregation deformation band, where grain crushing is absent or low.

Structures

In Figure 5.15 a selection of deformation bands are displayed, with a variety from easily recognisable to almost invisible structures. Backscatter-image B and F in Figure 5.15 illustrate a cataclastic deformation band with cementation in-between quartz grains. C, E and D have evidence of crushed grain-material, displayed as a cataclastic deformation band type without visible cementation. Backscatter-image A shows a compaction of grains in the rock with no evidence of grain crushing, which consequently is classified as a disaggregation band. The cementation within the cataclastic deformation bands predominantly contains quartz.

Porosity and grain size

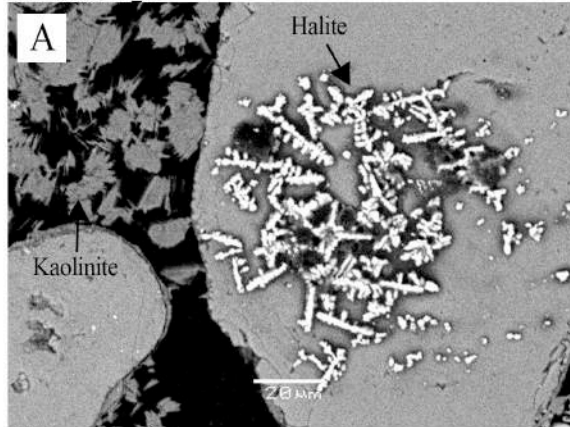
The porosity variation between deformation bands in IH_03, IH_04, IH_06 and IH_11 shows a range from a 10-19% in porosity. IH_03 that represent population 4 of the deformation bands (disaggregation band in this case) and the ladder structure, have higher porosity within the deformation band compared to population 2 in IH_04 and population 3 in IH_06. However, thin section IH_11 also has high porosity within the deformation band, regardless of a cataclastic deformation mechanism in population 3. In addition, population 4 in IH_03 and population 3 in IH_11 have smaller differences between the host rock and the deformation band porosity, than population 3 in IH_06 and population 2 in IH_04. The grain size variation is evenly distributed from 10-100 μm , except for population 3 in IH_06, which has a high measured peak above 100 μm .

Table 5.5: Result from analysis performed in SEM and electron microscope. The mineralogy is accomplished by SEM; the occurrence of size and percentage are observed with electron microscope. Be aware that size and percentage of the minerals are based on subjective measurement and are approximately estimates. The size and percentage vary between thin section and in- and outside of deformation bands.

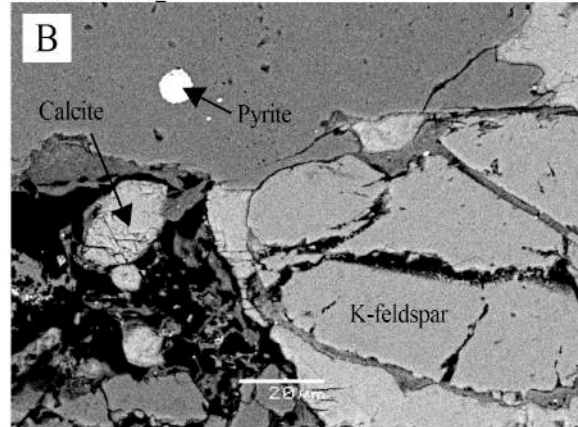
Mineralogical characteristics of deformation bands			
Mineral	Description	Grain size	Percentage
Quartz	Rounded grains and cementation.	10 -100 μm	80-90 %
K-feldspar	Altered grains	5 μm	2 %
Illite	Quartz coating	5 μm	5-10 %
Kaolinite	Cloudy appearance	5 μm	2-5 %
Calcite	Anhedral crystals	5-150 μm	5-10 %
Pyrite	Spherical crystals	10 μm	0-0,1 %
Titanite	Anhedral crystals	1-5 μm	0-0,1%
Halite	Crystal growth	1-2 μm	0-0,1 %
Albite	Replacing k-feldspar	10-100 μm	0-1 %

Figure 5.13 illustrates the mineral occurrence and crystal habit that are present in the backscatter-analysed thin sections. Note the illite coating around grains in fluid-accessible grain boundaries in image A-F (Figure 5.13). A large quantum of k-feldspar grains is in transition to alter into albite, as illustrated in Figure 5.13 F. In backscatter-image C, small calcite grains are clustered together with surrounding illite veins. Areas like this are present in all of the thin sections, commonly situated in host rock area. Kaolinite occurs in A and D, formed at a later stage in-between grains. The accessory minerals barite, apatite, halite and pyrite are demonstrated in Figure 5.13 and Figure 5.14, illustrating the variety of minerals present. Dolomite crystals are present as euhedral crystals in areas outside the deformation bands (Figure 5.14 E, Figure 5.13).

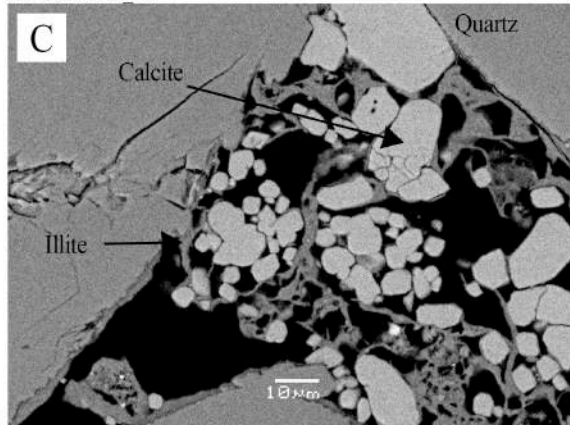
Thin section IH 03



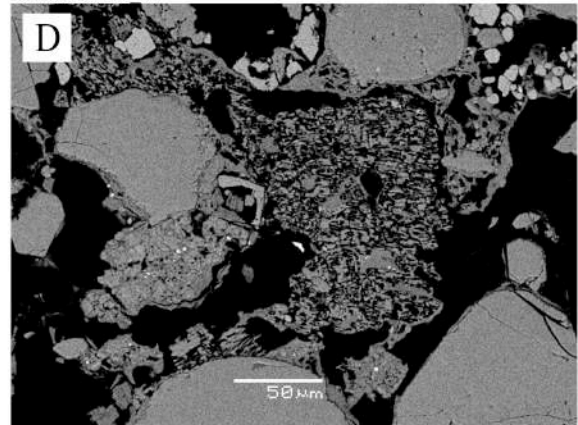
Thin section AB13 2



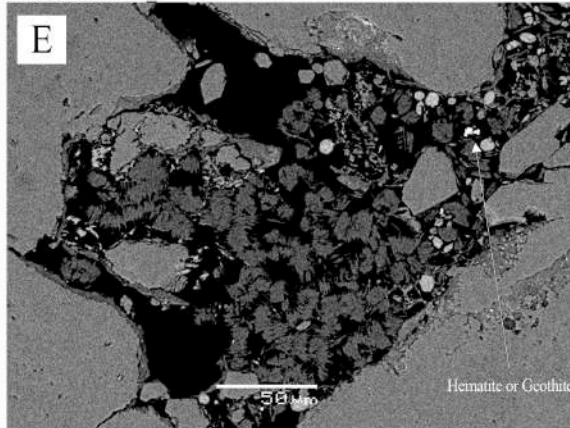
Thin section IH 04



Thin section IH 04



Thin section AB13 2



Thin section AB13 5

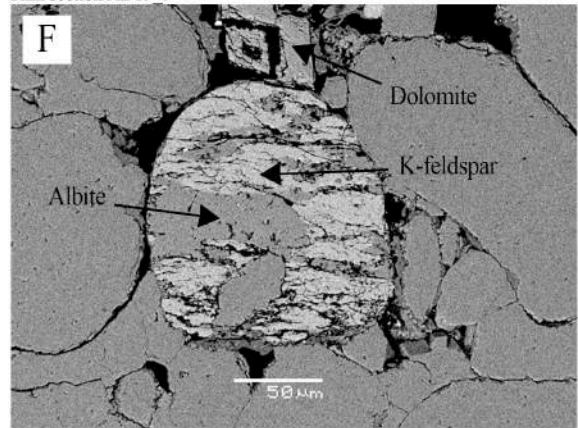
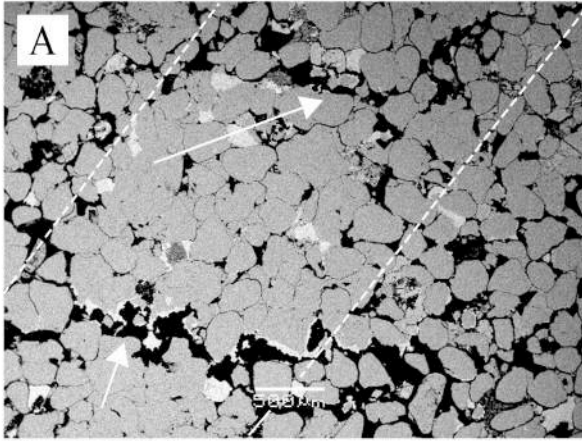
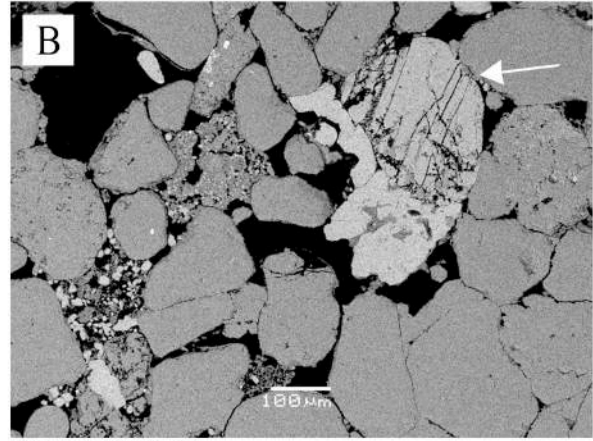


Figure 5.13: Mineralogy identified in SEM with backscatter-images. Backscatter-image A, B and F are within deformation band and C, D and E are situated in the host rock. **A)** Halite crystal present situated above a quartz grain. Illite and kaolinite clays are present: illite as coating around quartz grains and kaolinite as individual crystals. **B)** Calcite, pyrite, quartz and k-feldspar are present. The k-feldspar has fractures, which in this situation is a sign of dissolution possesses of existing k-feldspars. Calcite cleavage is visible. A spherical pyrite crystal is displayed inside the quartz grain. **C)** Small calcite grains are clustered in areas with an illite vein complex. **D)** Displaying a kaolinite area in-between quartz grains. The area with kaolinite displays a usual kaolinite habit, showing high porosity. Additional to kaolinite there are quartz, illite, calcite and dolomite present. **E)** Displays a close-up of the one mineral grain found of hematite. Pore space filled with kaolinite. **F)** Illustrates the on-going weathering process of albitization.

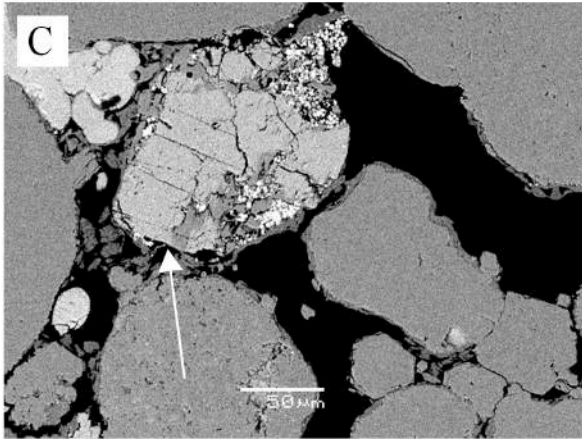
Thin section IH_06



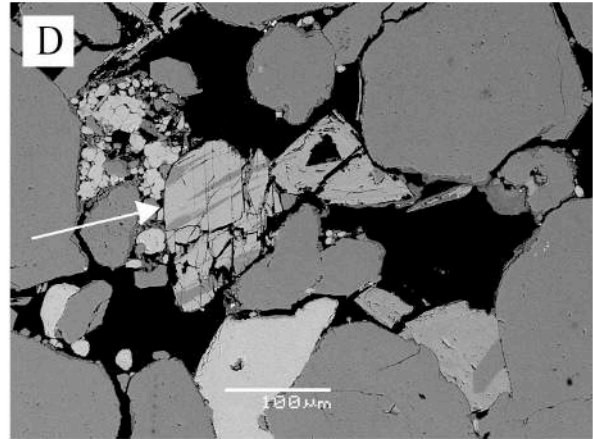
Thin section IH_03



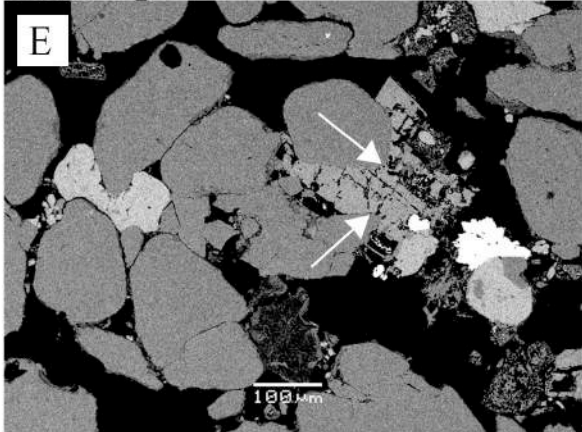
Thin section AB13_5



Thin section AB13_4B



Thin section A13_2



Thin section AB13_2

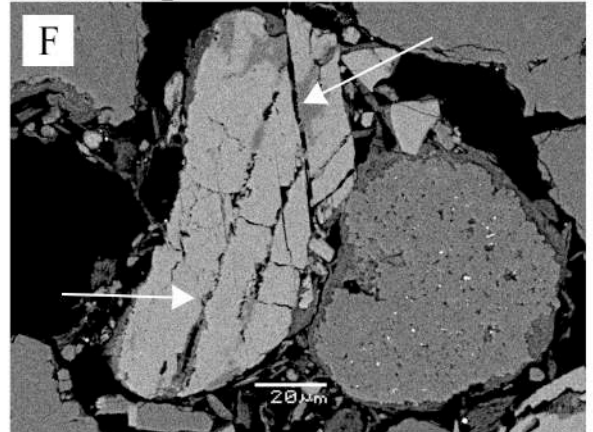
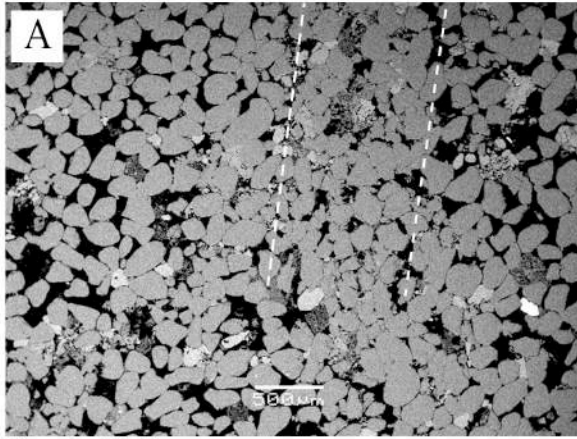
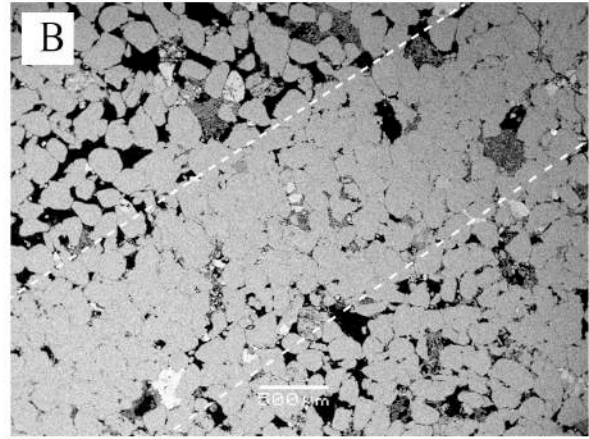


Figure 5.14: An overview of present structures in Backscatter-images. A) Deformation band with fractures crossing through. Inside the fractures, in the "northern" part, there is calcite around and along the quartz boundary. B) K-feldspar grain with parallel fractures, crosscut by a new angled fracture. C) K-feldspar grain with parallel fractures undergoing an albitization. In addition there are weak signs of two parallel fractures with a visible angle from the other parallel fractures. D) Displays a K-feldspar grain undergoing albitization in a 120°/60° relationship with present fractures. E) Displaying the dolomite growth in the field area. Such growth around the already established quartz grains illustrates a later phase of dolomite formation. F) K-feldspar grain with three sets of parallel fractures, all offsetting by another.

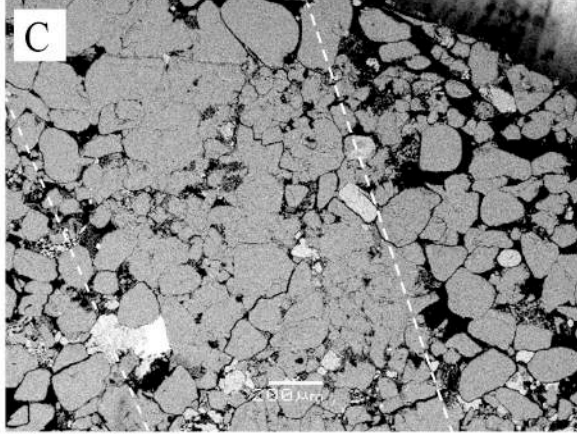
Thin section IH_03



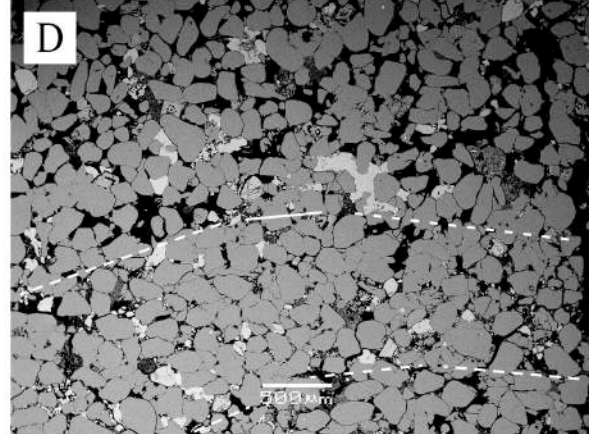
Thin section IH_04



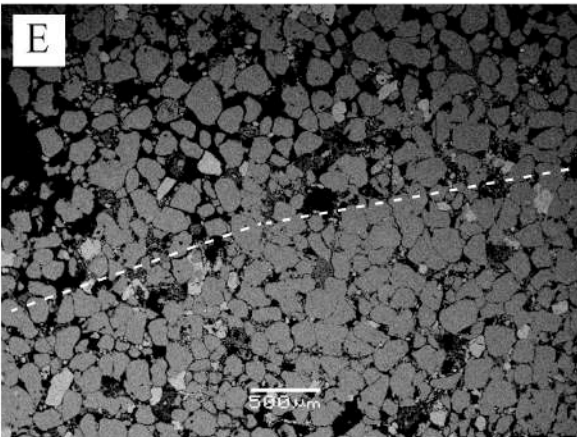
Thin section IH_11



Thin section AB13_5



Thin section AB13_2



Thin section IH_06

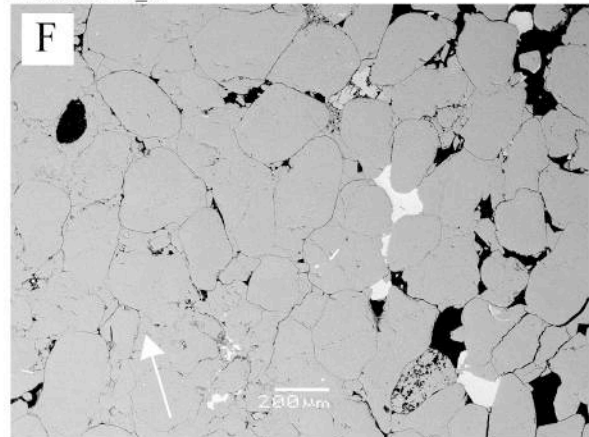


Figure 5.15: Backscatter-images overview of deformation band. A) Shows a deformation band with compaction and no visible grain crushing or cementation. There is lower porosity than in the host rock, nevertheless it is still high compared to other deformation bands. B) An easy recognisable cataclastic deformation band, with large difference between porosity in host rock and deformation band. There are both grain crushing and cementation present. C) Illustration of the vanished grain boundary often observed within deformation bands. A few open fractures show the crushed grain boundaries and the new angular grains. There are few signs indicating cementation, making dissolution and grain crushing the main mechanisms. D) A light porosity difference detaches the deformation band from the host rock. In addition pore space in the deformation band seems to be filled with smaller grains of quartz, some longitudinally and some oddly shaped grains. The lighter white calcite grains are even distributed between host rock and deformation bands. E) The deformation bands have a low porosity difference compared to the host rock, and are only affected by compaction. F) Close-up of a cataclastic deformation band. Grain crushing, dissolution and cementation mechanisms have all been present as a part of the diagenesis.

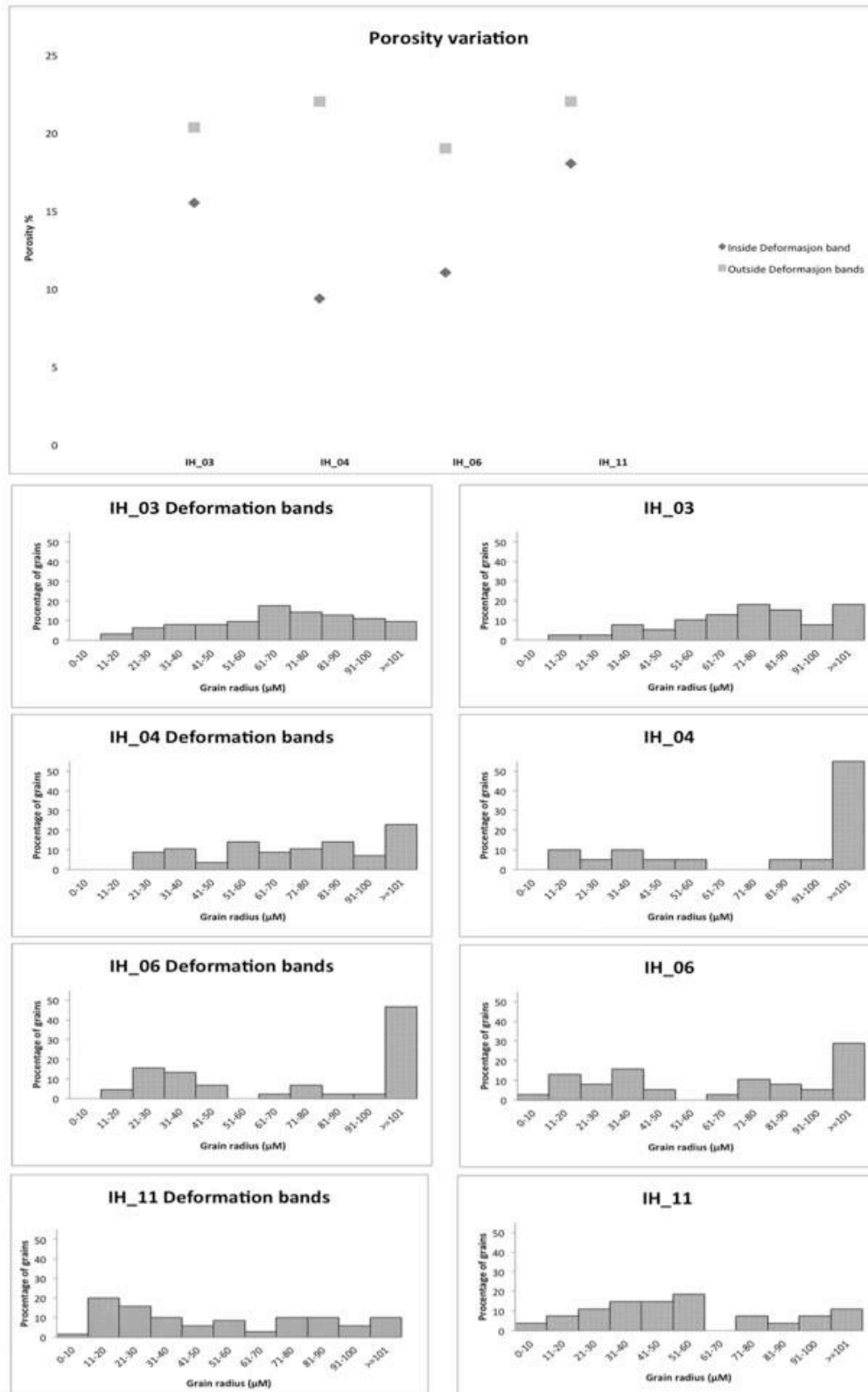


Figure 5.16: Showing relation of grain size and porosity. A) Porosity variation between thin sections and between deformation bands and host rock. Variations are smaller between deformation bands and host rock in thin section IH-03 and IH-11 than in thin section IH-04 and IH-06. B) Histograms showing grain size variation in deformation bands and in host rock for each thin section analysed. The grain size incidence is given in percentage, since the number of sites analysed differ for each thin section

6 | Discussion

The dataset and analysis show that deformation bands distributed differently along the Fremont Bedding. Noticeably there is no evidence recorded for previous hematite coating. However, alteration of k-feldspar was prevalent. Furthermore, the Fremont Bedding occurs in a domal structure, consisting of two anticlinal folds. The four hypothesis proposed in the introduction are summarised in the end of this chapter.

6.1 Regional setting

A few features observed in the study area indicate more than one stress regime affecting the Fremont Bedding. The large-scale structure demonstrates a complex folding, with both anticlinal and synclinal folds (Figure 5.3). The folds observed make up a dome structure based in at least two folding events almost perpendicular to one another. Due to the regional geological setting, stresses relating to the Laramide Orogeny with fault propagate folding and impacts of the Moab fault array can be expected. The SSE trending fold-hinges may represent the north edge of the San Rafael Swell monocline, formed during the Laramide Orogeny (Figure 1.1). The approximately perpendicular anticline WWS trending to the SSE trending folds is linked to an unknown stress regime.

The orientation of deformation bands indicates one or more paleo-stress regimes, which could contribute to the understanding of the folding events. Population 2 (see Table 5.2) has a large range in dip angles with WWS- EEN strikes. These bands are probably related to the folds of the unknown stress regime, since the strike is approximately parallel to the fold-hinges (Figure 5.3). The fracture population striking NNW-SSE (Figure 5.9 A) can be related to the fold-hinge plunging with the same direction (Figure 5.3). This fracture population are most likely a result of the San Rafael fault propagation fold. Deformation band population 1 have a WWN-EES striking sets similar with the fracture population and the fault situated in the study area in Figure 5.9 B. Deformation band population 4 includes the ladder structures, which geographically relates to the area of fault or pipe-structure.

Deformation band chronology

Of the four deformation band populations, population 2 are crosscut by deformation band population 3. Offsets and deflections that underpin the chronology of deformation band population 2 and 3, in which population 3 is crosscutting population 2, are indicating that

deformation band population 3 is younger. Unfortunately, deformation band population 4 and 1 does not have any intersecting deformation bands revealing the relative age.

In microscope examination, there are differences between deformation band population 2 and 3. Population 3 bands have more small, crushed grains relatively to population 2 deformation bands. The assumption of unchanged rock properties from when deformation band population 2 was formed until population 3 formed, leads to a change in stress regime causing the differences between population 2 and population 3 deformation bands. However, the properties or fluid pressure may have changed from when population 2 formed to when deformation band population 3 was formed. This could be in the form of more minerals weathering, causing lower failure strength. Anyhow, progressive shear can cause intense cataclasis, producing less strain hardening and increased displacement (Rotevatn et al., 2008). This might indicate that population 3 bands were exposed for higher stress than deformation band population 2. It can be both higher mean stress and/or higher differential stress. This change in stress state can be due to deeper burial or due to the dissolution of the grain supporting coating or due to increased pore pressure. These intense cataclastic deformation bands may develop to form a discrete slip along central fractures in later stage (Rotevatn et al., 2008), although there are no signs of this in the Humbug Flat.

WWS trending fold

There are no obvious explanations for the fold occurrence with the WWS trending fold-hinge. Anyhow, a discussion of a possible explanation is necessary. In addition to SSE trending San Rafael Swell, Miner Mountains and Uncompagne are NE trending folds/Swells (Bump and Davis, 2003). Bump and Davis (2003) suggest that an oblique slip surface may cause perpendicular fold-trends as a plausible explanation for the present structure in Colorado Plateau formed during the Laramide Orogeny (Bump and Davis, 2003). Hence, smaller oblique slip surfaces may also occur, whereas the WWS trending fold-hinge can be explained. Since population 3 are younger than population 2, the WWS trending anticlinal fold may have occurred before the San Rafael Swell.

A rebound caused by Moab fault WWS segment (see Figure 5.9) can be another plausible interpretation of the occurrence of WWS trending fold and deformation bands population 2. The study area is located between two faults in a horst structure, indicating a footwall rebound regime (Figure 1.1 c). Regarding the footwall location, a rebound had to occur at a

top of a fault tip monocline to explain the anticlinal structure (Erslev, 1991). Furthermore, there are several possible interpretations connecting the Moab Fault Array and the appearance of WWS fold. An alternative explanation to the oblique slip may be that the slip surface is connected to the Moab fault instead. The relative ages of the deformation band populations connected to the different folding events underpin none of the interpretations; population 3 are younger than type population 2, which means that type 2 and the WWS - folding event had to occur before or syn-tectonic to the Laramide Orogeny. Hence, the Moab Fault Array and Laramide oblique slip may both be possible sources for the WWS- trending fold and deformation band population 2.

6.2 Depositional characteristics of the Fremont Bedding and surrounding units

The characteristics of Fremont Bedding compared to beds above and below are different in several ways. Firstly, the distinctive pale colour differs from the surrounding red massive beds with hematite cement (Eivind B. Larsen, personal communication, May 20, 2015). Moreover, the lithostratigraphic log and depositional structures suggest a tabular cross-stratification fluvial bed, with mainly a southwestwards flow direction. At the uppermost part of the layer a bi-directional cross-stratification are observed, topped with a layer of pale-yellow sandstone with signs of rootlets and an uneven pillow-like exposure surface. The Humbug succession is changing from thick predominantly massive red sandstone to thinner massive red sandstone with interlayers of shifting pale silt to red fine sandstone layers in the upper part. According to Fillmore (2011c), during the Jurassic time in Utah the environment changed from an arid basin to a wetter fluvial environment (Figure 2.2). The depositional conditions correlates with the succession described in the lithostratigraphic log.

The Fremont Bedding is probably deposited from a river flowing through an arid area, which was infiltrated by aeolian deposits. Although the textural characteristics are not exclusively dependable indicators of fluvial sand, aeolian dunes are excluded since they commonly are well-sorted with well-rounded grains (Ahlbrandt and Fryberger, 1982; LeTourneau and Huber, 2006). Since analyses performed on the host rock show poorly sorted sandstone and sub-rounded grains, Fremont Bedding is interpreted as fluvial. The bi-directional cross-stratification observed in the upper part of Fremont Bedding may have formed when the flow direction changed.

Either way the river shifts path or demises from the area, in exchange of a floodplain forming the pale yellow layer with rootlets. Furthermore, the massive eolian beds replace the vegetation surface until thin layers of pale silt and red fine sandstone occur. A cyclic succession as these facies (C and D in Table 5.1), suggest repetitions of related deposits under similar conditions (Boggs, 2011a). Regarding the paleogeography for the middle Jurassic time, the cyclic succession may have been formed by seasonal flood plains in a normally arid area or as a tidal flat (Figure 2.2). However, there are no signs of bioturbation, fossils or mud-drapes, which would be expected in marginal-marine environments (Boggs, 2011b). According to Hintze and Kowallis (2009), the shallow marine waters retreated before the Entrada Formation was deposit. Because of no marginal-marine texture, the suggested environment is a river system. The cyclic succession is most likely natural-levee deposits or crevasse splay, which typically have a horizontally stratified fine sand overlain by laminated mud (Boggs, 2011b).

6.2.1 Pipe-structures, collapse or something else?

The collapsed structures and the present sandstone knob described in the study area, have cataclastic deformation bands at the top of the structure in addition to cataclastic deformation bands inside blocks in part of the pipe-structure. Moreover, the sandstone observed in the pipe areas has soft-sediment or water-escape structures, represented by flow-like pattern around the blocks. Soft-sediment appearances occur theoretically in low-burial conditions in sediments with high water content. It is possible that the field area's collapsed structures are soft-sediment dike intrusions. However, related deformation bands are cataclastic and not the expected disaggregation band type, usually formed in low burial conditions. According to Fossen (2010), granular flow is common deformation mechanism for shallow burial conditions whereas crushing and fracturing mechanisms, typical for cataclastic deformation bands forms at deeper level. Nevertheless, there are described cataclastic deformations in faults and in deformation bands associated with shallow-burial deposits in other sediment basins and deltas (Cashman and Cashman, 2000; Rawling and Goodwin, 2003). The cataclastic deformation bands are observed in low confining pressure conditions. Anyhow, it is no uniform explanation for why the cataclastic deformation bands form in low burial conditions. Rawling and Goodwin (2003) suggest that particulate flow may be the controlling factors in forming cataclastic deformation bands under low confining pressure. However, Cashman and Cashman (2000) propose that the cataclastic deformation bands in low burial environment are related to episodic slip during large earthquakes. The pipes and

sandstone knob in Humbug Flat may therefore be a syn-deposition soft-sediment dike, regardless of the presence of cataclastic deformation bands.

Even if the cataclastic deformation bands can form during low confining pressure, the presence of blocks with cataclastic deformation band within the collapsed structure is difficult to explain. If the collapsed structure occurred syn-depositional, why are blocks with cataclastic deformation bands located within the pipe? A plausible interpretation may involve a dividedness of the dike intrusion and later event(s) of block subsidence. Assumed that cataclastic deformation bands at the top are formed during dike intrusion, they somehow have to separate into blocks and sink down in a highly fluid-rich sandstone matrix. Nevertheless, there are suggested that sand intrusions may form in greater depths despite of the usual opinion that sand dikes only occur in surface conditions (Jolly and Lonergan, 2002). The assumed difference of surface to low burial is the increased distance between seal failure and the sill formation. At depth greater than 1 km, the deformation bands form as cataclastic rather than disaggregation (Fossen et al., 2007). However, shallower depth from 1 km to the surface, the probability decreases drastically closer to surface (Fossen et al., 2007). Regarding the potential depth of 100–500m for the sand-dike intrusion instead of surface conditions (Jolly and Lonergan, 2002), there are more likely that cataclastic bands actual formed due to the sand-dike.

Another possible explanation can be that the block-source originates from a layer underneath, brought up with the dike intrusion. Suppose the blocks are sourced below the dike, the deformation bands population 3 (at the top) may have formed at a later stage.

The Moab fault array affects the eastern part of the Humbug cliffs, juxtapositioning Entrada Sandstone Fm and Curtis Fm to be in contact. The age of Moab faulting are described as two active periods from Triassic to Mid-Jurassic and from Mid-Cretaceous to Early Paleogene. Due to no syn-tectonic deposits and the fault crosscutting Early-Cretaceous deposits, the age is assumed somewhere in-between of Mid-Cretaceous to Early Paleogene (Foxford, 1996). The faults are presumed to cause the bleaching appearance on the Fremont Bedding, since the thoroughgoing faults have a bleached rim above and below the bleached bedding. Faults with large displacement tend to have wider damage zones, (according to Shipton and Cowie (2001) approximately 2,5 times the total fault throw) especially when the sandstone are porous. Deformation bands caused by faulting may have a wide distribution into Fremont Bedding, probably formed as the deformation band population 1.

An interesting question is if the pipe-structure and the sandstone knob are related to the faults rather than a result of a dike intrusion. Small normal faults are observed beside the collapse V. (Figure 5.1), which may indicate a local extensional graben. A combination of high fluid pressure, sandstone with high porosity and permeability and extensional force may have caused the collapsed structures as well as the sandstone knob. Perhaps Fremont Bedding was an incompetent layer in relation to the surrounding beddings, behaving as a soft-sediment instead of faulting. If the fault collapse interpretation is correct, the blocks with cataclastic clusters of deformation bands had to be from the Fremont Bedding. Harms (1965), described several different sand-dike intrusions whereas sand-dikes connected to thrusting was explained. According to Harms (1965), a convex-upward reverse fault has extension zones within the hanging-wall causing space for sand-dikes to form. This interpretation are based on that sediments from Fremont Bedding filled the cracks caused by the extensional zone. However, the sandstone knob described from the study area (Figure 5.5), have bended layers indication an upward sediment transport.

Assumed that the NS-trending cataclastic deformation bands formed during Laramide Orogeny and not during the sand-dike-event (or dike-intrusion as Harms (1965) suggested), the problem would have been solved. However, the cataclastic deformation within the blocks is still difficult to explain in a soft sediment depositional environment. Nevertheless, except from the blocks, structures as the upward bended layer in the sandstone knob, the water-escape structures indicates a soft-sediment dike intrusion.

6.2.2 Is the Fremont Bedding bleached?

Fremont bedding has a lighter colour than surrounding strata, indicating a chemical deviation. Observations of deformation bands situated in the Fremont Bedding demonstrate a possible connection between the pale colour and the collapse. The beds below and above are not analysed in this thesis; however, Beitler et al. (2005) and Wigley et al. (2012) have performed detailed studies of comparable chemical diagenesis of the Jurassic Navajo and Entrada Sandstone fms. in Southern Utah. These publications enable an understanding of the possible diagenetic variance between the Fremont Bedding and neighbouring beds.

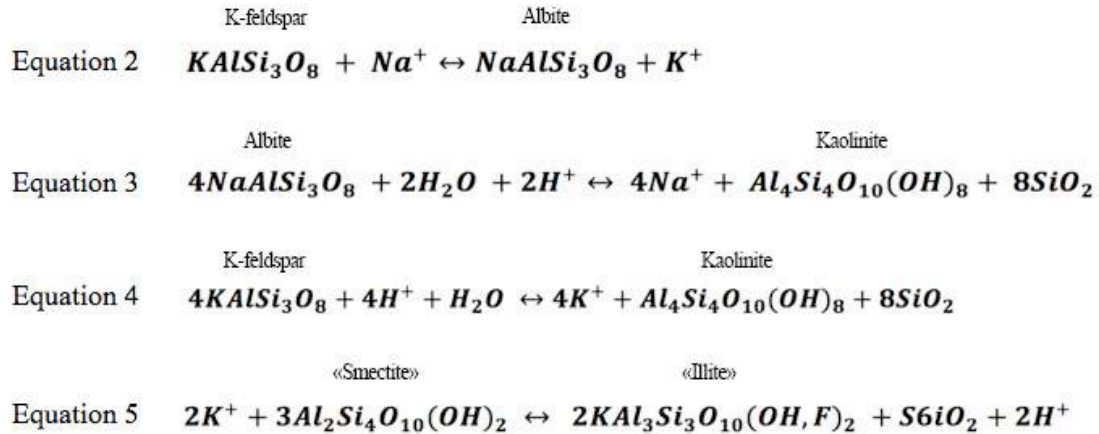
Above all, the bleaching or removal of the hematite coating has been impossible to prove. There is no hematite in the so-called bleached sandstone, suggesting either that the hematite never was present, or that the hematite coating was fully dissolved in an early diagenetic stage, leaving no trace. Anyhow, one small grain of hematite or goethite was discovered in

the host rock (Figure 5.13), but probably without any significance or relation with the hematite coating. Nevertheless, the bleached area around the fault whereas this structure cuts beds below and above makes the bleaching theory of the Fremont Bedding a plausible assumption, based on the fact that the fluid flowing through the fault somehow changes the red area around the fault leaving a white rim, which is probably hematite removal. However, this has not been proven because of deficient sampling from this area.

Regardless, the minerals, which actually are present, indicate chemical weathering due to a fluid phase. The SEM analysis performed shows a sandstone with k-feldspar weathering, calcite cement, quartz cement, illite coating, kaolinite and authigenic dolomite. According to Beitler et al. (2005) the primary evidence of bleaching are increased k-feldspar, weathering and calcite cement dissolution, which are equivalent to the weathering reactions observed in the study area.

K-feldspar observed in the analysed samples shows albitization (Figure 5.13 F). Equation 2 displays the weathering process that changes k-feldspar into albite by adding Na^+ to the chemical process (Table 6.1). The dissolved element Na^+ is probably originating from the deep buried halite-rich paleo-sabkha environment (Paradox Basin) or other halite rich deposits (evaporite)(Chan et al., 2000). The maximum burial for Entrada Sandstone is approximately 2500 m indicating a peak temperature of ca. 60 °C, accounting the “world-mean” geothermal gradient (24 °C/km) (Nuccio and Condon, 1996). According to Baccar et al. (1993), k-feldspar albitization occur at temperatures around 120-150 °C, which is twice the temperature that the Entrada Sandstone was exposed to.

Table 6.1: Equation used to explain the diagenetic features in the study area. Equation 2 shows the k-feldspar alteration into albite. Equation 3 displays the albite change into kaolinite. Equation 4 shows the direct alteration from k-feldspar into kaolinite. The last equation (Equation 5) describe the change from smectite into illite clays.



The study performed by Beitler et al. (2005) shows quartz, k-feldspar and high smectite/illite ratio as primary minerals in low diagenetic red sandstones. On the contrary, kaolinite, illite, and albite are secondary minerals (authigenic) found in bleached beds. According to Beitler et al. (2005)'s study, kaolinite has a negative correlation with k-feldspar, indicating a k-feldspar alteration to kaolinite in addition to albite. Nevertheless, the alteration process might as well be k-feldspar \rightarrow albite \rightarrow kaolinite (Equations 3 and 4). As with k-feldspar alteration, the expected temperature is too low for kaolinite weathering in regular standardisations (Bjorkum and Gjelsvik, 1988). The observed precipitations of illite are explained by Bjorkum and Gjelsvik (1988) as a closed system, with weathering processes in both kaolinite and k-feldspar releasing K^+ .

Meteoric water is a possible explanation for transitions of kaolinite and k-feldspar under low-burial conditions (Bjorlykke, 2010b). Rainwater contains carbon dioxide and sulphur acid, which could have dissolved the carbonate, k-feldspar and phyllosilicates (Bjorlykke, 2010b). Meteoric water flowing through the sandstone is associated with diagenetic processes in shallow marine environments (Bjorlykke, 2010b), similar to assumed environments in Utah during the middle Jurassic and Cretaceous (figure 2.1) (Fillmore, 2011c).

Beitler et al. (2005)'s study made observations of the relationship between smectite and illite from low to intermediate diagenetic sandstones. At low diagenetic evolution, the smectite/illite ratio was commonly > 90 %, and opposite in mature diagenetic layers (Beitler et al., 2005). Smectite is absent in the Fremont Bedding. Anyhow, based on previous studies (Beitler et al., 2005; Wigley et al., 2012) it is suggested that illite is an alteration product of past smectite, in accordance with Equation 5, which is the equilibrium equation between smectite and illite. According to Le Chatelier's principle, the oversaturation of K^+ , maintains the precipitation of illite until equilibrium is achieved. The pyrophyllite formula is used for representing the smectite group, and the muscovite formula is used for illite, which fulfils the silica-aluminium-potassium system (Helge Hellevang, personal communication, March, 06, 2015). This reaction occurs due to available K^+ from k-feldspar and kaolinite alteration.

The key question is if the diagenesis or bleaching actually had an influence on the bedding collapse? The answer is related to the porosity and the load-carrying principle (Figure 3.3). The bleaching of a fluid pathway would be restricted by the Fremont Bedding itself, indicating a high bedding permeability even before the diagenetic change occurred, since the fluid would flow the easiest way. The Fremont Bedding is regarded as fluvial the massive red sandstones below and above. The diagenetic hypothesis described in the introduction accounts for the possibility that hematite coating was present and later removed by bleaching. The absence of hematite does not underpin or exclude the hypothesis. Anyhow, calcite dissolution and k-feldspar weathering are results of fluid interaction and so-called bleaching, which removed grain coating (Beitler et al., 2005). Beitler et al. (2005) describes the presence of hematite coating between contact points, which is gone in the Fremont Bedding. By focusing the stress on grain boundary points, local stress for each grain increases. As shown in Figure 3.3 the removal of grain coating can be crucial for formation deformation bands or faults. Moreover increase in porosity by removal of grain coating is difficult to prove, but could be a key to collapse, a detailed study following the Fremont Bedding out of the field area to unbleached areas are recommended for further study of this topic. Besides, samples taken from the fault with both red and pale coloured rock, would also improve the study. In Frery et al. (2015)'s study there are discussed effects of fluid-rock interactions, which bleached areas around faults, are related to CO_2 . Moreover, Frery et al. (2015) suggest that brutal fault opening mechanism is linked to overpressure fluids, followed

by CO₂-enriched fluids. In addition the fault opening are implied to occur in multiple occurrences (Frery et al., 2015), which may be the case in Humbug Flat area as well.

6.2.3 Deformation band occurrence in the Fremont Bedding

Deformation bands are inconsistently distributed along the Fremont Bed, both in orientation and in localization (Figure 5.11). The deformation band populations correlate with structures situated around the study area. In the dataset and analysis chapter, the deformation bands are divided in four populations (Table 5.2), based in the orientation and properties of the individual band in outcrop.

Deformation band population 1 is cataclastic, conjugated set with a WWN-strike. Population 2 are similar to population 1 with a WWS-strike. Regardless of the similarities in both orientation and mechanism, the WWN-strike set is correlating with the fracture system and therefore separated from population 2. The third population (population 3) represents clustered single and conjugated sets with an overall NS-strike. The deformation band population 4 represents the ladder structure deformation bands.

Population 1 is widely distributed, with increased number closer to the faults or the sand-dikes. However, population 2 are frequent in this area too. Furthermore, population 1 is also predominant in the outer part of the study area. Accordingly, they appear both close to and further away from the fault. Population 3 bands are formed as single deformation bands or as parallel deformation bands in clusters, with NS-strike. They occur individually along the Fremont Bedding in small numbers, and in clusters near the sandstone-dikes. The last deformation band population (population 4) is associated with ladder structure, and are located nearby the fault and sand-dikes.

In extensional regimes cataclastic deformation bands tend to cluster into decimetre-thick zones, which can evolve into faults (Antonellini and Aydin, 1994; Fossen et al., 2015; Johansen and Fossen, 2008). The most common deformation band reported in literature according to Fossen et al. (2015) is the compaction shear band, that is characterised by shear-induced grain crushing and compaction and with a few cm of shear offset (Fossen et al., 2015). In contractional regimes shear-enhanced compaction bands and pure compaction bands are described (Ballas et al., 2013; Eichhubl et al., 2010). However, Eichhubl et al. (2010) suggests that pure compaction band are uncommon, since the tectonic stress contribution needs to be large at the burial depth shallow. Eichhubl et al. (2010) describes

the compactive shear bands to have large shear offset and extensive grain-size reduction, in contrary to the characteristics of the shear enhanced compaction bands.

Population 1 has the same orientation as the fault with a throw on 1,14 m (Eivind B. Larsen, personal communication, May, 20 2015). Anyhow, population 1 is distributed all along the Humbug Flat cliff, which is not an expected distance for the damage zone related to a fault throw on 1,14 m. According to Shipton and Cowie (2001), approximately 2,5 times the total throw are expected damage zone, which in this case are $1,14 \text{ m} \times 2,5 = 2,85$. Population 1 and 2 may therefore be the same conjugated set, after all. Population 1 and 2 have high amounts of cementation, which makes it difficult to indicate if this is a shear enhanced compaction band or a compactional shear band. Anyhow, the grain sortation seems to be intact, the porosity is lower (not taking the cementation in consideration) and no slip surfaces is observed, indicating shear enhanced compaction bands. Population 3 was analysed in two thin sections IH_06, IH_11 and partly in an additional thin section for examine the crosscuts (Figure 5.6.) In thin sections IH_06 and IH_11, the suggested kinematic mechanism is shear enhanced compaction bands and not compactional shear bands, because of the low presence of cataclasis. However, the additional thin section was clearly a compactional shear band with high amount of cataclase. Population 4 has a small porosity change and in outcrop a clear shear-distance, indicating shear-bands with minor compaction.

6.2.4 How did the deformation band form?

The three types of deformation bands are all cataclastic (except the Reidel/ladder structure), consisting either of clusters, of conjugate sets or single bands.

A microscopic analysis of four different thin sections, show different deformation band populations (Figure 6.1). Thin section IH_03 contains two rungs from a ladder structure, IH_04 displays deformation band population 3 sampled from a cluster, IH_06 shows deformation band population 2 also sampled from a cluster, and IH_11 represents a deformation band sampled from an semi-consolidated sandstone block in at the top of the sandstone knob/sand-dikes. The question is if the host rock grain size and porosity impose control on the population of deformation band?

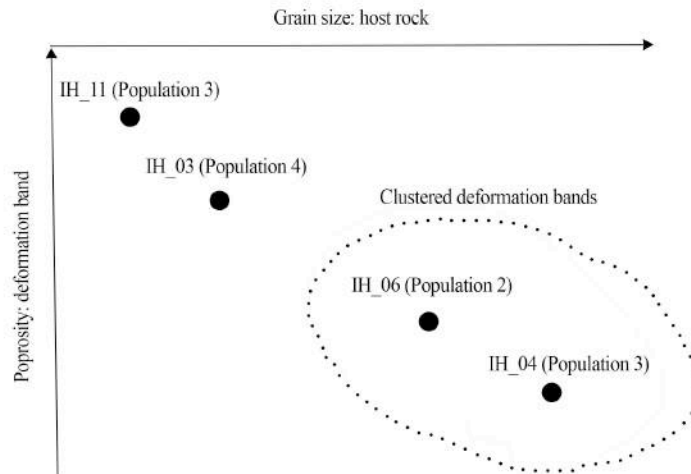


Figure 6.1: Relations between deformation band porosity, clusters and grain size in host rock. There can be two interpretations according to the diagram. 1) Coarse grain size give low porosity within the deformation band, in addition to formation in clusters. 2) Clusters of deformation band will reduce the permeability (i.e. less fluids flowing trough the host rock), which will result in less alteration and dissolution in host rock in areas of clustered deformation bands.

The four thin sections have low variety in host rock porosity, ranging from 20% to 23%.

Anyhow, the grain size within the host rock seems to vary greatly. IH_04 (population 3) and IH_06 (population 2) have the higher count of grain sizes above 100 μM , contrary to IH_03 (population 4) and IH_11 (population 3) with low number of large grains (Figure 5.16; Figure 6.1). The correlation between large grains and low deformation band porosity are significant for the four thin sections analysed, i.e. large grains generate more cataclasis.

Another correlation is observed between large grains in host rocks and deformation bands formed in clusters. If the area has clusters of deformation bands the in-between grain size is coarse. Based on the observation at least two interpretations can be suggested:

- (1) High amount of coarse grains in the host rock contributes to lower porosity within the deformation band than for bands formed in a more fine grained host rock. (This is due to higher stress concentration on grain contacts for coarser grained sandstone)
- (2) Clusters of deformation bands provide strain “protection”, which allow large grains to be present in the host rock (protected from alteration and dissolution processes caused by reduced fluids).

Interpretation 2 is underpinned by the large differences between grain sizes in the same bed. Even though it is possible to have variation in grain size and sorting within a bed, the

variation change from a mean value at $40 \mu\text{M}$ in some areas to mean values above $100 \mu\text{M}$ in other areas. Are the possible the large grain size differences are due to cluster protecting the host rock? Areas 2a and 2b (Figure 5.12) are geographically close, whereas the thin section IH_4 (population 3) and IH_03 (population 4) are sampled from (Figure 5.12), have large differences in host rock grain sizes.

The relationship between host rock grain size and formation of cataclastic deformation bands are described by several authors (Balsamo and Storti, 2010; Soliva et al., 2013). Soliva et al. (2013) substantiate the results from analysis performed on the viable deformation band sampled in the study area. In Figure 6.2, mean stress, differential stress, host rock grain size and pore pressure is used to display occurrence of shear bands, compactional shear bands and shear enhanced compaction bands. The host rock grain size is similar with thin section observations on IH_03 (disaggregation band), IH_04 (cataclastic bands), IH_06 (cataclastic bands) and IH_11 (cataclastic bands). However, the kinematic equivalent (Figure 3.1) to the mechanical description can be described as this; IH_03 as shear bands, IH_04 shear-enhanced compaction bands, and IH_06 and IH_11 as shear-enhanced compaction bands. In

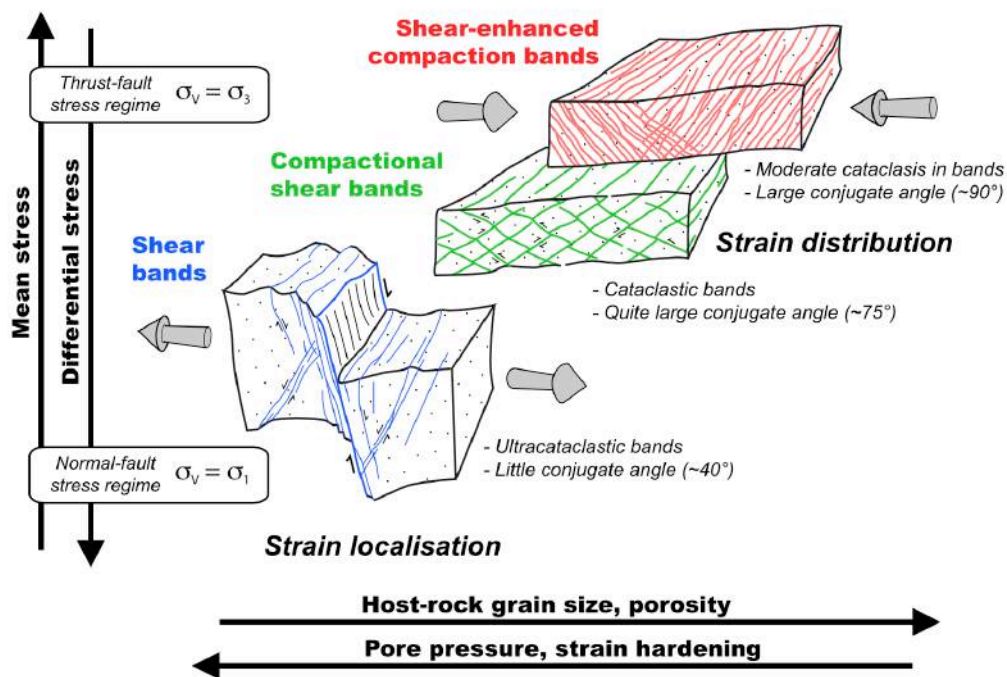


Figure 6.2: figure showing relations between host rock grain size, pore pressure, strain hardening, mean stress and differential stresses. Field study performed on Fremont Bedding shows similar relations, especially between deformation band type and host rock grain sizes. Figure is from Soliva et al. (2013), page 58, figure 10.

Soliva et al. (2013)'s study several field areas was used, whereas large grain sizes variation can be expected.

Interpretation (2) describes a strain hardening process “protecting” the host rock, keeping the grain size unchanged. Grain size reductions can be performed by grain crushing, alteration or/and dissolution. Deformation bands are tabular areas with larger amount of grain crushing compared to the host rock, making alteration and dissolution the main mechanism for decreasing grain sizes in the host rock. Several deformation bands forming in clusters, due to strain hardening, can theoretically cause less permeability (especially areas with perpendicular flow direction related to deformation band orientation). Dissolution is often connected with fluids flowing through the rock, which may have been prevented in area 2a (population 3) and 3 (population 2)(Figure 5.12), because of deformation band clusters.

However, the alteration and dissolution processes should have been more common in host rocks in normal spaced deformation band areas, because of the exposure for more fluid flow (if interpretation 2 is right). Even though dissolution might have been less in host rock within deformation bands clusters compared to regular spaced deformation band, the host rock mineralogy seems to be similar for any type of deformation band analysed. At least the chemical weathering process should have been more mature in normal spaced deformation band areas than in deformation band clusters, if dissolution and fluid flow affected the host rock areas differently. Regarding the similarities in amount of dissolution and alteration between host rocks situated in-between clusters and normal spaced deformation bands, interpretation 1 is more plausible than interpretation 2.

6.2.5 Burial evolution and deformation band formation

Burial history, regional geology and deformation band formation are related to one another. Soliva et al. (2013) have a range of different deformation band types (Figure 6.2), compared to deformation bands described in Humbug Flat area. Nevertheless, this is because of the differences of burial conditions in the areas Soliva et al. (2013)'s study was situated and the burial conditions of Humbug flat. In Humbug Flat the deformation bands occur as shear enhanced compaction bands and shear-isochoric bands (with minor compaction). Moreover, the small range of deformation band types, indicate a small range of burial depth tectonic- and structural events. In Figure 6.3 the suggested deformation band occurrence related to burial depth and tectonic and structural events are present. Population 1 and 2 are proposed to be the same population after all, crosscut by population 3 formed in a later stage.

Population 4 consist of mainly disaggregation bands, which occur in low burial depth. Since disaggregation bands form with granular flow (i.e. less consolidated sandstone present), population 4 are suggested to have formed before population 1 and 2.

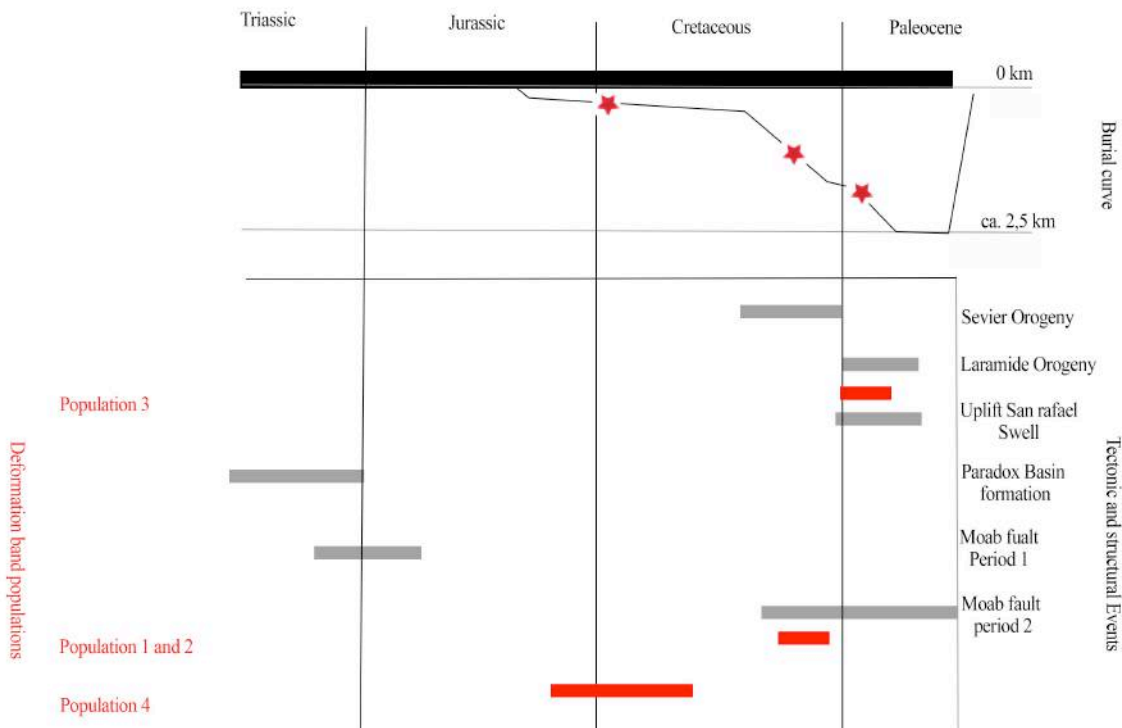


Figure 6.3: Timing of events in Utah with deformation band occurrence. The red lines are approximately occurrence of the deformation band formations. The red stars displayed in the burial curve, showing the approximately burial depth occurrence of the deformation bands.

6.2.6 Are there a relationship between the dome-structure and the pale-colour?

To affect the porosity and remove the grain coating a reducing fluid had to be present. The field study shows an overall complex structure with at least two folding events (Figure 5.3). Since the fluid is assumed to behave with buoyancy, the accumulation of reducing fluid within the anticlinal trap is expected. The surrounding strata have low porosity and the fluid had to flow through available fractures and faults to disperse through Fremont Bedding. In the field area, there are two larger faults with vertical pale-coloured successions below and above Fremont Bedding. The faulting seems to be a plausible explanation regarding to the large fault segments linked to Moab Fault. Anyhow, the meteoric water interpretation

presumes that rainwater is the reducing/bleaching source. The faults located in the study area have small bleached zones around the fault core indicating the pathway of the fluid flow. The bleached parts of the faults seem wider in lower strata and disappear further up the succession, demonstrating that the fluid sourced is originated from the depth. However, the first appearance of fluid may have been with the soft-sediment dike-intrusion.

Regardless of the fluid origin, the fluid contained a reducing chemical composition with Na^+ . Meteoric water is suggested as the solution, though other sources of reducing fluid may also be present. Beitler et al. (2005) suggest that the bleaching was either caused by interaction with hydrocarbons or other organic acids, producing CO_2 as a by-product. Due to the records from the bleached structures around the faults, it is clear that the fluvial solution had an upward transport direction. CO_2 are naturally trapped in sedimentary rocks in the Colorado plateau and it is questioned if groundwater saturated with CO_2 could cause bleaching of red sandstones (Allis et al., 2001). Wigley et al. (2012) suggest that the fluid in the Green River area, not far from Humbug Flat, was CO_2 -charged brine. Whereas Wilkinson et al. (2009) proposed that CO_2 springs in Green River are sourced from Navajo, whereas the water is supplied mostly from meteoric recharged water. However, migration of free CO_2 gas or fluid might have been present too (Wilkinson et al., 2009).

6.3 The key to the collapse of Fremont Bedding

Due to low evidential material revealing removal of hematite coating, the pore pressure is the most plausible explanation for the collapse with a deformation bands forming event. The pore pressure increase is suggested as the main origin of the collapse, the alteration weakness in the rock, the dome-structure and other rock properties may have influenced the final Fremont Bedding collapse.

Firstly, the high porosity and permeability of the rock is the main reason for the collapse. Since Fremont Bedding is a fluvial deposit with high porosity, this made it possible for fluids to flow through the rock. Moreover, changing the chemistry and the failure criteria of the rock makes it possible to form deformation bands.

Three out of four hypotheses proposed in the introduction, are directly or/and indirectly affecting the Fremont Bedding to collapse.

- Hypothesis 1 – Diagenesis: suggested that a reducing fluid causing a hematite-removal as the main trigger for the sandstone to collapse. Hematite removal can not be documented, but diagenesis and dissolution is present.
- Hypothesis 2 – Fold strain: the already reduced strength of the rock combined with folding may have been the trigger for the collapse. There are two folding events causing two deformation populations within the study area.
- Hypothesis 3 – Fault leakage: the fluid is transported along a fault in addition to a sand-dike intrusion. The presence of the fluid is changing the rock properties, which indirectly cause the sandstone to collapse. However, a cyclic development of the fault leakage does not correlate with the deformation band formation, making the fault leakage as an indirect cause of collapse.
- Hypothesis 4- Cap-rock burst: There are no signs of fractures continuing upward the fault into the cap rock, which make the cap-rock burst an unlikely cause for the collapse.

7 | Conclusion

The motivation for this thesis was to reveal possible sources causing sandstone reservoirs to collapse. It is based on data and analysis collected from the Fremont Bedding, a pale-coloured, likely bleached sandstone reservoir situated in Utah, USA. The data material is limited to one bed, which means that correlations and other relations found in this study may or may not be an overall trend/rule for collapsed sandstone reservoirs. To identify main source of collapsed reservoirs, several reservoirs need to be studied and compared. However, this study may contribute to identifying potential reasons causing a reservoir to collapse, which might be of importance in optimizing production/extraction related to petroleum industry, water aquifers and well-suited areas of CO₂ storage.

Four hypothesis posed in the introduction presupposed that folding, fluid pressure, cap-rock burst or/and diagenesis were the main triggers of the collapse. Out of these four hypotheses, pore fluid pressure, fold strain and diagenesis had with certainty an effect on the rock. On the other hand the cap-rock burst hypothesis is discarded, because of few signs of bleached fractures continuing through overlaying layers of Fremont Bedding.

The field and laboratory analysis revealed a reservoir affected by reduced fluids, causing diagenesis at shallower depth than expected. Deformation bands are located through all of the Fremont Bedding, more frequently around the sand-dikes and the fault. The clusters and conjugated deformation bands are distributed in three different populations, based on orientation and deformation mechanisms.

The sand-dikes are associated with the first appearance of reduced fluids. If there have been hematite coat removal, it might have been removed already at this early stage. Assumed that the hematite removal did occur, the yield-strength of the sandstone was reduced in low burial conditions. The first population to form may or may not have occurred because of the lowered strength of the sandstone. Later on, Fremont Bedding and surrounding areas are affected by folding, creating fluid traps and increased strain. There are suggested episodic fluids flowing through the fault, the sandstone-strength decreased even more. The low rock-strength of the Fremont Bedding caused by the trapped fluids may have triggered the massive deformation band formation distributed all along Humbug Flat cliffs. At last, deformation bands formed in relation to the San Rafael Swell uplift.

These results suggest that pore fluid pressure can cause collapse of sandstone reservoir, if the conditions are right. The petroleum industry, who wishes to use injection of fluids for fracturing to obtain increased permeability (Ochi and Vernoux, 1998), may have to consider this risk of actually reducing the permeability by forming deformation bands instead.

8 | Recommendation

For further work on deformation bands in collapsed sandstone reservoirs, I recommend that first priority should be to reveal if there have been extensive hematite grain carrying cement and coating present. If there are possible to prove a hematite removal, this may be the main trigger for collapse of Fremont Bedding.

I suggest mapping out Fremont Bedding is a good way to prove bleaching. By following the Fremont Bedding to outer part of the dome, areas without fluid influence may occur. A sample from both the red and the pale-coloured part of the fluid influence boarder, are the main thing to do.

However, sampling from pale-coloured areas around the present fault may also show hematite removal.

9 | References

- Google Earth 7.1, (2015). Utah State Map 12 S 540167.79 m"E 4346339.14 m"N. Image Landsat. Available through: <http://www.google.com/earth/index.html> [Accessed:4 August 2015].
- AHLBRANDT, T. S. & FRYBERGER, S. G. (1982). Introduction to eolian deposits. *In:* SCHOLLE, P. A. & SPEARING, D. (eds.) *Sandstone Depositional Environments*. Tulsa, American Association of Petroleum Geologists, 11-47.
- ALLIS, R., CHIDSEY, T., GWYNN, W., MORGAN, C., WHITE, S., ADAMS, M. & MOORE, J. Natural CO₂ reservoirs on the Colorado Plateau and southern Rocky Mountains: Candidates for CO₂ sequestration. *In:* Proceedings of the First National Conference on Carbon Sequestration, May 15-17, 2001 2001 National Energy Technology Laboratory, Washington, DC. p. 14-171.
- ANTONELLINI, M. & AYDIN, A. (1994). Effect of faulting on fluid-flow in porous sandstones -petrophysical properties. *AAPG Bull.-Am. Assoc. Petr. Geol.*, 78, p. 355-377.
- ARMSTRONG, R. L. (1968). Sevier orogenic belt in Nevada and Utah. *Geological Society of America Bulletin*, 79, p. 429-458.
- ATWATER, T. (1970). Implications of plate tectonics for the Cenozoic tectonic evolution of western North America. *Geological Society of America Bulletin*, 81, p. 3513-3536.
- AUBREY, W. M. (1996). Stratigraphic Architecture and Deformational History of Early Cretaceous Foreland Basin, Eastern Utah and Southwestern Colorado. *In:* HUFFMAN, A. C., LUND, W.R. AND GODWEIN, L. H. (ed.) *Geology and resources of the Paradox Basin*. Salt Lake City, Utah Geol. Assoc., 211-220.
- AYDIN, A. & AHMADOV, R. (2009). Bed-parallel compaction bands in aeolian sandstone: Their identification, characterization and implications. *Tectonophysics*, 479, p. 277-284.
- AYDIN, A., BORJA, R. I. & EICHHUBL, P. (2006). Geological and mathematical framework for failure modes in granular rock. *Journal of Structural Geology*, 28, p. 83-98.
- AYDIN, A. & JOHNSON, A. (1978). Development of faults as zones of deformation bands and as slip surfaces in sandstone. *pageoph*, 116, p. 931-942.
- BALLAS, G., SOLIVA, R., SIZUN, J.-P., BENEDICTO, A., CAVAILHES, T. & RAYNAUD, S. (2012). The importance of the degree of cataclasis in shear bands for fluid flow in porous sandstone, Provence, France. *AAPG bulletin*, 96, p. 2167-2186.
- BALLAS, G., SOLIVA, R., SIZUN, J.-P., FOSSEN, H., BENEDICTO, A. & SKURTVEIT, E. (2013). Shear-enhanced compaction bands formed at shallow burial conditions; implications for fluid flow (Provence, France). *Journal of Structural Geology*, 47, p. 3-15.
- BALSAMO, F. & STORTI, F. (2010). Grain size and permeability evolution of soft-sediment extensional sub-seismic and seismic fault zones in high-porosity sediments from the Croton basin, southern Apennines, Italy. *Marine and Petroleum Geology*, 27, p. 822-837.
- BEITLER, B., PARRY, W. & CHAN, M. A. (2005). Fingerprints of fluid flow: chemical diagenetic history of the Jurassic Navajo Sandstone, southern Utah, USA. *Journal of Sedimentary Research*, 75, p. 547-561.
- BEN BACCAR, M., FRITZ, B. & MADE, B. (1993). Diagenetic albitization of K-feldspar and plagioclase in sandstone reservoirs; thermodynamic and kinetic modeling. *Journal of Sedimentary Research*, 63, p. 1100-1109.

- BERG, S. S. & SKAR, T. (2005). Controls on damage zone asymmetry of a normal fault zone: outcrop analyses of a segment of the Moab fault, SE Utah. *Journal of Structural Geology*, 27, p. 1803-1822.
- BJORKUM, P. A. & GJELSVIK, N. (1988). An isochemical model for formation of authigenic kaolinite, K-feldspar and illite in sediments. *Journal of Sedimentary Research*, 58.
- BJORLYKKE, K. (2010a). Introductions to Geomechanics. In: *Petroleum Geoscience: From Sedimentary Environment to Rock Physics*. Berlin, Springer, 117-139.
- BJORLYKKE, K. (2010b). *Petroleum Geoscience: From Sedimentary Environments to Rock Physics*, Berlin, Springer.
- BLAKEY, R. No date. *Global Paleogeography* [Online]. Paleogeography Library. Available: <http://cpgeosystems.com/globehighres.html> c 21 January 2015].
- BLAKEY, R. C., PETERSON, F. & KOCUREK, G. (1988). Synthesis of late Paleozoic and Mesozoic eolian deposits of the Western Interior of the United States. *Sedimentary Geology*, 56, p. 3-125.
- BOGGS, J. S. (2011a). Stratigraphy and Basin Analysis, Lithostratigraphy. In: *Principles of Sedimentology and Stratigraphy*. New Jersey, Pearson prentice Hall, 337-364.
- BOGGS, S. (2011b). Depositional Environments. In: *Principles of sedimentology and stratigraphy*. New Jersey, Pearson, 207-329.
- BONNET, E., BOUR, O., ODLING, N. E., DAVY, P., MAIN, I., COWIE, P. & BERKOWITZ, B. (2001). Scaling of fracture systems in geological media. *Reviews of geophysics*, 39, p. 347-383.
- BRANDENBURG, J., ALPAK, F. O., SOLUM, J. G. & NARUK, S. J. (2012). A kinematic trishear model to predict deformation bands in a fault-propagation fold, East Kaibab monocline, Utah. *AAPG bulletin*, 96, p. 109-132.
- BUMP, A. P. & DAVIS, G. H. (2003). Late Cretaceous–early Tertiary Laramide deformation of the northern Colorado Plateau, Utah and Colorado. *Journal of Structural Geology*, 25, p. 421-440.
- BURCHFIELD, B. C. & HICKCOX, C. W. (1972). Structural development of central Utah. *Utah Geological Association* 2, p. 55-66.
- CASHMAN, S. & CASHMAN, K. (2000). Cataclasis and deformation-band formation in unconsolidated marine terrace sand, Humboldt County, California. *Geology*, 28, p. 111-114.
- CATER, F. W. & CRAIG, L. C. (1970) *Geology of the salt anticline region in southwestern Colorado, with a section on stratigraphy*. Professional Paper 637. Washington, OFFICE, U. S. G. P.
- CHAN, M. A., PARRY, W. T. & BOWMAN, J. R. (2000). Diagenetic hematite and manganese oxides and fault-related fluid flow in Jurassic sandstones, southeastern Utah. *AAPG Bulletin*, 84, p. 1281-1310.
- COE, A. L., ARGLES, T. W., ROTHERY, D. A. & SPICER, R. A. (2010). *Geological field techniques*, Milton Keynes, UK, John Wiley & Sons.
- CONEY, P. J. (1978). Mesozoic-Cenozoic Cordilleran plate tectonics, Cenozoic tectonics and regional geophysics of western Cordillera. *Geological Society of America Memoir*, 152, p. 33-50.
- CRITTENDEN JR, M. D., CHRISTIE-BLICK, N. & LINK, P. K. (1983). Evidence for two pulses of glaciation during the late Proterozoic in northern Utah and southeastern Idaho. *Geological Society of America Bulletin*, 94, p. 437-450.
- CURRIE, B. S. (1997). Sequence stratigraphy of nonmarine Jurassic–Cretaceous rocks, central Cordilleran foreland-basin system. *Geological Society of America Bulletin*, 109, p. 1206-1222.

- CURRIE, B. S. (2002). Structural Configuration of the Early Cretaceous Cordilleran Foreland Basin System and Sevier Thrust Belt, Utah and Colorado. *The Journal of Geology*, 110, p. 697-718.
- DAVATZES, N. & AYDIN, A. (2003). Overprinting faulting mechanisms in high porosity sandstones of SE Utah. *Journal of Structural Geology*, 25, p. 1795-1813.
- DAVIS, G. H. (1999). *Structural geology of the Colorado Plateau region of southern Utah, with special emphasis on deformation bands*, Geological Society of America.
- DICKINSON, W. R., KLUTE, M. A., HAYES, M. J., JANECKE, S. U., LUNDIN, E. R., MCKITTRICK, M. A. & OLIVARES, M. D. (1988). Paleogeographic and paleotectonic setting of Laramide sedimentary basins in the central Rocky Mountain region. *Geological Society of America Bulletin*, 100, p. 1023-1039.
- DICKINSON, W. R. & LAWTON, T. F. (2003). Sequential intercontinental suturing as the ultimate control for Pennsylvanian Ancestral Rocky Mountains deformation. *Geology*, 31, p. 609-612.
- DOCKRILL, B. & SHIPTON, Z. K. (2010). Structural controls on leakage from a natural CO₂ geologic storage site: Central Utah, U.S.A. *Journal of Structural Geology*, 32, p. 1768-1782.
- DU BERNARD, X., EICHHUBL, P. & AYDIN, A. (2002). Dilation bands: A new form of localized failure in granular media. *Geophysical Research Letters*, 29, p. 29-1-29-4.
- EICHHUBL, P., HOOKER, J. N. & LAUBACH, S. E. (2010). Pure and shear-enhanced compaction bands in Aztec Sandstone. *Journal of Structural Geology*, 32, p. 1873-1886.
- ERSLEV, E. A. (1991). Trishear fault-propagation folding. *Geology*, 19, p. 617-620.
- ERSLEV, E. A. & ROGERS, J. L. (1993). Basement-cover geometry of Laramide fault-propagation folds. In: SCHMID, C. J., CHAS, R. B. & ERSLEV, E. A. (eds.) *Laramide basement deformation in the Rocky Mountain foreland of the Western United States*. Pap. Geol. Soc. Amer, 125-146.
- FARMER, G. L. & DEPAOLO, D. J. (1983). Origin of Mesozoic and Tertiary granite in the western United States and implications for Pre-Mesozoic crustal structure: 1. Nd and Sr isotopic studies in the geocline of the Northern Great Basin. *Journal of Geophysical Research: Solid Earth (1978–2012)*, 88, p. 3379-3401.
- FERREIRA, T. & RASBAND, W. (2011). The ImageJ user guide. USA: National Institutes of Health.
- FILLMORE, R. (2011a). The Cretaceous Period: The Sea Appears. In: *Colorado Plateau of Eastern Utah and Western Colorado*. Salt Lake City, The University of Utah Press, 219-255.
- FILLMORE, R. (2011b). *Geological Evolution of the Colorado Plateau*, Salt Lake City, The University of Utah Press.
- FILLMORE, R. (2011c). The Jurassic Period: Sand and More Sand. In: *Colorado Plateau of Eastern Utah and Western Colorado*. Salt Lake City, The University of Utah Press, 177-218.
- FILLMORE, R. (2011d). The Pennsylvanian Period: The Rise of the Ancestral Rocky Mountains. In: *Colorado Plateau of Eastern Utah and Western Colorado*. Salt Lake City, The University of Utah Press, 27-102.
- FILLMORE, R. (2011e). The Tertiary period: The Rise of the Colorado Plateau. In: *Colorado Plateau of Eastern Utah and Western Colorado*. Salt Lake City, The University of Utah Press.
- FILOMENA, C. M., STOLLHOFEN, J., HORNUNG, H. & FILOMENA, H. (2014). Assessing accuracy of gas-driven permeability measurements: A comparative study of diverse Hassler-cell and probe permeameter devices. *Solid Earth*, 5, p. 1-11.

- FOSSSEN, H. (2010). Deformation bands formed during soft-sediment deformation: Observations from SE Utah. *Marine and Petroleum Geology*, 27, p. 215-222.
- FOSSSEN, H., SCHULTZ, R. A., SHIPTON, Z. K. & MAIR, K. (2007). Deformation bands in sandstone: a review. *Journal of the Geological Society*, 164, p. 755-769.
- FOSSSEN, H., ZULUAGA, L. F., BALLAS, G., SOLIVA, R. & ROTEVATN, A. (2015). Contractional deformation of porous sandstone: Insights from the Aztec Sandstone, SE Nevada, USA. *Journal of Structural Geology*, 74, p. 172-184.
- FOXFORD, K. A., GARDEN, I. R., GUSCOTT, S. C., BURLEY S. D., LEWIS, J. J. M., WALSH, J. J. AND WATTERSON, J. (1996). The field geology of the Moab Fault. In: HUFFMAN, A. C., LUND, W.R. AND GODWEIN, L. H. (ed.) *Geology and Resources of the Paradox Basin*. Utah, Utah Geological Society Guidebook 25, 265-283.
- FOXFORD, K. A., WALSH, J. J., WATTERSON, J., GARDEN, I. R., GUSCOTT, S. C. & BURLEY, S. D. (1998). Structure and content of the Moab Fault Zone, Utah, USA, and its implications for fault seal prediction. *Geological Society, London, Special Publications*, 147, p. 87-103.
- FRERY, E., GRATIER, J.-P., ELLOUZ-ZIMMERMAN, N., LOISELET, C., BRAUN, J., DESCHAMPS, P., BLAMART, D., HAMELIN, B. & SWENNEN, R. (2015). Evolution of fault permeability during episodic fluid circulation: Evidence for the effects of fluid–rock interactions from travertine studies (Utah–USA). *Tectonophysics*, 651-652, p. 121-137.
- GOODGE, J. W., VERVOORT, J. D., FANNING, C. M., BRECKE, D. M., FARMER, G., WILLIAMS, I., MYROW, P. & DEPAOLO, D. (2008). A positive test of east Antarctica-Laurentia juxtaposition within the Rodinia supercontinent. *Science*, 321, p. 235-240.
- HANDIN, J., HAGER JR, R. V., FRIEDMAN, M. & FEATHER, J. N. (1963). Experimental deformation of sedimentary rocks under confining pressure: pore pressure tests. *Aapg Bulletin*, 47, p. 717-755.
- HARMS, J. C. (1965). Sandstone dikes in relation to Laramide faults and stress distribution in the southern Front Range, Colorado. *Geological Society of America Bulletin*, 76, p. 981-1002.
- HETTINGER, R. D. & KIRSCHBAUM, M. A. (2002). *Stratigraphy of the Upper Cretaceous Mancos Shale (upper part) and Mesaverde Group in the southern part of the Uinta and Piceance basins, Utah and Colorado*, US Geological Survey.
- HINTZE, L. F. & KOWALLIS, B. J. (2009). *Geological History of Utah*, Provo, Utah, Brigham Young University Geology Studies.
- HINTZE, L. F., WILLIS, G. C., LAES, D. Y. M., SPRINKEL, D. A. & BROWN, K. D. (2000). *Digital Geologic Map of Utah*, 1: 500000. Utah: Utah Geological Survey. [Online] Available: <http://mrdata.usgs.gov/geology/state/state.php?state=UT> [Accessed 21.1.2015].
- HITE, R. & BUCKNER, D. (1981). Stratigraphic correlations, facies concepts, and cyclicity in Pennsylvanian rocks of the Paradox Basin. In: WIEGAND, D. L. (ed.) *Geology of the Paradox Basin*. Rocky Mountain Association of Geologists, 1981 Field Conference, p.147-159.
- HUMEZ, P., NÉGREL, P., LAGNEAU, V., LIONS, J., KLOPPMANN, W., GAL, F., MILLOT, R., GUERROT, C., FLEHOC, C., WIDORY, D. & GIRARD, J.-F. (2014). CO₂–water–mineral reactions during CO₂ leakage: Geochemical and isotopic monitoring of a CO₂ injection field test. *Chemical Geology*, 368, p. 11-30.
- JOHANSEN, T. E. S. & FOSSSEN, H. 2008. Internal geometry of fault damage zones in interbedded siliciclastic sediments. In: WIBBERLEY, C. A. J., KURZ, W., IMBER,

- J., HOLDSWORTH, R. E. & COLLETTINI, C. (eds.) *Geological Society Special Publication*.
- JOLLY, R. J. & LONERGAN, L. (2002). Mechanisms and controls on the formation of sand intrusions. *Journal of the Geological Society*, 159, p. 605-617.
- JONES, G., FISHER, Q. J., KNIPE, R. J., FOXFORD, K. A., WALSH, J. J., WATTERSON, J., GARDEN, I. R., GUSCOTT, S. C. & BURLEY, S. D. (1998). Structure and content of the Moab fault zone, Utah, USA, and its implications for fault seal prediction. *Geological Society Special Publications*, 147, p. 87-103.
- KIRKLAND, J. I., CIFELLI, R. L., BRITT, B. B., BURGE, D. L., DECOURTEN, F. L., EATON, J. G. & PARRISH, J. M. (1999). Distribution of vertebrate faunas in the Cedar Mountain Formation, east-central Utah. *Vertebrate Paleontology in Utah, Utah Geological Survey*, 99-1, p. 201-242.
- KLEIN, C. & DUTROW, B. (2007). Analytical and Imaging methods in mineral science. In: FLAHERTY, R. & NELSON, C. (eds.) *Mineral Science*. New Jersey, Jay O'Callaghan, 307-330.
- LAWTON, T. (1986). Fluvial Systems of the Upper Cretaceous Mesaverde Group and Paleocene North Horn Formation, Central Utah: A Record of Transition from Thin-Skinned to Thick-Skinned Deformation in the Foreland Region. In: PETERSON, J. A. (ed.) *Paleotectonics and sedimentation in the rock Mountain Region, United States*. American Association of Petroleum Geologists Memoir, 423-442.
- LETOURNEAU, P. M. & HUBER, P. (2006). Early Jurassic eolian dune field, Pomperaug basin, Connecticut and related synrift deposits: Stratigraphic framework and paleoclimatic context. *Sedimentary Geology*, 187, p. 63-81.
- MADSEN, D. B. & CURREY, D. R. (1979). Late Quaternary glacial and vegetation changes, Little Cottonwood Canyon area, Wasatch Mountains, Utah. *Quaternary Research*, 12, p. 254-270.
- MAGNABOSCO, C., BRAATHEN, A. & OGATA, K. (2014). Permeability model of tight reservoir sandstones combining core-plug and Miniperme analysis of drillcore; Longyearbyen CO. *Norwegian Journal of Geology*, 94, p. 189-200.
- MATHIS, A. C. (2000). *Capital Reef National Park and vicinity geologic road logs, Utah*, Utah, Utah Geological Association.
- MOLENAAR, C. (1981). Mesozoic stratigraphy of the Paradox Basin-an overview. In: WIEGAND, D. L. (ed.) *Geology of the Paradox Basin: Rocky Mountain Association of Geologists Guidebook*. 119-127.
- MOLLEMA, P. & ANTONELLINI, M. (1996). Compaction bands: a structural analog for anti-mode I cracks in aeolian sandstone. *Tectonophysics*, 267, p. 209-228.
- NELSON, S. T. & DAVIDSON, J. P. (1997). The petrogenesis of the Colorado plateau laccolith and their relationship to regional magmatism. *USGS Bulletin*, 2158, p. 85-100.
- NICOL, A., CHILDS, C., WALSH, J. J. & SCHAFER, K. W. (2013). A geometric model for the formation of deformation band clusters. *Journal of Structural Geology*, 55, p. 21-33.
- NUCCIO, V. F. & CONDON, S. M. (1996). Burial and thermal history of the Paradox Basin, Utah and Colorado, and petroleum potential of the Middle Pennsylvanian Paradox Formation.
- OCHI, J. & VERNOUX, J.-F. (1998). Permeability decrease in sandstone reservoirs by fluid injection: hydrodynamic and chemical effects. *Journal of Hydrology*, 208, p. 237-248.

- PIPERINGOS, G. N. & O'SULLIVAN, R. B. (1978). Principal unconformities in Triassic and Jurassic rocks: western Interior United States—a preliminary survey. *US Geological Survey Professional Paper*, 1035-A.
- RAWLING, G. C. & GOODWIN, L. B. (2003). Cataclasis and particulate flow in faulted, poorly lithified sediments. *Journal of Structural Geology*, 25, p. 317-331.
- REED, S. J. B. (2005). *Electron Microprobe Analysis and Scanning Electron Microscopy in geology*, Cambridge, Cambridge University Press.
- ROTEVATN, A., TORABI, A., FOSSEN, H. & BRAATHEN, A. (2008). Slipped deformation bands: a new type of cataclastic deformation bands in Western Sinai, Suez rift, Egypt. *Journal of Structural Geology*, 30, p. 1317-1331.
- RYER, T. A. & MCPHILLIPS, M. (1983). Early Late Cretaceous paleogeography of east-central Utah. In: REYNOLDS, M. W. & DOLLY, E. D. (eds.) *Mesozoic Paleogeography of the West-central United States*. Rocky Mountain Section, 253-272.
- SCHULTZ, R. A. & BALASKO, C. M. (2003). Growth of deformation bands into echelon and ladder geometries. *Geophysical Research Letters*, 30.
- SCHULTZ, R. A. & FOSSEN, H. (2008). Terminology for structural discontinuities. *Aapg Bulletin*, 92, p. 853-867.
- SHIPTON, Z. & COWIE, P. (2001). Damage zone and slip-surface evolution over μm to km scales in high-porosity Navajo sandstone, Utah. *Journal of Structural Geology*, 23, p. 1825-1844.
- SOLIVA, R., SCHULTZ, R. A., BALLAS, G., TABOADA, A., WIBBERLEY, C., SAILLET, E. & BENEDICTO, A. (2013). A model of strain localization in porous sandstone as a function of tectonic setting, burial and material properties; new insight from Provence (southern France). *Journal of Structural Geology*, 49, p. 50-63.
- SPIKER, E. M. & REESIDE, J. B. (1925). Cretaceous and Tertiary Formations of the Wasatch Plateau, Utah. *Geological Society of America Bulletin*, 36, p. 435-454.
- STEWART, J. H. (1998). Regional characteristics, tilt domains, and extensional history of the late Cenozoic Basin and Range province, western North America. In: FAULDS, J. E. & STEWART, J. H. (eds.) *Accommodation zones and transfer zones: The regional segmentation of the Basin and Range province*. Geological Society of America Special Paper, 47-74.
- STOKES, W. L. (1944). Morrison Formation and related deposits in and adjacent to the Colorado Plateau. *Geological Society of America Bulletin*, 55, p. 951-992.
- TORABI, A. & FOSSEN, H. (2009). Spatial variation of microstructure and petrophysical properties along deformation bands in reservoir sandstones. *AAPG Bull.*, 93, p. 919-938.
- TWISS, R. J. & MOORES, E. M. (2007a). Mechanics of Fracturing and Faulting. In: RAYMOND, V., CLENCH, W. & SERVICE, J. C. P. (eds.) *Structural Geology*. New York, W. H. Freeman and Company, 220-221.
- TWISS, R. J. & MOORES, E. M. (2007b). *Structural geology*, New York, W. H. Freeman and Company.
- WEIMER, R. J. (1960). Upper cretaceous stratigraphy, rocky Mountain area. *AAPG Bulletin*, 44, p. 1-20.
- WHITMEYER, S. J. & KARLSTROM, K. E. (2007). Tectonic model for the Proterozoic growth of North America. *Geosphere*, 3, p. 220-259.
- WIGLEY, M., KAMPMAN, N., DUBACQ, B. & BICKLE, M. (2012). Fluid-mineral reactions and trace metal mobilization in an exhumed natural CO₂ reservoir, Green River, Utah. *Geology*, 40, p. 555-558.

- WILKINSON, M., GILFILLAN, S. M., HASZELDINE, R. S. & BALLENTINE, C. J. (2009). Plumbing the depths: Testing natural tracers of subsurface CO₂ origin and migration, Utah. In: GROBE, M., PASHIN, J.C., DODGE, R.L. (ed.) *Carbon Dioxide Sequestration in Geological Media d State of the Science*. AAPG Studies, 1-16.
- WILLIS, G. C. (1999). The Utah thrust system -an overview. *Utah Geological Association Publication*, 27, p. 1-9.
- YINGLING, V. L. & HELLER, P. (1992). Timing and record of foreland sedimentation during the initiation of the Sevier orogenic belt in central Utah. *Basin Research*, 4, p. 279-290.
- YOUNG, R. G. (1970). Lower Cretaceous of Wyoming and the southern Rockies. *The Mountain Geologist*, 7, p. 105-121.
- ZULUAGA, L. F., FOSSEN, H. & ROTEVATN, A. (2014). Progressive evolution of deformation band populations during Laramide fault-propagation folding: Navajo Sandstone, San Rafael monocline, Utah, U.S.A. *Journal of Structural Geology*, 68, Part A, p. 66-81.